ISTANBUL TECHNICAL UNIVERSITY
ELECTRICAL-ELECTRONICS FACULTY

ELECTROMAGNETIC MODELLING OF THE WIRELESS COMMUNICATION CHANNELS ASSISTED WITH RECONFIGURABLE INTELLIGENT SURFACES (RIS)

SENIOR DESIGN PROJECT

Serden Sait ERANİL
Ramazan Umut AKTAŞ

ELECTRONICS AND COMMUNCATION ENGINEERING DEPARTMENT

JUNE, 2022

ISTANBUL TECHNICAL UNIVERSITY
ELECTRICAL-ELECTRONICS FACULTY

ELECTROMAGNETIC MODELLING OF THE WIRELESS
COMMUNICATION CHANNELS ASSISTED WITH
RECONFIGURABLE INTELLIGENT SURFACES (RIS)

SENIOR DESIGN PROJECT

Serden Sait ERANİL
(040170025)
Ramazan Umut AKTAŞ
(040190762)

ELECTRONICS AND COMMUNCATION ENGINEERING
DEPARTMENT

Thesis Advisor: Assoc. Prof. Mehmet Nuri AKINCI
Thesis Co-Advisor: Prof. Dr. İbrahim ALTUNBAŞ

JUNE, 2022

AYARLANABİLİR AKILLI YÜZEYLER İÇEREN KABLOSUZ HABERLEŞME KANALLARININ ELEKTROMANYETİK OLARAK MODELLENMESİ

LİSANS BİTİRME TASARIM PROJESİ

Serden Sait ERANİL
(040170025)
Ramazan Umut AKTAŞ
(040190762)

Tez Danışmanı: Doç. Dr. Mehmet Nuri AKINCI
Eş Danışman: Prof. Dr. İbrahim ALTUNBAŞ

ELEKTRONİK VE HABERLEŞME MÜHENDİSLİĞİ BÖLÜMÜ

HAZİRAN, 2022

We are submitting the Senior Design Project Report entitled as "ELECTROMAG-NETIC MODELLING OF THE WIRELESS COMMUNICATION CHANNELS AS-SISTED WITH RECONFIGURABLE INTELLIGENT SURFACES (RIS)". The Senior Design Project Report has been prepared as to fulfill the relevant regulations of the Electronics and Communication Engineering Department of Istanbul Technical University. We hereby confirm that we have realized all stages of the Senior Design Project work by ourselves and we have abided by the ethical rules with respect to academic and professional integrity .

Serden Sait ERANİL   ....
(040170025)

Ramazan Umut AKTAŞ   ....
(040190762)

FOREWORD

We sincerely remercie to our supervisors Prof. Dr. İbrahim Altunbaş and Assoc. Prof. Dr. Mehmet Nuri Akıncı for their support and guidance through the project. We are grateful to academic staff and laborers of Istanbul Technical University for their efforts, who provide us the opportunity of completing our Bachelor of Science degree in the Istanbul Technical University Department of Electronics and Communication Engineering, which is a great privilege. Finally, we would like to thank our families and friends who stood by us and supported us in all circumstances.

June, 2022
Serden Sait ERANİL

Ramazan Umut AKTAŞ

TABLE OF CONTENTS

ABBREVIATIONS

3GPP	**:**	3rd Generation Partnership Project
5G	**:**	Fifth Generation
6G	**:**	Sixth Generation
AWGN	**:**	Additive White Gaussian Noise
BER	**:**	Bit Error Rate
EM	**:**	Electromagnetic
ETSI	**:**	European Telecommunications Standards Institute
FET	**:**	Field-Effect Transistor
FPGA	**:**	Field Programmable Gate Array
GSTCs	**:**	Generalized Sheet Transition Conditions
IRS	**:**	Intelligent Reflecting Surface
LIS	**:**	Large Intelligent Surface
LOS	**:**	Line of Sight
MEMS	**:**	Electromechanical Devices
NLOS	**:**	Non-line of Sight
OFDM	**:**	Orthogonal Frequency-Division Multiplexing
PDF	**:**	Probability Distribution Function
PMF	**:**	Probability Mass Function
RIS	**:**	Reconfigurable Intelligent Surface
SEM	**:**	Surface Electromagnetics
SISO	**:**	Single Input Single Output
SNR	**:**	Signal-to-Noise Ratio
TE	**:**	Transverse Electric
TM	**:**	Transverse Magnetic
XPR	**:**	Cross Polarization Power Ratio

LIST OF FIGURES

ELECTROMAGNETIC MODELLING OF THE WIRELESS COMMUNICATION CHANNELS ASSISTED WITH RECONFIGURABLE INTELLIGENT SURFACES (RIS)

SUMMARY

Contrary to the classical paradigm, which assumes that the channel is an uncontrollable entity, partial control over the wireless environment can be obtained by deploying a RIS in the channel. Thus, RIS can increase achievable rate, block eavesdropping, decrease channel sparsity, etc. These capabilities of RIS usage imply that proper settlement of RIS on the wireless channel can provide various advantages, and these advantages make RIS a promising technology of beyond 5G communication systems. Even though there exist active RIS technologies, studies in literature mainly focused on passive RIS. Passive RIS technology consumes power only for control of the RIS itself, making it a nearly passive device because of its low power consumption. Having provided control over the channel with low power consumption makes RIS technology energy efficient and this feature is one of the most significant aspects of RIS.

In order to obtain optimum performance in RIS-assisted channels, an synthesis of the link should be performed by considering the realistic constraints. Realistic constraints stem from the model that encompasses the response of the overall channel. The channel model consists of two main parts, which are the RIS response and the stochastic channel model. RIS response is a deterministic equation that models the interaction between the surface and impinging electromagnetic (EM) waves. Stochastic parameters in the channel are included in the stochastic channel model.

In this project, it is aimed to obtain a physical channel model which models the RIS response and stochastic channel. As a result, the equation for the overall channel model is obtained. This equation includes both deterministic RIS response and generation stochastic channel parameters. The model is valid for the sub-6GHz band and mmWave band and it is based on clustered statistical channel model. Also, the model assumes single input single output (SISO) communication link. In the model, it is assumed that the transmitter and receiver have a fixed location, which eliminates the effect of the Doppler shift. There are plenty of statistical parameters in the channel equation. These are the number of clusters, clusters powers, path losses, angles of elevation and azimuth, cross-polarization powers, phase shifts, line-of-sight (LOS) probabilities, and the number of scatterers per cluster. These random parameters are also environment dependent, which means that their statistical characteristics are dependent on the environment that which the communication link is placed. Deterministic parameters are operating frequency, RIS size, transceiver antennas' radiation pattern, transmit power and EM parameters of the RIS. The meaning of those parameters will be explained in detail in the following sections. The electromagnetic response of the RIS is modeled by using the transmission line model. As a result, a

model is obtained for the RIS-assisted channel which includes both the EM parameters such as operating frequency, polarization, radiation patterns, and random parameters in a single equation.

The model's accuracy was tested by comparing the achievable rate's dependency on RIS size, positioning, and transmit power with the existing results in the literature. Since models in the literature assume ideal RIS response, in order to obtain comparable results we also assumed ideal RIS response. However, it is not guaranteed that RIS can provide an ideal response. Hence, by using the overall channel model, we have formulated a constrained optimization problem for achieving the maximum achievable rate with a given design. Solutions to this problem show how much RIS response varies from ideal response with given constraints and pre-determined design parameters. This optimization problem can be constructed differently by using various approaches. For example, the objective function is dependent to channel information. Thus, there are two different optimization cases. Obtained results are used to show a realistic perspective about RIS usage in wireless channels.

AYARLANABİLİR AKILLI YÜZEYLER İÇEREN KABLOSUZ HABERLEŞME KANALLARININ ELEKTROMANYETİK OLARAK MODELLENMESİ

ÖZET

Artan veri hızı, spektral verimlilik, güvenilir iletişim ihtiyaçları sebebiyle her zaman yeni teknolojilere olan ihtiyaç artmaktadır. Araştırmacılar bunun için sürekli yeni teknolojiler geliştirmeye çalışmakta veya var olan teknolojileri geliştirmek için yeni metotlar ve modifikasyonlar geliştirmektedir. RIS bu yeni teknolojilerden birisidir. Potansiyeli sebebiyle araştırmacılar arasında hızla büyük bir ilgi görmüş, daha sonra 6G ve sonrası teknolojilerde kullanılmak üzere çalışmalara başlanmıştır. Bu teknoloji yeni yeni gelişmekte olduğu için birçok yeni ölçüme, fiziksel kanal modellerine, avantajları ve dezavantajların belirlenmesine ihtiyaç vardır.

Örnek verecek olursak bu avantajlardan birisi RIS'ın neredeyse tamamen pasif bir yapıda olmasıdır. Pasif yapıda olmaktan kasıt, RIS'ın neredeyse hiç güç harcamadan, sadece üzerindeki kontrol mekanizmasını çalışır kılabilecek kadar güç harcayarak istenilen işlemleri gerçekleştirebilmesidir. Literatürde aktif kuvvetlendirici içeren RIS'ların kullanımına dair bazı çalışmalar bulunmasına rağmen RIS, literatürdeki çalışmalar ana olarak pasif RIS yapılarına odaklanmıştır. Bu da RIS yüzeylerinin enerji açısından verimli olmasının önemini ortaya çıkarmaktadır.

Telsiz iletişim kanalındaki bozucu etkilerden biri olan sönümleme nedeniyle kanalda çoklu kopyalar oluşur. Bu çoklu kopyalar farklı yönlerde rastgele saçılma yaptığı için hem diğer iletişim kanallarında girişime sebep olur hem de kullanılabilecek gücün bir kısmının kayıplara karışmasına sebep olur. RIS kullanımı ile bu farklı yönlerde rastgele saçılan çoklu işaretleri alıcıya iletebiliriz. Bu sayede hem girişim azaltılmış olur hem de alıcıdaki SNR iyileştirilebilir.

RIS'ın telsiz iletişimin kontrol edilemeyen ortamının kısmen kontrol edilebilmesine olanak vermesi sebebiyle birçok avantajı bulunur. Bu çalışmalardan birkaçına örnek verecek olursak; kanalların birbirinden farklı olmasını kullanan uzaysal modülasyon gibi tekniklerde kanalın korelasyonunu artırmak için ortama RIS gibi bir saçıcı yerleştirilerek kasıtlı olarak kanalın korelasyonu düşürülebilir. Öte yandan RIS yapıları izinsiz dinleme ve fiziksel kanal güvenliği açısından da birçok avantaj sağlayabilir. Fakat bu çalışmanın ana amacı RIS'ın potansiyel avantajları ve kullanım alanlarının anlatılmasının aksine elektromanyetik açısından tutarlı bir kanal modelinin bulunmasıdır.

RIS yapılarının telsiz iletişim kanalında nasıl davrandığının anlamlandırılabilmesi ve gerçek hayattaki davranışına ilişkin optimum modeller bulunabilmesi için önce telsiz kanalının nasıl davrandığını yani içerisinde yayılan dalgaların nasıl etkilere maruz kaldığını sonra da RIS yüzeylerinin üzerine gelen bu dalgalara nasıl bir tepki verdiğini

anlamak önemlidir. Bu etkiler öğrenildikten sonra RIS'ın telsiz iletişim kanalındaki davranışı incelenebilir, modellenebilir ve optimizasyonu gerçeklenebilir.

Bu çalışmanın 1. bölümünde telsiz iletişiminin nasıl bir kanal olduğundan ve bozucu etkilerinden bahsedilmiştir. Telsiz iletişimin hayatımızda önemli bir yer tutmasının ana sebeplerinden bazıları her yere kablo döşemenin pratik olmaması, pahalı olması ve çok yer kaplamasıdır. Bunun yerine eğer biz bilgiyi havadan iletirsek bu insanların hayatını çok kolaylaştırır. Bu da telsiz iletişimin ana amacıdır.

Telsiz iletişimde büyük çapta ve küçük çapta olmak üzere yayılma etkileri çeşitleri vardır. Bu yayılma etkileri çeşitleri sinyalin genliğinde yarattığı değişimlere göre adlandırılır.

Örnek verecek olursak, yol kaybı olarak adlandırılan ve dalga yayılımının doğasından kaynaklanan güç kaybı büyük çapta bir yayılma etkisidir. Bu yol kaybı dalganın dalga boyuna önemli miktarda bağlıdır. O yüzden yüksek frekanslarda dalgalar çok büyük kayıplara uğramaktadır. Bu büyük kayıplar iletişim kanalının performansını büyük ölçüde kısıtlamaktadır. Bir diğer büyük çaptaki yayılma etkisi de gölgeleme olarak adlandırılan ve iletim yolundaki engellemelerin ya da bloklamaların alınan güçte büyük dereceli salınımlara sebep olmasıdır. Bu salınımlar iletim yolundaki ormanlık bir alan, bir dağ gibi çevresel etmenler olabilir. Gölgeleme etkileri istatistiksel olarak log-normal dağılımı ile modellenebilir.

Küçük çaptaki yayılım etkilerine sönümleme örnek olarak verilebilir. Sönümleme etkisi yine yayılımın doğasından kaynaklanan saçılma etkilerinden kaynaklanır. Mesela, ortamdaki nesneler yayılan dalganın dalga boyuna göre belirli bir orandan küçük olduğu zaman bu nesneler dalga için saçıcı olarak davranır ve bu saçılmalar aynı dalganın farklı yönlerde ve farklı genliklerde kopyalarının oluşmasına sebep olur. Bu farklı yönlerde ve farklı genliklerde yayılan kopyalar alıcıya farklı zamanlarda ulaştıklarında elde edilen işaretin fazının ve genliğinin rastgele değişmesine sebep olur. Bu da hata performansını kötüleştirir.

Farklı kanal sönümleme çeşitleri vardır. Bunlar, frekans seçici, frekans seçici olmayan (düz), hızlı ve yavaş olmak üzere 4 çeşittir. Fakat kanal aynı anda hem frekans seçici hem de hızlı olabilir. Yani, ilk iki kanal ve ikinci iki kanal birbirinden bağımsız değildir. Frekans seçici kanal isminden de anlaşılabileceği üzere farklı frekanslar için farklı sönümleme katsayıları uygularlar. Öte yandan frekans seçici olmayan kanallar belirli bir frekans için sabit bir kanal cevabı uygular. Bu sabit kanal cevabından dolayı bazen düz kanal olarak da adlandırılırlar. Düz kanal çeşitlerine Rayleigh, Rician, Nakagami-m kanalları ve bu dağılımların istatistiksel dağılımları örnek olarak verilmiştir.

Kanalın frekans seçici olup olmaması, sinyalin bant genişliğine göre tanımlanır ve sinyalin bant genişliği kanalın karakteristiğini ifade eden uyumluluk bant genişliği ile karşılaştırılarak belirlenir. Frekans seçici kanalların kötü etkilerini yok etmek için birçok teknik geliştirilmiştir. OFDM, yayılmış spektrum (SS) ve kanal dengeleme sayesinde kanallar düz olarak kabul edilebilirler.

Hızlı ve yavaş sönümleme kanalları ise kanalın zamanla nasıl değiştiğinin bir belirticisidir. Mesela hızlı sönümleme kanallarında sönümleme katsayısı zamanın bir fonksiyonudur ve zamanla farklı sönümleme katsayıları uygularlar. Bunun sebebi iletişimin sağlandığı ortamın durgun olmaması ve zamanla değişmesinden ya da verici, alıcının hareket etmesinden kaynaklanabilir. Fakat kanalın hızlı ya da yavaş olması,

frekans seçiciliğinde olduğu gibi sinyale de bağlıdır. Eğer gönderilen sembollerin süresi kanalın uyumluluk süresinden küçük ise kanal yavaş olarak değişir. Tam tersi durumda ise kanal hızlı değişir. Günümüzde iletişim frekanslarının sürekli artması dolayısıyla bu koşul genelde sağlanır ve kanallar yavaş değişen kanallar olarak kabul edilebilirler.

Bu çalışmanın 2. bölümünde ise RIS cihazının nasıl bir yapısı olduğundan ve RIS tepkisinin elektromanyetik olarak nasıl modellenebileceğine dair bazı yaklaşımlardan bahsedilmiştir. RIS yapılarını metamateryal olarak adlandırılan ve doğada bulunmayan bazı dalga dönüşümlerini uygulayabilen yapıların bir alt kümesi olarak inceleyebiliriz. Bu dalga dönüşümlerinden en önemlisi olarak geliş açısından farklı bir açıyla yansıtma örnek verilebilir. Bu durum Snell yasalarına aykırıdır çünkü Snell yasalarına göre yüzeye çarpan dalga geldiği açıyla geri yansıtılmaktadır. Metamateryellerin bu özelliği sebebiyle iletişim kanalında kullanılmasında büyük bir potansiyel görülmüştür. Metamateryaller, 3 boyutlu ve kalın yapılar oldukları için direkt olarak haberleşme sistemlerinde kullanılması pek pratik değildir. Fakat Huygens'in prensibine göre bu 3 boyutlu yapıların sağladıkları elektromanyetik özellikler 2 boyutlu yüzeylerle tamamen sağlanabilir. Bu prensip sayesinde bu yüzeyleri 2 boyutlu sentezlemek haberleşme sistemi için çok daha uygundur. Bu sayede bu yapılar artık yüzeyler olarak adlandırılır. Bu yapıların neden ayarlanabilir olarak adlandırıldığına gelecek olursak eğer, bu yüzeylerin üzerinde boyutları dalga boyundan küçük olan birçok eleman bulunur ve bu her elemanın elektromanyetik özellikleri bu elemanın üzerine uygulanan voltaj, akım veyahut elemanların geometrisindeki değişimler sayesinde kontrol edilebilir. Bu sayede bu yapılar kanalı takip ederek gerekli elektromanyetik özellikleri bu elemanlar üzerinden sağlayabilir. Bu elemanların kontrolleri için tüm elemanlar bir adet kontrolöre bağlanırlar. Bu kontrolör bir FPGA veyahut programlanmış bir mikrokontrolör olabilir. Akıllı olarak adlandırılmalarının sebebi de alışılageldiğin dışındaki dalga dönüşümlerini uygulayabilmeleridir.

Elde edilen bu yüzeylerin kontrolünün istenildiği gibi sağlanabilmesi için bu yüzeylerin doğru bir şekilde modellenmesi gerekmektedir. Bu yüzden farklı modelleme teknikleri literatürde yer bulmaktadır. Bu modellemeleri RIS yüzeyini tamamen yüzey elektromanyetiği kullanarak modellenmesi ve eleman bazında iletim hattı modellemesi olarak iki farklı başlıkta gruplandırabiliriz. Yüzey elektromanyetiği modellemeleri, iletim hattı modellemesine göre çok daha doğru olmasına rağmen karmaşıklığı çok yüksek olduğu için literatürde haberleşme araştırmacıları tarafından pek tercih edilmez. Fakat yüzey elektromanyetiği model karşılıklı kuplaj gibi diğer elemanların birbirleri üzerindeki etkileri de içerdiği için bazı durumlarda daha çok tercih edilebilir. Öte yandan iletim hattı modellemeleri yüzey elektromanyetiğine göre birçok varsayım yapılarak türetilmiştir. Kullanılması ve analizi çok daha basittir. Fakat RIS'a çarpan elektromanyetik dalgalarının polarizasyon değişmelerini ve yükselim açıları gibi değerleri kullanmadığı için uygulamadan uygulamaya kolaylığından dolayı kazandırdığı avantajı kaybedebilir. Bu araştırma çalışmasında da referans alınan çalışmada polarizasyon değişimleri hesaba katılmadığı için iletim hattı modellemesi tercih edilmiştir. Ayrıca operasyon frekansı çok yüksek olduğu için karşılıklı kuplajın da küçük olduğu varsayılmıştır.

Telsiz iletişim kanalının yayılan dalga üzerinde nasıl etkilere sahip olduğu ve RIS yapısının ne olduğu, nasıl çalıştığı ve modellemesi hakkında fikir verildikten sonra RIS yapılarının telsiz iletişim kanallarındaki davranışlarından literatürdeki mevcut

çalışmalar perspektifinden bahsedilmiştir. Önce RIS yüzeylerinin teorik olarak basit bir çalışmasından performans analizi hakkında bilgi verilmiştir. RIS yapılarının mevcut potansiyelini gösteren bu çalışmada alıcı, RIS, verici arasında saçıcı bir ortamın olmadığı varsayılmış ve direkt olarak kanallar LOS kabul edilmiştir. Bu model gerçekteki ortamları çok iyi modellemediği için 6 GHz altındaki bantlar için saçıcı ortamlarda incelenmiş bir kanal modeli incelemeye alınmıştır. Bu kanalda saçılmalar olduğu için RIS üzerine gelen açıların istatistiksel olarak modellenmesi gerekmektedir. Bu açılar için istatistiksel olarak bazı olasılık dağılım işlevleri önerilmiş ve diğer çevresel kanal parametreleri üretilerek analizleri ve simülasyonları yapılmıştır. Fakat bu model de seçilen ortam için LOS olasılığını sabit kabul etmiş ve aynı LOS koşulları için incelemiştir. Bu tezde referans olarak alınan başka bir çalışmada, verici, alıcı ve RIS'ın konumlarının önemine, daha doğru istatistiksel açı modellerine, uzaklığa bağlı olarak verilen LOS olasılıklarına ve kanalların arasındaki korelasyonlara değinilmiştir. Bu sebeple de gerçeğe daha yakın bir modellemedir. Fakat söz konusu çalışmada ideal bir RIS cevabı olduğu için ve saçılmalardaki polarizasyon değişimlerinden kaynaklanan kayıpların bir modeli bulunmadığı için bunları kapsayan bir model bu araştırma çalışmasında verilmiştir.

Önerilen bu yeni kanal modelinin parametreleri öncelikle bahsedilmiş, daha sonra alt bölümlerde tek tek açıklanmıştır. RIS cevabı için kullanılan iletim hattı modelinin çıkarımına yer verilmiş, sonrasında da kanal modelindeki direkt (SISO), LOS ve NLOS kanallarının açıklamalarına yer verilmiştir. Bu çalışmada bina içi (indoor) ve bina dışı (outdoor) olmak üzere iki farklı çevre için haberleşme kanalının özellikleri incelenmiştir. Örnek verecek olursa bina içinde RIS ve alıcı yapısının yakın olması beklendiğinden bu kanalın LOS olasılığı yüzde 50'nin üzerindedir. Bu sebeple bu kanal direkt olarak LOS kabul edilmiştir. Ayrıca yine bina içideki bu yakınlık sebebiyle verici alıcı arasındaki kanalın verici ve RIS arasındaki kanal ile aynı saçıcıları tecrübe ettiği kabul edilebilir ki kötü bir varsayım değildir. Öte yandan bina dışı için bu iki kanalın tamamen farklı bir saçıcı ortam tecrübe ettiği varsayılmıştır. O yüzden konumlamalara bağlı olarak farklı performanslar elde edilmiştir.

Bunların yanında, elde edilen model için farklı SNR değerleri, farklı konumlar ve konum değişimlerinin etkisi, eleman sayısının artmasının etkisi gibi etkilerin başarılabilir hız (achievable rate) için ne kadar önemli olduğunun grafikleri verilmiştir. Burada bu tüm simülasyonlar için alıcı ve verici arasındaki direkt kanal RIS kullanılan kanala göre çok daha güçlü ve rastgeledir. Bunun sebebi RIS kullanılan kanalda dalgaların daha çok mesafe kat etmesi dolayısıyla daha fazla yol kaybına uğramalarıdır. Bu sebeple RIS'ın kullanılmasının uygun görüldüğü ortamların genelde direkt kanalın kurulamadığı senaryolar için uygun olduğu çıkarımı yapılmıştır.

Son olarak kullanılan RIS cevabının alıcıdaki performansı azami seviyeye getirilmesi için nasıl bir optimizasyon yapılması gerektirdiğinden bahsedilmiş ve 3. bölümde de bu sistemin gerçeklenmesi üzerindeki gerçekçi kısıtlamalar ve sonuçlardan bahsedilmiştir. Bu projenin nerede kullanılabileceğinden ve sosyal, ekonomik, çevresel katkılarının ne olduğuna da değinilmiştir. Çalışmanın maliyetinden ve sağlık açısından bir probleminin olup olmadığına değinilmiş ve bu projeye ilerde ne gibi katkılar yapılabileceğinden bahsedilmiştir.

1. INTRODUCTION

1.1 Abstract of the Interim Project

Increased data transfer rate requirements, scarcity in the spectrum, and the need for more reliable communication due to developing internet of things technology make usage of novel communication technologies capable of satisfying required communication standards inevitable. The utilization of a RIS in the channel makes the communication users benefit from high speed data rates and more reliable communication by altering the channel properties. Therefore, the RIS deployment offers a solution to the users' higher data rate, increased bandwidth, and reliable communication requirements. The wireless communication channels which are assisted with reconfigurable intelligent surfaces have different channel characteristics and different channel impulse responses compared to classical ones. The overall channel characteristic is both a function of the wireless environment, which is modeled statistically, and the function of the deployed surface, which is modeled by deterministic wave transformations. In order to acquire proper channel models, the electromagnetic response of the surface must be determined and applied to the channel model. This senior design project aims to combine the modeled EM response of the RIS with the 3D polarized mmWave clustered channel model.

1.2 Wireless Channel Model

As the name completely suggests, wireless channel is a type of communication technique which utilizes no wire to convey information from one place to another. By the advent of more mobile devices, the benefits, and importance of wireless communication come to realization. However, wireless channels have inherent challenges to the quality of communication such as noise, interference, and other channel impediments. Some of these impediments are called path-loss, shadowing, Doppler effect, fading, etc. Path-loss and shadowing effects are called large-scale

propagation effects, since they attenuate the signal on a large scale with respect to the signal's amplitude. On the other hand, fading is also referred to as small-scale propagation effects because it causes small deviations from the signal's amplitude. Fading is a phenomenon caused by the fact that scattered signals arrive to the receiver at different times, thereby causing constructive and destructive summation. The scattered signals may propagate through different paths; therefore, it is also called the multipath effect.

The effects of large-scale and small-scale propagation can be seen in Figure 1.1. While path-loss reduces the received signal's power directly, shadowing and multipath causes large and small variation on the signal's amplitude, respectively.
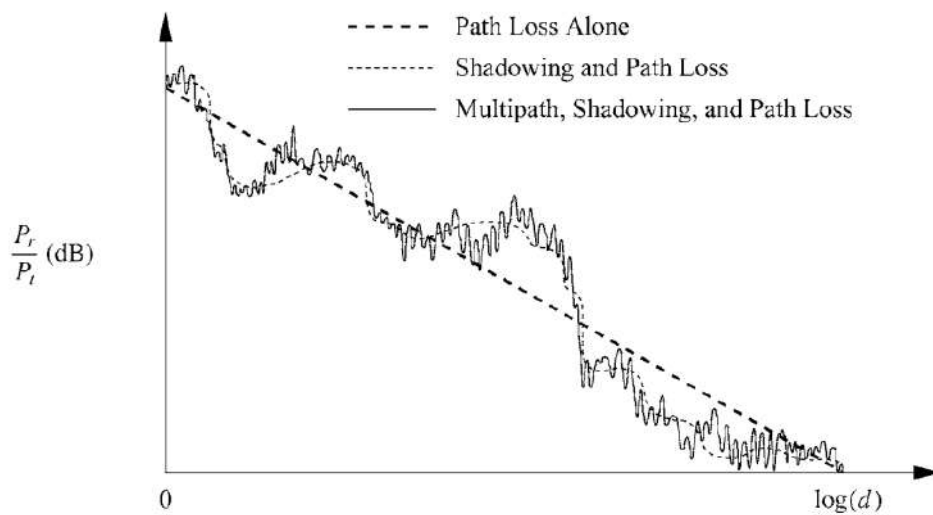
Figure 1.1 : Large-scale and small-scale propagation effects on the received power with respect to logarithmic distance [1].

Path-loss is a type of parameter mainly caused by the distance traveled by the wave and the operating frequency of the wave. There are some empiric models that quantify the amount of path-loss, such as Okumura Model, Hata Model, COST 231, etc. However, shadowing and fading are required to be modeled statistically, since it is not possible to know the state of the channel at every point and time and solve Maxwell's Equations at these points to find the variations on the amplitudes.

Generally, the wireless channel is subject to change and there are different wireless environments such as indoor, outdoor etc. For example, it is obvious that the physical properties of the medium are different in a metropolitan area than that of an urban area. The metropolitan areas are an environment with more scattering properties, since

there are much more interacting objects compared to the suburban areas. Suburban areas, on the other hand, have less interacting objects in surroundings; hence, cause less scattering. Due to these differences, different channels requires different channel properties.

1.2.1 Complex representation of signals

Before diving into channel models, we need to incorporate the usage of complex representation since it simplifies the analysis and reduces unnecessary complexity. Generally speaking, the transmitted symbols can be shown as

$$s(t) = a(t)\cos\left(w_c t + \theta(t)\right) \tag{1.1}$$

where $a(t)$ represents the variations in the signal's amplitude, $w_c = 2\pi f_c$ represents the angular operation frequency, and $\theta(t)$ represents variations in the phase of the signal. If we expand (1.1) and define $s_I(t)$ and $s_Q(t)$ as

$$s(t) = \underbrace{a(t)\cos\theta(t)}_{s_I(t)}\cos\omega_c t - \underbrace{a(t)\sin\theta(t)}_{s_Q(t)}\sin\omega_c t \tag{1.2}$$

we obtain

$$s(t) = s_I(t)\cos w_c t - s_Q(t)\sin w_c t \tag{1.3}$$

where $s_I(t)$ and $s_Q(t)$ represents the in-phase and quadrature-phase terms of $s(t)$. From now on, we can define the complex envelope or low pass equivalent of $s(t)$ by using the form

$$s(t) = Re\left[\tilde{s}(t)e^{jw_c t}\right] \tag{1.4}$$

where $\tilde{s}(t) = s_I(t) + js_Q(t) = a(t)e^{j\theta(t)}$ is the complex envelope of $s(t)$. Writing signals in the form of (1.4) prove to be very useful since it does not include the operating frequency term in the analysis.

1.2.2 Fading

In an environment, the transmitted signal will interact with the surrounding objects and these objects will cause the reflections and scattering of the signal that result in extra copies of the signal. These copies may follow different paths and therefore may have different attenuation and phase differences with respect to the original signal. When all the copies reach to the receiver, they will add up and result in fluctuations in the signal's amplitude.

If we had known every interaction of the signal with every object in the environment and their boundary conditions, we would have solved Maxwell's Equations and found the exact attenuation, phase, delay etc. However, it is not possible in practical approach, although it seems theoretically doable. The environment generally changes, and we cannot know every interaction; therefore, we employ some statistical techniques to model the signal's fluctuations and phase shifts. Additionally, since Maxwell's equations cannot be solved, a common approximation of plane waves which is known as ray tracing will be employed. This method takes reflection and refraction of the plane wave into consideration; however, ignores the complex scattering from the objects. Hence, allow us to use geometric equations instead of coupled differential equations. Since the ray tracing approximation is based upon plane waves, in order for this approximation to be accurate the receiver must be several wavelengths further than the interacted object and the dimensions of the interacted objects must be large.

In this subsection, some fading types will be introduced. Before we introduce these fading types, it is required to mention the channel model with ray tracing approach. The received signal without the Gaussian noise at the receiver is

$$
\begin{aligned}
r(t) &= Re\left\{ \sum_{n=1}^{N} c_n e^{j\psi_n - j2\pi f_c \tau_n + j2\pi\left(f_c + f_{D,n}\right)t} \tilde{s}\left(t - \tau_n\right) \right\} \\
&= Re\left\{ \tilde{r}(t) e^{j2\pi f_c t} \right\}
\end{aligned}
\tag{1.5}
$$

where c_n and ψ_n are random variables representing the amplitude and the phase change through the path n. τ_n represents the delay of the path n, $f_{D,n}$ represents the Doppler's frequency shift caused by the path n, and $\tilde{r}(t)$ represents the low pass equivalent of the received signal $r(t)$. For the sake of simplicity, one term can be defined for all phase terms as

$$\phi_n(t) = \psi_n - 2\pi f_c \tau_n + 2\pi f_{D,n} t. \tag{1.6}$$

Then, (1.5) simplifies to

$$\tilde{r}(t) = \sum_{n=1}^{N} c_n e^{\phi_n(t)} \tilde{s}(t - \tau_n) \tag{1.7}$$

which is the most general form of received signal under the assumption of the ray tracing method, regardless of the channel type. Since transmitted signal and received signal are known, the channel impulse response can be found as

$$g(t, \tau) = \sum_{n=1}^{N} c_n e^{j\phi_n(t)} \delta(\tau - \tau_n). \tag{1.8}$$

With the channel equation is obtained, the channel can now be investigated further. The channel may be frequency selective, non-frequency selective (flat) and also these channels can be classified further into slow and fast channels.

1.2.2.1 Frequency selective multipath fading

When the maximum delay of the multipath components greater or equal to the symbol duration, the transmitted signal is exposed to different amplitude changes for different frequencies; hence, gaining the name frequency selective channel. Also, the inverse of the amount of maximum delay among the multipath components is known as coherence bandwidth. With the same logic, if the coherence bandwidth of the channel is smaller or equal to the symbol bandwidth, then the symbol experiences a frequency selective channel. As it can be easily deduced, frequency selective channels are generally an undesired channel type since it experiences a different attenuation at each different frequency. It is both unpredictable, and compensating these attenuations in different frequencies is costly for the receiver.

An example of a frequency selective channel can be seen in Figure 1.2. It applies different attenuation values at different frequencies; thereby, reducing the performance of the channel.

With the techniques developed such as OFDM, Spread Spectrum and Channel Equalization methods, the effect of frequency selective channels can be mitigated.

Therefore, it is not required to delve into the details of the frequency selective channel. In this project, the proposed models accept the channel as a non-frequency selective (flat) channel.
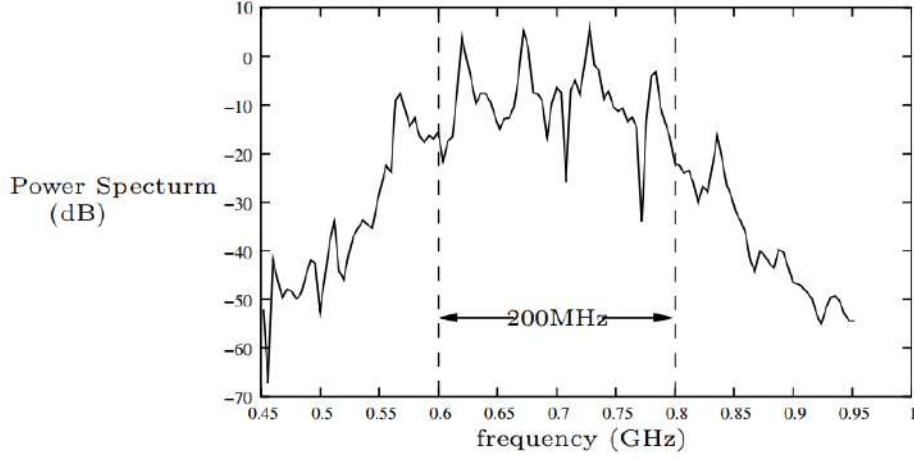
Figure 1.2 : An example of frequency selective channel [2].

1.2.2.2 Non-frequency selective multipath fading (flat fading)

When the maximum delay spread of the multipath components smaller than symbol duration or, in other words, the coherence bandwidth of the channel is greater than the symbol bandwidth, the channel experiences a constant frequency response over that duration. If all the delay spreads are assumed to be equal, namely, $\tau_i \approx \tau_j = \hat{\tau}, \quad \forall i, j$, then channel impulse response (1.8) can be written as

$$g(t, \tau) = \sum_{n=1}^{N} c_n e^{j\phi_n(t)} \delta(\tau - \hat{\tau}) \qquad (1.9)$$

where summation before $\delta(\tau - \hat{\tau})$ is only dependent on t; therefore, it can be defined as $g(t)$. Then the channel equation becomes

$$g(t, \tau) = g(t)\delta(\tau - \hat{\tau}) \qquad (1.10)$$

where $g(t) = \sum_{n=1}^{N} c_n e^{j\phi_n(t)}$. By taking the Fourier Transform of $g(t, \tau)$, it can be shown that the amplitude of the channel impulse response is constant over the frequency range. Also, $g(t)$ can be further decomposed as

$$g(t) = \sum_{n=1}^{N} c_n \cos \phi_n(t) + j \sum_{n=1}^{N} c_n \sin \phi_n(t) = g_I(t) + jg_Q(t) = \rho(t)e^{j\varphi(t)} \qquad \textbf{(1.11)}$$

where $g_I(t) = \sum_{n=1}^{N} c_n \cos \phi_n(t)$, $g_Q(t) = \sum_{n=1}^{N} c_n \sin \phi_n(t)$, $\rho(t) = \sqrt{g_I^2(t) + g_Q^2(t)}$, and $\varphi(t) = \text{arctg} \frac{g_Q(t)}{g_I(t)}$.

$g(t)$ can be addressed as channel coefficient since it is multiplied with the transmitted signal. The amplitude of the channel coefficient is $\rho(t)$ and the phase of the channel coefficient is $\varphi(t)$.

The statistical distributions of the amplitude and the phase of the channel coefficient is dependent on the environment. For example, if there is no LOS component and NLOS components have zero mean and roughly the same power, then g(t) is said to have a complex Gaussian distribution since $g_I \sim N(0, \sigma^2)$ and $g_Q \sim N(0, \sigma^2)$. Moreover, $\rho(t)$ will follow Rayleigh Distribution and $\varphi(t)$ will follow uniform distribution between $-\pi$ and π. The PDF of Rayleigh distribution is given as

$$p_\rho(x) = \frac{2x}{\Omega} \exp\left(-\frac{x^2}{\Omega}\right) \qquad \textbf{(1.12)}$$

where $\Omega = E\left[\rho^2\right] = \int_0^\infty x^2 p_\rho(x)dx = 2\sigma^2$ is the power of the channel.

If there exist a dominant path such as LOS, then $\rho(t)$ will follow a Rician Distribution. This dominance can be modeled as non-zero mean Gaussian $g_I \sim N(m_I, \sigma^2)$ and $g_Q \sim N(m_Q, \sigma^2)$. Then $\rho = \sqrt{g_I^2 + g_Q^2}$ is Rician distributed.

The PDF of Rician Distribution can be given as

$$p_\rho(x) = \frac{2x(K+1)}{\Omega} \exp\left(-K - \frac{(K+1)x^2}{\Omega}\right) I_0\left(2x\sqrt{\frac{K(K+1)}{\Omega}}\right), x \geqslant 0 \qquad \textbf{(1.13)}$$

where $s^2 = m_I^2 + m_Q^2$ is a mathematical parameter representing the means of different paths, $K = \frac{s^2}{2\sigma^2}$ is the ratio of power of direct path and indirect path, Ω is again the power of the fading, and

$$I_0(x) = \frac{1}{\pi} \int_0^\pi e^{x\cos\theta} d\theta \qquad \textbf{(1.14)}$$

is the zeroth degree first type modified Bessel function.

In Rician Distribution, when $K = 0$ then Rician Distribution becomes Rayleigh Distribution because the power of direct path is zero. On the other hand, as $K \rightarrow \infty$ Rician fading converges to AWGN Channel.

One of the other most used fading types is Nakagami-m fading, which can model fading conditions that are severe than Rayleigh fading channels. Its PDF is given as

$$\rho_\rho(x) = \frac{2m^m x^{2m-1}}{\Gamma(m)\Omega^m} \exp\left(-\frac{mx^2}{\Omega}\right) \tag{1.15}$$

where m is the shaping parameter and

$$\Gamma(m) = \int_0^\infty y^{m-1} e^{-y} dy \tag{1.16}$$

is the Gamma function (generalized factorial). When $m = 1$, Nakagami-m fading becomes Rayleigh fading.

1.2.2.3 Fast and slow fading

Channels can experience fast and slow fading depending on the environment and especially on Doppler's Shift. If the bandwidth of the signal is much greater than the Doppler frequency, then this channel is said to be under slow fading. On the other hand, if the bandwidth of the signal is much smaller than the Doppler frequency, then that channel is said to be under fast fading. Under fast fading conditions, the channel coefficient is assumed to change at every time sample and under slow fading conditions it is assumed to be constant for a particular time set of interest. Therefore, as it can be easily guessed, having a slow fading channel is a desired thing. Fortunately, it can be said that channels generally is slow fading channel since data rates and frequencies are very large compared to the generic environments. Therefore, assuming a slow fading channel is generally not a harm to the channel performance.

1.2.2.4 Shadowing and path loss effects

Shadowing is a phenomenon that the received power fluctuates due to the obstruction or blockages of in the transmission path. These fluctuations come from the local means that is computed by averaging envelope power over a spatial averaging interval. This interval is generally chosen to be 20 wavelengths of the transmitted signal [3]. The

received power is constant through that interval, actually, this interval is chosen so that the received power changes smoothly. If there is a building or something in the transmission path, then the averaging in this interval is no longer smooth. This change in local mean is called the shadowing effect and empirical calculations showed that the local mean follows a log-normal distribution whose PDF is given as

$$p_{\Omega_p}(x) = \frac{1}{x\sigma_\Omega\xi\sqrt{2\pi}}\exp\left\{-\frac{\left(10\log_{10}\{x\} - \mu_{\Omega_p(\text{dBm})}\right)^2}{2\sigma_\Omega^2}\right\} \qquad (1.17)$$

where

$$\mu_{\Omega_p(\text{dBm})} = 10\text{E}\left[\log_{10}\{\Omega_p\}\right], \qquad (1.18)$$

Ω_p denotes the local mean, σ_Ω is the standard deviation of shadowing effect in dB, and $\xi = \ln(10)/10$.

There are also composite models for envelope that accompanies both the effect of multipath and the effect of shadowing in one parameter. One such example of composite models is Gamma-Log-Normal Distribution, which models the fading channel as Nakagami-m and local mean as log-normal.

Path loss, as the name suggests, loss due to the propagation of radio wave in the medium. It is the largest cause of attenuation in a wireless channel, therefore it is the most important parameter in the budget of network designers. Path loss occurs due to the spherical expansion of the electromagnetic wave in every direction. There are quite a lot of path loss formulas in the literature, some of which are theoretical and some of which are empirical. One of the most basic and popular theoretical path loss formula is the free space path loss formula, which given as

$$L_{\text{ps}} = \left(\frac{4\pi d}{\lambda_c}\right)^2 = \left(\frac{4\pi d f_c}{c}\right)^2 \qquad (1.19)$$

where d is the travelled distance, c is the light speed, λ_c is the wavelength of the propagating wave, and f_c is the operating frequency of the wave.

Moreover, there are some empirical path loss models such as Okumura-Hata, COST-231, etc. and other models presented by 3GPP and WINNER II.

1.3 RIS Technology

In order to obtain a physical channel model, RIS interaction with impinging EM waves should be modeled. These interactions depend on the both surface's technology and the properties of the impinging wave, such as wavelength (λ), polarization (TE, TM) and arrival angle of elevation (θ). RIS applies wave transforms to the impinging wave, and these transformations enable the operator to have partial control over the wireless channel. There are various wave transforms that RIS can apply, and RISs' capability of applying certain transforms stems from their design. Thence, to obtain desired transformation capabilities, proper technology should be used. Consequently, the model that depicts RIS's interaction with EM waves should be determined with respect to its design.

There are passive and active RIS technologies already studied in the literature. Since being an almost passive device is one of the most significant aspects of the RIS, passive RIS technology is explored in this study. In the passive RIS technology, the only power consuming elements are the controllers that adjust the RIS's response. In the active RIS technology, in addition to controllers, there are amplifiers that consume power. These amplifiers allow RIS to amplify the incoming signal. If we express the interaction of impinging waves with the RIS as a matrix that consists of reflection coefficients, the magnitude of these coefficients should be less than or equal to one in the case of passive RIS technology usage. If active RIS technology is used, then the magnitude of reflection coefficients can take values over positive real numbers.

RISs can be classified as metasurfaces that have adjustable parameters which are controlled by certain control elements. The configurability of these surfaces stems from these controllable parameters. The following section is dedicated to explaining the structure of the RIS.

1.3.1 Metamaterials and metasurfaces

In this section, metamaterials and metasurfaces are briefly introduced. Then the overall RIS structure is explained.

While designing a RIS structure for a wireless communication link, the designer should consider the requirements that the channel imposes. These requirements should be satisfied by exploiting the features of the designed RIS in a controlled manner. Since controllable features stem from the metasurface substrate in the RIS structure, metasurface technology should be known for designing the proper structure.

Metasurfaces can be considered as a specific type of metamaterial that shows similar properties to metamaterials to some extent, and metamaterials can be thought of as pioneer technology for metasurfaces. So, metamaterials will be explained in the first place.

Metamaterials used in EM applications can be broadly defined as artificial homogeneous materials that have EM features not seen in nature. Homogeneity implies that the average cell size of the metamaterial is smaller than a quarter wavelength. When this condition is satisfied, the response of the EM metamaterial can be calculated by using averaged parameters (susceptibility, polarizability, etc.) over the volume. Thus, for the entire material, well-defined constitutive parameters can be obtained. And these constitutive parameters depend only on the structure of the unit cell. As a result, in the direction of propagation, the surface behaves as an electromagnetically uniform material [4]. Configurability of the EM properties of the metamaterial can be obtained by changing the geometry of the cells, or by altering the near-field interactions of cells [5]. Metamaterials have widespread applications in usage. Lens and superlens structures, subwavelength imaging, scattering cancellation, cloaking, EM band gap filtering, multiband resonators, microwave phase shifters, and metamaterial-based antennas are examples of applications in that metamaterials are used [6]. It can be seen that various metamaterials are engineered for controlling the EM wave properties with respect to desired characteristics. If the thickness of the metamaterial becomes much smaller than the wavelength, variations along this axis can be assumed zero. This means that the thickness of the metamaterial can be ignored. Thus, one can obtain a 2D metamaterial or a metasurface by designing a metamaterial with a thickness less than a wavelength [7]. Similar to metamaterials, metasurfaces also consist of subwavelength elements called meta-atoms. Metasurfaces' reduced thickness provides lower loss in the medium and makes them easier to design. Similar to metamaterials, metasurfaces also consist of elements that have sizes smaller than

wavelength, called meta-atoms. Metasurfaces' reduced thickness provides lower losses in the medium and makes them easier to design [8]. Meta-atoms of the surface construct a periodic or quasi-periodic structure. Metasurfaces can perform similar responses as metamaterials. This equivalence between metamaterial and metasurface responses can be shown by using Huygens' principle. Huygens'principle states that arbitrary sources of EM radiation (charges and currents) excited by impinging waves in a closed volume create electric and magnetic fields on the outside of this volume. And these created fields can be expressed as fields that are scattered by sources in an arbitrarily thin layer of electric and magnetic currents enclosing the volume [9]. It should be noted that, since the magnetic currents exist as electric current loops, the thickness of the surface should be greater than zero. Effective parameters of surfaces are calculated by taking the average of EM parameters over the surface. While metamaterial properties are defined in terms of effective permeability and permittivity in general, effective parameters for metasurfaces could be surface polarizabilities, surface susceptibilities, or surface impedances. Moreover, these different representations for effective surface parameters are equivalent, and it is possible to define transformations that allow one to switch between them [8]. Figure 1.3 illustrates the Huygens' principle. As it can be seen, the response of the excited cells in the enclosed volume of metamaterial is equivalent to the response of the magnetic and electric currents in an arbitrarily thin region.

The term metasurface includes a broad class of engineered 2D materials. There are metafilms, metascreens, metagratings and various types of surfaces that can be considered as metasurface. These different classes of metasurfaces can be separated by the topology that forms the metasurface. Different topologies provide different features for surfaces. The features that are desired to be provided by metasurface may vary with respect to its usage. In wireless communication applications, RIS can have multifarious functionalities such as: beamforming, mitigating the fading, blocking eavesdropping, etc. Many of these functions stem from RIS's capability of providing control over phase, polarization, amplitude, direction of reflection of impinging EM waves. And RIS's ability to provide these properties stems from metasurface used in RIS design.
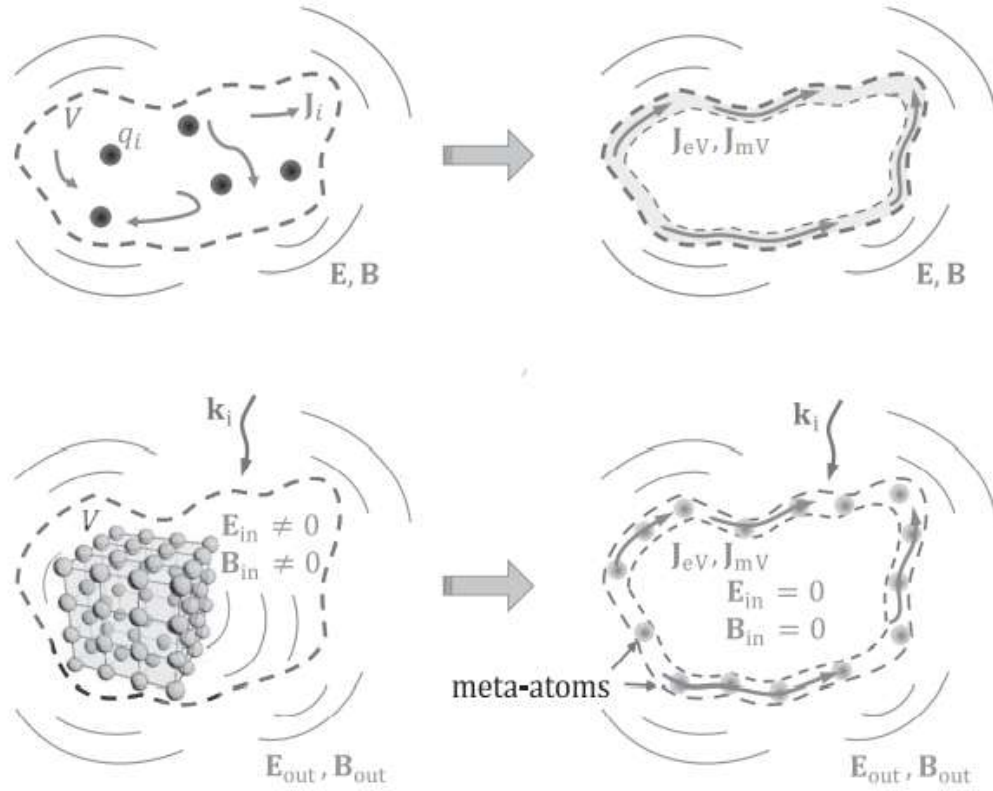
Figure 1.3 : Huygens' principle [9].

Thus, properly engineered metasurfaces should be used in RIS design and RIS's overall structure should be designed by considering its function.

1.3.2 RIS structure

A RIS consists of different layers. Each layer carries out specific tasks. Figure 1.4 demonstrates the architecture of a RIS device. As it can be seen, RIS consists of three major layers and a controller device that tunes the response of the meta-atoms of the metasurface.

The top-most layer is the metasurface layer, which consists of meta-atoms, the copper backplane layer and the control circuit board. Metasurface layer performs the wave transformations to the impinging waves. The copper backplane layer is a good reflector. Thus, it restrains the energy leakage. The control circuit board allows the operator to control the response of the RIS. It provides reconfigurability to the system. Thus, the response of the RIS can be tuned with respect to the requirements of the dynamic channel conditions in real-time. For tuning the RIS response, varactor diodes,
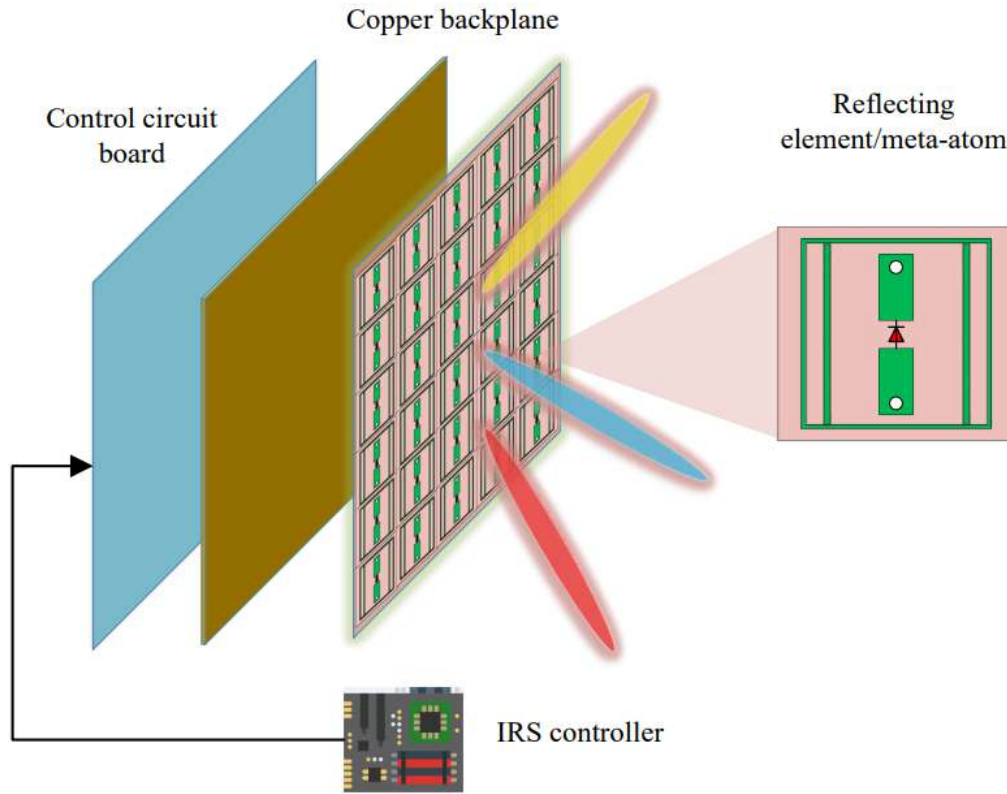
Figure 1.4 : RIS architecture [10].

PIN diodes, MEMS, FETs or an FPGA can be used in the control board layer. The controller device controls the control board layer [10].

Figure 1.5 shows a more simplified model of the RIS structure. In this figure, it can be seen that a RIS element may consist of smaller elements called unit cells [11]. These unit cells correspond to meta-atoms in the metasurface.

The tuning circuit can provide either discrete adjustments or continuous adjustments. For instance, if varactor diodes are used as tuning elements, then by controlling their capacitance with voltage, continuous phase adjustments can be made. However, if an FPGA is used as a tuning element, then discrete phase adjustments can be made.

By using different configurations, different RIS architectures can be obtained. For instance, when the active devices such as amplifiers are implemented to a RIS device, an active RIS can be obtained. Figure 1.6 shows a novel RIS architecture called dual polarized RIS. This architecture allows the operator to have a control over different polarized components of the impinging EM wave. TE and TM polarized components

14
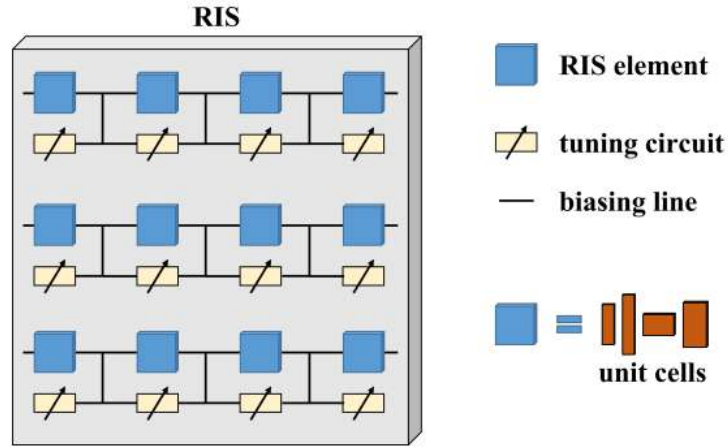
Figure 1.5 : Simplified RIS model [11].

of the EM wave can be manipulated simultaneously and independently by using this device [12].
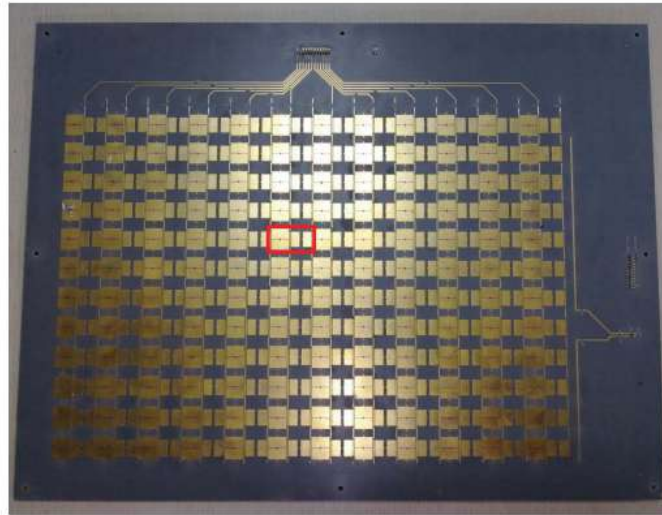
Figure 1.6 : Dual polarized RIS [12].

1.3.3 RIS response modelling approaches

When performing a specific task for wireless communication, the RIS reconfigures its response with respect to the channel conditions. Reconfiguration means changes in the RIS response. The problem of obtaining a proper response can be summarized as: given the channel conditions, which response optimizes the target? The target function can vary with respect to the function of the RIS, it can be achievable rate, SER performance, received power, etc. However, the response is a pre-determined function and a proper RIS response can not be tuned without knowing its formulation. Thus,

for determining the required adjustments to obtain proper response, RIS's interaction with impinging waves should be modeled.

While modeling the RIS response, the response of each cell forming the surface can be modeled and the overall response can be modeled as a superposition of the cell responses. It should be noted that cells forming the RIS can be larger than the wavelength, meta-atoms forming these cells must be smaller than the wavelength. It is plausible to represent the cell response as a 2-by-2 matrix. Entries of this matrix represent the different cases of which the polarization of impinging and reflecting wave. Thus, for the nth cell of the RIS, response can be represented as

$$\Gamma_n(\mathbf{x}) = \begin{bmatrix} f_n^{HH}(\mathbf{x}) & f_n^{HV}(\mathbf{x}) \\ f_n^{VH}(\mathbf{x}) & f_n^{VV}(\mathbf{x}) \end{bmatrix} \tag{1.20}$$

where $f_n^{HH}(\mathbf{x})$ represents the response function for the waves impinging and reflecting with horizontal polarization. $f_n^{VV}(\mathbf{x})$ represents the response function for the waves impinging and reflecting with vertical polarization. Off-diagonal entries represent the response for the waves which are changing polarization after the interaction with the RIS. The vector $\mathbf{x}$ represents the parameters that RIS response depends on.

It should be noted that, $\Gamma_n(\mathbf{x})$ has one input parameter, which is the vector $\mathbf{x}$. This means that in this type of model, all responses for impinging waves are controlled by a single device, yielding the entries of the matrix becoming dependent. However, it is not compulsory to control all responses for incoming waves from a single device. As in the dual-polarized RIS architecture, different responses for different polarizations can be obtained by separate devices by building a proper system. In this case, the response matrix becomes

$$\Gamma_n(\mathbf{x,y,w,z}) = \begin{bmatrix} f_n^{HH}(\mathbf{x}) & f_n^{HV}(\mathbf{y}) \\ f_n^{VH}(\mathbf{w}) & f_n^{VV}(\mathbf{z}) \end{bmatrix}. \tag{1.21}$$

If a RIS architecture could be developed that is capable of supplying the response shown in (1.21), then each entry of the response matrix becomes independent. Modeling the RIS response means that modelling the entries of the RIS response matrix. The modeling process can be divided into two parts, which are determining

the parameters that the response depends on and expressing each entry of the response matrix as a function of those parameters.

Based on the works already studied in the literature, approaches for modelling the RIS response can be classified into two major groups, which are transmission line models and SEM based models. Transmission line models offer low computational complexity models for overall response, but they do not reflect all the capabilities of the RIS, and they neglect some effects observed on the surface such as high order Floquet harmonics and adjacent cell interference. In general, SEM based models characterize surfaces' response in a more detailed and accurate manner. The downside of using SEM based models is they are computationally complex so that in real-time operation using these models may not be feasible.

1.3.3.1 Transmission line models

Transmission line models are based on the assumption that constitutive parameters of the surface change only in the one direction in the meta-atom. Thus, since the metasurface's thickness is much smaller than the wavelength of the impinging wave and there are no variations in terms of constitutive parameters in one direction, Maxwell's equations are reduced to transmission line equations. This assumption forces the designer to neglect some effects actually observed in the real scenario. For example, RIS can change the polarization of the impinging wave if its phase gradient is sufficiently small [9]. However, transmission line neglects this feature and assumes that the polarization of the impinging wave remains the same. Thus, in the transmission line models, off-diagonal entries of the RIS response matrix becomes zero. Response matrix for transmission line models can be written as

$$\Gamma_n(\mathbf{x}) = \begin{bmatrix} f_n^{HH}(\mathbf{x}) & 0 \\ 0 & f_n^{VV}(\mathbf{x}) \end{bmatrix}. \tag{1.22}$$

Transmission line models express the response of the surface in terms of reflection coefficient of the surface, which is found by using intrinsic parameters of the surface. In general, these parameters are impedances related to surface and control devices. Impedance can be calculated once the inductances, capacitance, and resistance are known for the related cell. And once the impedances are known, the reflection

coefficient can be expressed in terms of equivalent impedance and free space impedance. The equation of reflection coefficient in terms of the impedances is

$$\Gamma = \frac{Z_{eq} - Z_0}{Z_{eq} + Z_0},$$ (1.23)

where Z_0 represents the impedance of the medium that EM waves propagate, and Z_{eq} represents the equivalent impedance of the surface that EM waves impinge. Equivalent impedance depends on both surface parameters such as permeability, susceptibility, dimensions, the geometry of the cell, and properties of an impinging wave such as frequency, polarization, and incidence angle. The equivalent impedance of the RIS cell should be determined by following the proposed transmission line model for the cell. Figure 1.7 shows a transmission line model for a RIS cell.
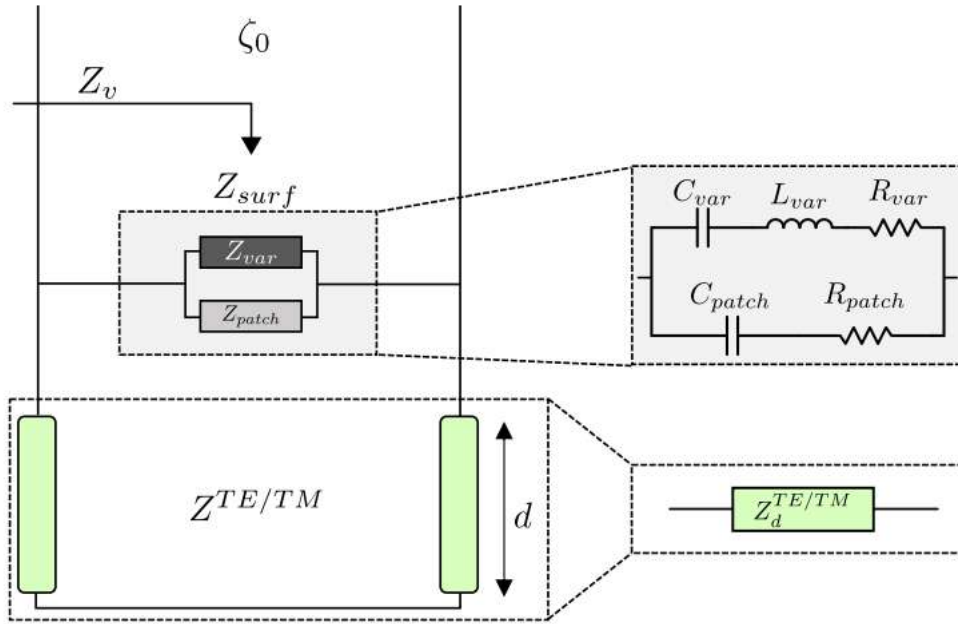
Figure 1.7 : Transmission line model for RIS cell [13].

The impedance of the surface consists of the impedance of the varactor diode and the impedance of the patch. The impedance of the patch is dependent on both materials used to fabricate the surface and the geometry of the patch. For instance, if the patch has rectangular geometry, impedance includes resistive and capacitive terms. If the patch has circular geometry, then the additional inductive term contributes to overall impedance [13]. The term $Z_d^{TE/TM}$ stems from the polarization dependent bulk impedance, which means that this model accounts for polarization. Calculations of

18

equivalent impedance parameters are given in the study. This model also considers the arrival angle of elevation when calculating the impedance. This model will be used in the next sections, thus, detailed explanation for surface impedance parameters will be done later.

One major limitation of using this model is the fact that the formulation for calculating equivalent impedance is valid if there is no high order propagating Floquet harmonics. This condition is satisfied if the following inequality holds:

$$f_0 < \frac{c}{D\left(\sqrt{\varepsilon_r} + \sin\theta^i\right)}. \tag{1.24}$$

In this expression, c denotes the speed of light, D denotes the periodicity of the cells, θ^i denotes the arrival angle of elevation, ε_r denotes the relative electric permittivity of the material and f_0 denotes the frequency of the impinging wave [13].

In this model, patch impedance parameters modeled as independent of arrival angle. However, more detailed models such as [14] consider those parameters as angle dependent parameters. Nonetheless, the more detailed the response modeled, the more computationally complex it becomes. And if extensiveness is crucial in modeling, then SEM based models should be preferred. For the ease of simplicity, in this project the model proposed by [13] is preferred.

1.3.3.2 SEM based models

Surface electromagnetics focuses on the interaction of the EM waves with objects lie in 2D world. As in the transmission line models, if some dimensions are much smaller than the component of the EM wave in that direction, electric and magnetic fields in that direction can be assumed to be constant. In the 2D case, two of the dimensions are comparable with wavelength, but the remaining dimension is much smaller. Hence, Maxwell's equations can be solved in 2D with given boundary conditions and the interaction of the surface with EM waves can be modeled.

As mentioned before, SEM based models represent the surface's interaction in a much more detailed manner, which results in more complicated equations for RIS response. These equations change form with respect to the design of the metasurface. For instance, in [9], different equations are proposed for metafilm, metagrating

and metascreen. Response of the metasurface can be modeled by using different approaches in the SEM based models. There are polarizability based, susceptibility based, and equivalent matrix impedance based models.

Polarizability based models are built upon the relation between the polarizations and the fields that which cause these polarizations. These relations are expressed by using the magnetic, electromagnetic, and magnetoelectric polarizability tensors. These tensors are independent of external fields, they only depend on the properties of inclusions, such as their geometry in the lattice and material properties. However, since metasurfaces consist of dense arrays of inclusions with periodicity smaller than the wavelength, fields inside the medium may be dependent on the inclusion structure. Thus, in polarizability based models, effective polarizability dyadic tensors are used since they also account for the interactions over inclusions in the lattice [9]. Susceptibility based models relate the averaged polarization surface densities to averaged fields on each side of the surface.

Parameters that relate macroscopic fields on a surface can be found by utilizing GSTCs. GSTCs can be thought of as a boundary conditions for solutions of Maxwell's equations over the surface. Once they are properly characterized, electric and magnetic fields over the region of interest can be found. However, their expressions are quite complex in general because metasurfaces are bi-anisotropic mediums. The equations

$$
\mathbf{a}_z \times \boldsymbol{H}\big|_{z=0^-}^{0^+} = j\omega\varepsilon \overleftrightarrow{\chi}_{\text{ES}} \cdot \boldsymbol{E}_{t,\text{av}}\big|_{z=0}
$$
$$
- \mathbf{a}_z \times \nabla_t \left[\chi_{\text{MS}}^{zz} H_{z,\text{av}}\right]_{z=0} \tag{1.25}
$$

and

$$
\boldsymbol{E}\big|_{z=0^-}^{0^+} \times \mathbf{a}_z = j\omega\mu \overleftrightarrow{\chi}_{\text{MS}} \cdot \boldsymbol{H}_{t,\text{av}}\big|_{z=0}
$$
$$
+ \mathbf{a}_z \times \nabla_t \left[\chi_{\text{ES}}^{zz} E_{z,\text{av}}\right]_{z=0} \tag{1.26}
$$

show the GSTCs that relating the electric and magnetic fields on the both sides of a metafilm [15]. These equations are obtained under the assumption of surface susceptibility dyadics are diagonal [15]. These assumptions simplify the equations for GSTCs, since being diagonal implies a certain type of symmetry in the lattice, eliminating the bi-isotropy and bi-anisotropy conditions. Even though very simplifying assumptions have been made, it can be seen that equations that describe GSTCs are yet quite complex.

By using GSTCs, reflection and transmission coefficients of the metasurface can be found. However, in general, these coefficients are quite complex too. The set of equations

$$R_{TE}(\theta) = -\frac{\mathscr{A}\mathscr{B} - k_0^2 \chi_{MS}^{yx} \chi_{MS}^{xy}}{2\left(\mathscr{A}\mathscr{C} + k_0^2 \chi_{MS}^{yx} \chi_{MS}^{xy}\right)} + \frac{\mathscr{E}\mathscr{N} - k_0^2 \chi_{ES}^{yx} \chi_{ES}^{xy}}{2\left(\mathscr{D}\mathscr{E} + k_0^2 \chi_{ES}^{yx} \chi_{ES}^{xy}\right)},$$

$$T_{TE}(\theta) = \frac{\mathscr{A}\mathscr{B} - k_0^2 \chi_{MS}^{yx} \chi_{MS}^{xy}}{2\left(\mathscr{A}\mathscr{C} + k_0^2 \chi_{MS}^{yx} \chi_{MS}^{xy}\right)} + \frac{\mathscr{E}\mathscr{N} - k_0^2 \chi_{ES}^{yx} \chi_{ES}^{xy}}{2\left(\mathscr{D}\mathscr{E} + k_0^2 \chi_{ES}^{yx} \chi_{ES}^{xy}\right)},$$

$$R_{TE}^{TM}(\theta) = -\frac{jk_0 \chi_{MS}^{yx}(\mathscr{B} - \mathscr{C})}{2\left(\mathscr{A}\mathscr{C} + k_0^2 \chi_{MS}^{yx} \chi_{MS}^{xy}\right)} + \frac{jk_0 \chi_{ES}^{xy}(\mathscr{N} - \mathscr{D})}{2\left(\mathscr{D}\mathscr{E} + k_0^2 \chi_{ES}^{yx} \chi_{ES}^{xy}\right)},$$

$$T_{TE}^{TM}(\theta) = \frac{jk_0 \chi_{MS}^{yx}(\mathscr{B} - \mathscr{C})}{2\left(\mathscr{A}\mathscr{C} + k_0^2 \chi_{MS}^{yx} \chi_{MS}^{xy}\right)} + \frac{jk_0 \chi_{ES}^{xy}(\mathscr{N} - \mathscr{D})}{2\left(\mathscr{D}\mathscr{E} + k_0^2 \chi_{ES}^{yx} \chi_{ES}^{xy}\right)}, \qquad \textbf{(1.27)}$$

$$\mathscr{A} = 2 + \frac{jk_0}{\cos\theta}\chi_{MS}^{yy} + \frac{jk_0}{\cos\theta}\chi_{ES}^{zz}\sin^2\theta; \mathscr{B} = 2 - jk_0\chi_{MS}^{xx}\cos\theta,$$

$$\mathscr{N} = 2 - \frac{jk_0}{\cos\theta}\chi_{ES}^{yy} - \frac{jk_0}{\cos\theta}\chi_{MS}^{zz}\sin^2\theta; \mathscr{E} = 2 + jk_0\chi_{ES}^{xx}\cos\theta,$$

$$\mathscr{D} = 2 + \frac{jk_0}{\cos\theta}\chi_{ES}^{yy} + \frac{jk_0}{\cos\theta}\chi_{MS}^{zz}\sin^2\theta; \mathscr{C} = 2 + jk_0\chi_{MS}^{xx}\cos\theta$$

show the reflection and transmission coefficients of the metafilm, for different polarizations and cross polarization reflections [9]. Unlike the transmission line models, in these models cross polarization reflections are also considered, which shows that SEM based models are more detailed. Nonetheless, by comparing the equations for reflection coefficients, it can be seen that SEM based models produce more complicated results than the transmission line models.

Another problem with the SEM based models is the fact that expression of the tunable parameters are more complex compared to transmission line models. In transmission line models, by altering the impedance of the tuning circuit, surface impedances are adjusted. However, in SEM based models, control elements change the surface polarizability or susceptibility tensors. The effect of the control elements over these tensors should be modeled separately.

Since SEM based models are more complex compared to transmission line models, and since it is not known how the control elements in the RIS device change the polarizability or susceptibility tensors, transmission line models are used to model RIS response in the senior design project.

1.4 RIS Assisted Wireless Channel

The RIS-assisted wireless channel consists of two main parts, which are mmWave clustered stochastic channel and RIS response. Stochastic channel parameters are generated by following the model proposed by [16] and these parameters model the channel excluding the RIS response. By appropriately modeling of those two parts and combining them in one equation, one can obtain an end-to-end physical channel model for RIS-assisted wireless systems. In the following sections, generation of the stochastic channel parameters and modeling of RIS response are explained.

1.4.1 Overall Channel Models and Existing Researches

Since the nature of the wireless channel is quite complex, it is not always possible to consider all parameters in the RIS assisted wireless channel model. Thus, existing models in the literature for these channels vary with respect to the scope of the study.

1.4.1.1 Hypothetical RIS-assisted channel model

Firstly, when RIS has emerged as a potential technology in wireless communication, preliminary and basic models are introduced to demonstrate the effects of RIS utilization in the wireless channel. These models were too idealized. Study [17] is an example of these models. In this study, RIS is used as an access point when there is no LOS channel between the transmitter and receiver. Figure 1.8 shows the setup for a proposed model, where S denotes the transmitter antenna, D denotes the receiver antenna, and h_i, g_i denotes the channel coefficients between transmitter and i^{th} element of the RIS, receiver and i^{th} element of the RIS, respectively. These channel coefficients are complex numbers that represent total attenuation and phase shift. They are modeled as complex Gaussian random variables with zero mean and unit variance.

In this study, RIS both creates a channel between transmitter and receiver, and it eliminates the phase mismatches on the receiver side by applying certain wave transformations with unit gain. Thus, RIS also mitigates the effect of multipath fading. As a result, the overall channel can be modeled as

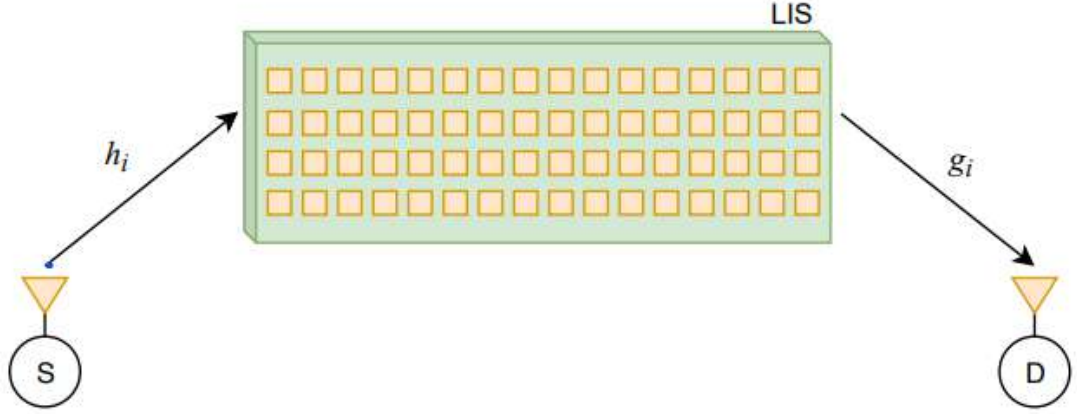$$r = \left[\sum_{i=1}^{N} h_i e^{j\phi_i} g_i\right] x + n. \tag{1.28}$$

Figure 1.8 : Access point RIS setup [17].

where r represents the received signal, x represents the transmitted signal, index i stands for the ith multipath component of the transmitted signal, N represents the total number of RIS elements, and n represents the additive noise. The term $e^{j\phi_i}$ stems from the phase adjustment that RIS applied to the ith multipath component. Phase adjustment provided by RIS is given by

$$\phi_i = -arg(h_i) - arg(g_i) \tag{1.29}$$

where *arg* is a function that returns the phase of the input. As a result of this adjustment, the received signal r can be expressed as

$$r = \left[\sum_{i=1}^{N} |h_i||g_i| \right] x + n. \tag{1.30}$$

It is obvious that the phase adjustment provided by RIS increases the received power. Thus, SNR increases and BER decreases. Figure 1.9 demonstrates the effect of the RIS on the BER performance under AWGN channel [17]. It is observed that with increased number of RIS elements, BER performance advances since transmitted power increases.

This study shows that RIS utilization in wireless channel can be exploited for getting better BER performances, or for providing communication under blocked LOS conditions. However, the channel model used for simulations in this model is oversimplified and neglects significant amount of parameters. Also, it is assumed
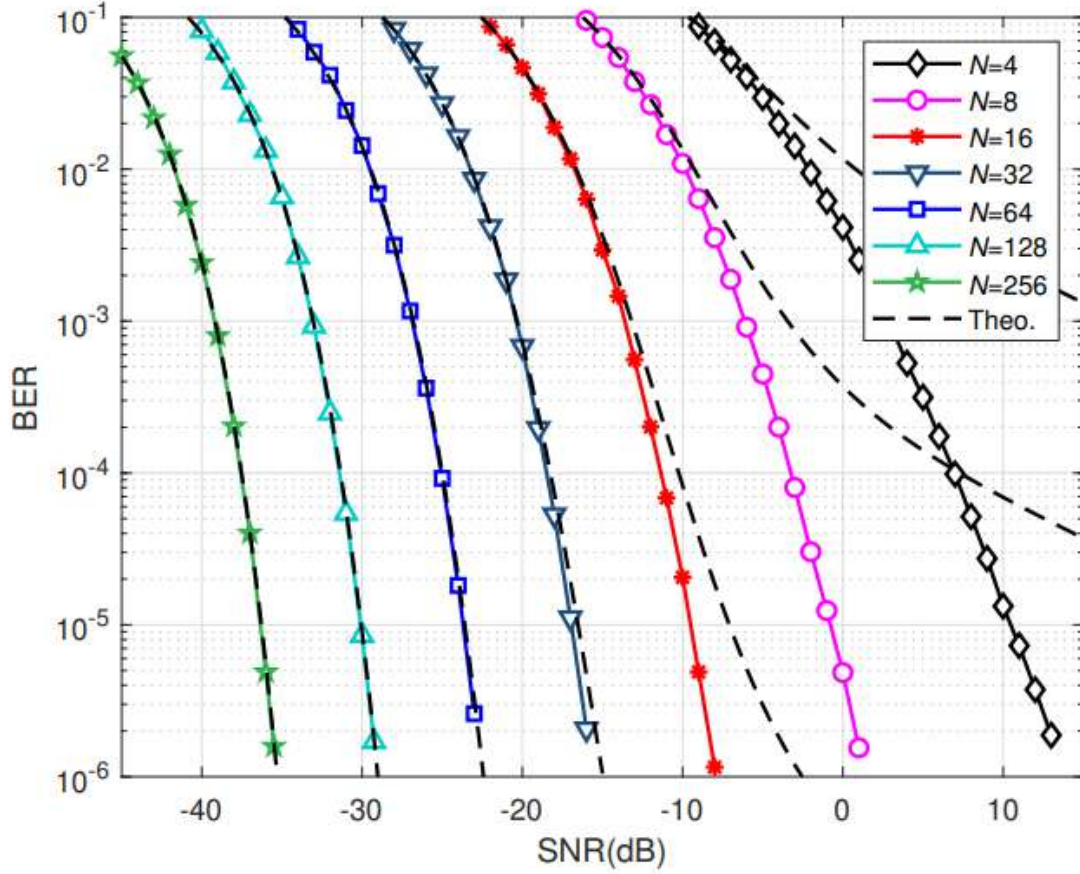
Figure 1.9 : BER performance of the system with increasing number of RIS elements [17].

that RIS can cancel all the phase mismatches without any error and with no power loss. RIS response used in this study is ideal, which is not applicable in reality because of physical constraints. Finally, random variables that model the channel coefficients in this study are complex Gaussian distributed. However, in practice, the distribution of those complex parameters is not complex Gaussian. The distribution of those parameters are studied in [18] and it has been shown by the authors that the distribution of those parameters does not fit complex Gaussian. More realistic channel models should consider more detailed process of generating random variables for channel. Path loss, shadowing, and multipath fading should be modeled for different scenarios and physical parameters such as radiation pattern of transceiver antennas, distribution of elevation angle of arrival.

1.4.1.2 Physical sub 6GHz channel model

A little further extensive modelling approach is considered in [19]. This model incorporates a scattering environment in the sub 6GHz band. Also, it contains generation of statistical parameters for angle of arrival, angle of departure, cluster powers, path loss, and shadowing. Moreover, this model includes physical parameters such as radiation pattern of RIS cells and array response vector of the overall surface. End-to-end channel setup is illustrated in the Figure 1.10 where RIS is placed on the xz-plane. From Figure 1.10, it can be seen that there are both direct and indirect paths between channels. However, this was not the case in [17] which has only direct paths between the channels. Therefore, this model is a little further extensive than [17].
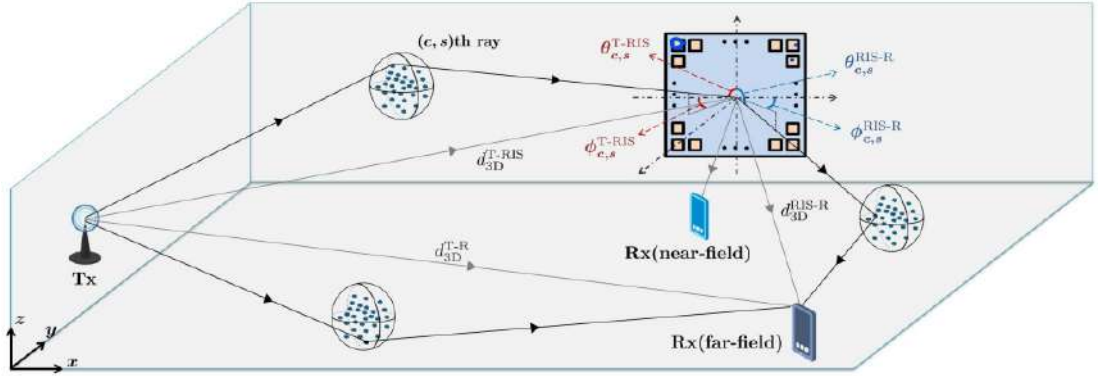
Figure 1.10 : Sub 6GHz channel setup [19].

The channel equation incorporating the scatterers, radiation patterns, array response vectors, and the RIS response is given in vector form as

$$y = \sqrt{P_t}\left(\mathbf{g}^{\mathrm{T}}\boldsymbol{\Theta}\mathbf{h} + h_{\mathrm{SISO}}\right)s + w \qquad (1.31)$$

where P_t is the transmitted signal's power, $\mathbf{h}$ and $\mathbf{g}$ are the channel vectors between RIS and transmitter, RIS and receiver, respectively. $\boldsymbol{\Theta}$ is a matrix of responses of every RIS element in diagonal entries; namely, $\boldsymbol{\Theta} = \mathrm{diag}\left(\beta_1 e^{j\alpha_1}, \cdots, \beta_N e^{j\alpha_N}\right)$. w is a complex Gaussian noise with zero mean. y is the complex envelope of the received signal and s is the complex envelope of the transmitted signal. Finally, h_{SISO} is the scalar channel between transmitter and receiver, it consists of the sum of all LOS and NLOS components that propagated directly towards the receiver.

The equations for the channel between transmitter-RIS and transmitter-receiver can be written respectively as

$$\mathbf{h} = \sum_{c=1}^{C} \sum_{s=1}^{S} \sqrt{\frac{P_c}{S}} \sqrt{\frac{G_e\left(\theta_{c,s}^{\text{T-RIS}}\right)}{P_L}} e^{j\Phi_{c,s}} \mathbf{a}\left(\theta_{c,s}^{\text{T-RIS}}, \phi_{c,s}^{\text{T-RIS}}\right), \qquad \textbf{(1.32)}$$

$$h_{\text{SISO}} = \sum_{c=1}^{C} \sum_{s=1}^{S} \sqrt{\frac{P_c}{S}} \sqrt{\frac{1}{P_L}} e^{j\Phi_{c,s}} \qquad \textbf{(1.33)}$$

where C is the number of clusters in the environment, S is the number of scatterers per cluster, P_c is the cluster power, $G_e\left(\theta_{c,s}^{\text{T-RIS}}\right)$ is the radiation gain of the RIS in the direction of $\theta_{c,s}^{\text{T-RIS}}$ which is the angle of zenith from $(c,s)^{th}$ path to the receiver, P_L is the path loss component whose equations are given in [19], $\Phi_{c,s}$ is the random initial phase, and finally $\mathbf{a}(\theta_{c,s}^{\text{T-RIS}}, \phi_{c,s}^{\text{T-RIS}})$ is the array response vector calculated for the zenith angle $\theta_{c,s}^{\text{T-RIS}}$ and azimuth angle $\Phi_{c,s}^{\text{T-RIS}}$.

One of the important distinctions presented in this study is the dependency of the generation of the RIS—receiver channel on the placement of the setup. If far-field channel conditions are valid, then receiver RIS channel is generated in the same way as RIS—transmitter channel. However, if near channel conditions are valid, then the equation for the RIS-receiver channel drastically changes. Channel equation in the near-field condition is shown as

$$|g_n|^2 \approx \frac{1}{4\pi} \sum_{x \in \mathbb{X}} \sum_{z \in \mathbb{Z}} \left(\frac{\frac{xz}{y^2}}{3\left(\frac{z^2}{y^2}+1\right)\sqrt{\frac{x^2}{z^2}+\frac{z^2}{y^2}+1}} + \frac{2}{3}\tan^{-1}\left(\frac{\frac{xz}{y^2}}{\sqrt{\frac{x^2}{y^2}+\frac{z^2}{y^2}+1}}\right) \right) \qquad \textbf{(1.34)}$$

where $\mathbb{X} = \left\{d/2+x^n-x^{\text{Rx}}, d/2+x^{\text{Rx}}-x^n\right\}, \mathbb{Z} = \left\{d/2+z^n-z^{\text{Rx}}, d/2+z^{\text{Rx}}-z^n\right\}$, and $y = \left|y^n - y^{\text{Rx}}\right|$. The phase of g_n can be calculated as follows:

$$\gamma = 2\pi \bmod \left(\frac{\left\|\mathbf{r}^n - \mathbf{r}^{\text{Rx}}\right\|}{\lambda}, 1 \right) \qquad \textbf{(1.35)}$$

where $\mathbf{r}^n$ is the position vector of the nth cell of RIS, $\mathbf{r}^{Rx}$ is the position vector of the receiver, and λ is the wavelength.

In [19], it has been shown that RIS utilization in the wireless channel increases the achievable rate. Figure 1.11 shows that, with the increasing number of RIS elements, achievable rate increases. The effect of the height of the RIS can also be seen.

Compared to [17], the channel model for sub 6GHz band in this study considers the random parameters that determine the channel behavior in a more detailed manner. Also, physical parameters such as radiation pattern, angle distributions, and array response vector are introduced. Thus, this study is more realistic. Random variables used in this study defined by considering their dependency on the environment and operating frequency. So, instead of modelling the channel coefficients by using a selecting single random variable, such as in [17], they are modeled as functions of several random variables. Thus, this modelling approach is more suitable for modelling realistic cases. However, this approach still neglected some of the parameters that should be considered. For example, polarization of the impinging waves is not mentioned, it is assumed that all clusters are common, RIS response assumed to be ideal, and LOS probabilities are assumed to be unity, although it is not the case in real-life applications. The radiation pattern of the transceivers is also not considered. In addition to all these simplifications, there is also frequency restriction to the higher data rates since it operates under the 6GHz band.

1.4.1.3 More realistic channel model

In [20], the channel model proposed in [19] enhanced by integrating more physical parameters, which are determinant in practical scenarios. In this model, LOS probabilities in all channels, a more general formula for different clusters, amount of scatterers per cluster, distribution of the clusters have been proposed. Also, the effect of positioning on the system performance, and the correlation between channel coefficients have been emphasized. Figure 1.12 illustrates the placement of the RIS in the proposed model.

It is similar to the channel used in sub 6GHz model. The difference is there is no cluster between RIS and the receiver. In [20], it is stated that if the distance between the RIS and receiver becomes smaller than a certain value, the LOS component dominates the overall channel. Thus, NLOS components can be neglected and RIS-receiver channel can be simplified. The distance that provides LOS dominated
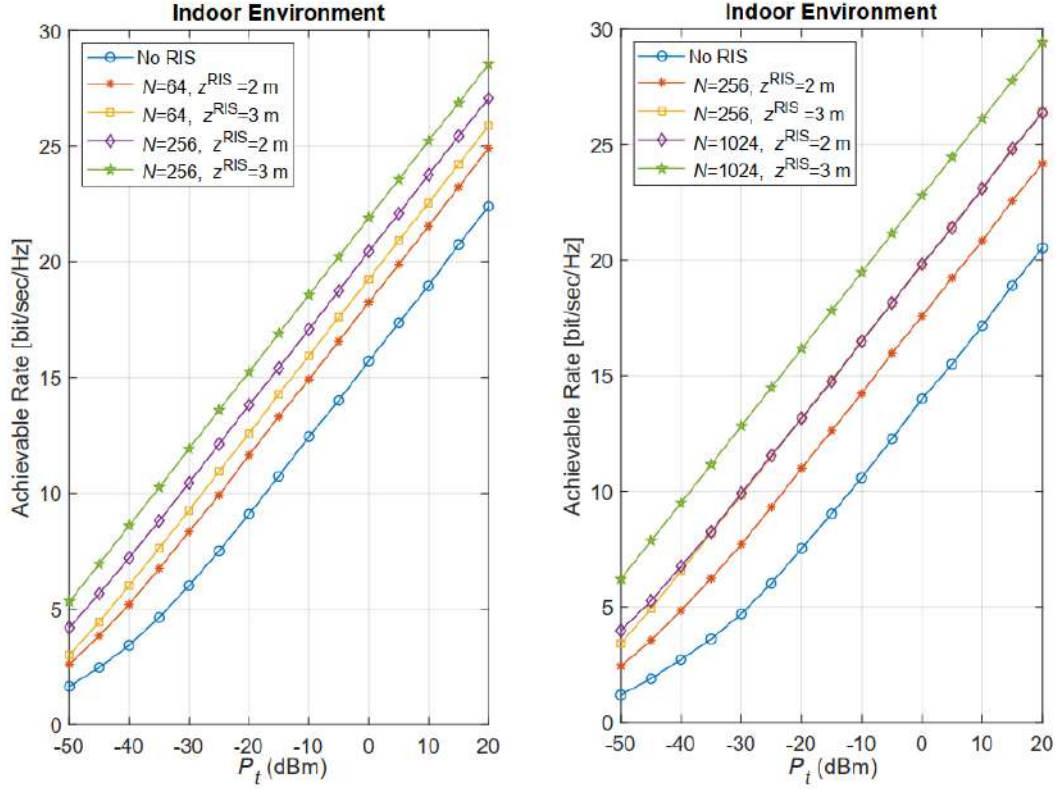
Figure 1.11 : Achievable rate analysis in the indoor environment for different numbers of RIS cells [19].

channel conditions is determined as the distance where LOS probability becomes greater than 50%. Note that, LOS probability is defined as a random variable which is a function of the distance. In this model, the overall channel model is the same as in [19] and it is represented by using equation (1.31). However, the expression of the channel coefficients in terms of channel parameters has been updated under the novel considerations. One of the significant aspects of this study is proposed channel models are placement dependent. For example, if RIS placed near to receiver, they may experience common clusters and therefore better performances. Consequently, the existence of shared clusters, LOS dominated channels cause changes in the overall channel model.

A random variable that defines RIS-transmitter channel behavior is given as

$$\mathbf{h} = \gamma \sum_{c=1}^{C} \sum_{s=1}^{S_c} \beta_{c,s} \sqrt{G_e \left(\theta_{c,s}^{\mathrm{RIS}} \right) L_{\mathrm{T-RIS}}} \mathbf{a} \left(\phi_{c,s}^{\mathrm{RIS}}, \theta_{c,s}^{\mathrm{RIS}} \right) + \mathbf{h}_{\mathrm{LOS}} \qquad \textbf{(1.36)}$$
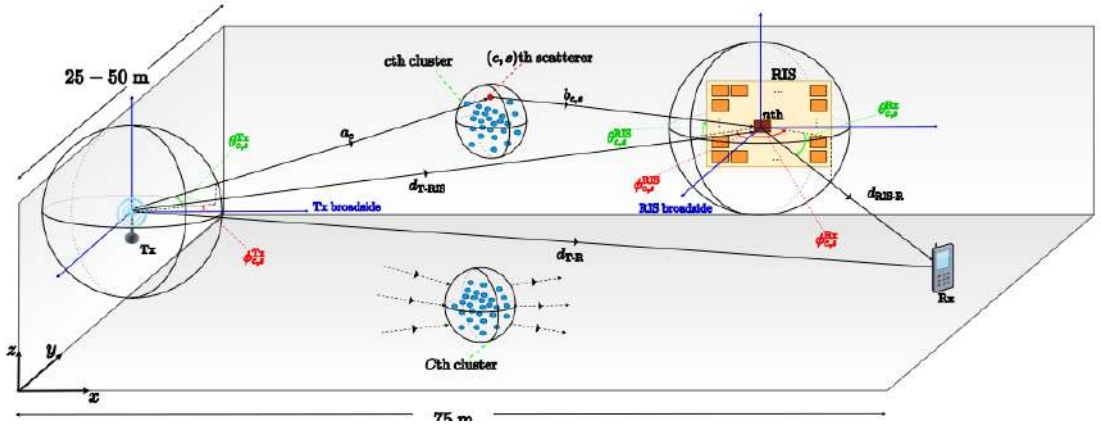
Figure 1.12 : RIS setup in channel model [20].

where $\gamma = \sqrt{\frac{1}{\sum_{c=1}^{C} S_c}}$ is a parameter coming from the assumption that cluster powers are uniformly distributed, C is the number of clusters and whose distribution is $C \sim \mathscr{P}(\lambda_p)$ where λ_p is the environment dependent Poisson rate, S_c is the number of scatterers contained in the cluster c whose distribution is $S_c \sim \mathscr{U}[1,30]$, $\beta_{c,s} \sim \mathscr{CN}(0,1)$ is the complex path gain, $G_e(.)$ is the radiation pattern of an RIS element, $L_{\text{T-RIS}}$ is the path loss of the ray propagating transmitter-csth scatterer-RIS, $\mathbf{a}(.,.)$ is the array response vector of RIS, $\theta_{c,s}^{\text{RIS}}$ and $\phi_{c,s}^{\text{RIS}}$ are the azimuth and zenith angle of arrival from csth scatterer to RIS, respectively, and h_{LOS} describes the LOS channel coefficient of the transmitter-RIS channel whose equation given as

$$\mathbf{h}_{\text{LOS}} = I_{\mathbf{h}}(d_{\text{T-RIS}}) \sqrt{G_e\left(\theta_{\text{LOS}}^{\text{RIS}}\right) L_{\text{T-RIS}}} e^{j\eta} \mathbf{a}\left(\phi_{\text{LOS}}^{\text{RIS}}, \theta_{\text{LOS}}^{\text{RIS}}\right) \qquad \textbf{(1.37)}$$

where $e^{j\eta}$ is a random variable that describes the phase shift in the LOS channel. Since the proposed model considers the operation in high frequency ranges, such as mmWave band, small variation in the distance taken for the ray may cause large phase shifts. Thus, even though the LOS channel is deterministic except for LOS probability, phase shift is defined by using a uniform random variable $\eta \sim \mathscr{U}[0,2\pi]$. $I_{\mathbf{h}}(d_{\text{T-RIS}})$ is a Bernoulli random variable that takes the values 0 or 1, with the PMF given in equations (1.38) and (1.39) depending on the environment. The remaining parameters of the LOS channel are deterministic, since there is nothing random in the direct path between transmitter and RIS.

LOS probabilities are defined depending on the environment and depending on the distance. For example, LOS probability for indoor environment is given as

$$p = \begin{cases} 1 & d_{\text{T-RIS}} \leq 1.2 \\ e^{-\left(\frac{d_{\text{T-RIS}} - 1.2}{4.7}\right)} & 1.2 < d_{\text{T-RIS}} \leq 6.5 \\ 0.32 e^{-\left(\frac{d_{\text{T-RIS}} - 6.5}{32.6}\right)} & d_{\text{T-RIS}} > 6.5. \end{cases} \tag{1.38}$$

where $d_{\text{T-RIS}}$ represents the distance between transmitter and the center of RIS and LOS probability for the outdoor environment is given as

$$p = \min(20/d, 1)\left(1 - e^{-d/39}\right) + e^{-d/39} \tag{1.39}$$

where d is the distance that is particularly interested. These LOS probabilities are one of the deviating points in the model from [19]. Generation of remaining random parameters such as angles, positions of scatterers, and shadowing are explained in [20]. RIS-receiver channel g is generated as h channel. However, if the g channel is LOS dominated, NLOS components can be neglected and the channel equation reduces to

$$\mathbf{g} = \sqrt{G_e\left(\theta_{\text{Rx}}^{\text{RIS}}\right) L_{\text{RIS-R}}} e^{j\eta} \mathbf{a}\left(\phi_{\text{Rx}}^{\text{RIS}}, \theta_{\text{Rx}}^{\text{RIS}}\right). \tag{1.40}$$

Generation of the g_{LOS} channel is also similar to generation of h_{LOS}. The direct channel between transmitter and receiver is, h_{SISO} and it is generated similar to LOS channels in RIS- transceiver channels. The equation of the SISO channel is given as

$$h_{\text{SISO}} = \tilde{\gamma} \sum_{c=1}^{\tilde{C}} \sum_{s=1}^{\tilde{S}_c} \tilde{\beta}_{c,s} \sqrt{L_{\text{SISO}}} + h_{\text{LOS}}. \tag{1.41}$$

By omitting the parameters that stem from RIS deployment in LOS channels, one can obtain SISO channel equation. $\tilde{\gamma}$ is the normalization constant of the SISO channel, and it is calculated as in the h channel equation. The number of clusters and the amount of scatterer per cluster is different from h channel, which implies that those two channels possess different clusters. This difference is denoted by adding the tilde on top of the relevant parameters in SISO channel. Finally, it should be noted that, since it is beneficial to place receiver and RIS close, SISO channel and RIS-receiver channel can possess common clusters.

It has been mentioned that, existence of LOS channels is probabilistic and the contribution of LOS parameters cannot be neglected. For example, quite different achievable rate results can be obtained depending on the existence of LOS channel; therefore, the relative positions of transceivers and RIS are quite important. Figure 1.13 is self-explanatory graphics from [20] that show how great the effect of position can be on the achievable rate. For example, in Figure 1.13 the x and y coordinates of the receiver are changed in a specified interval and the effect of that on the achievable rate is observed. It can be easily seen that the existence of direct link, which is another probabilistic channel, fluctuates and increases the achievable rate considerably.
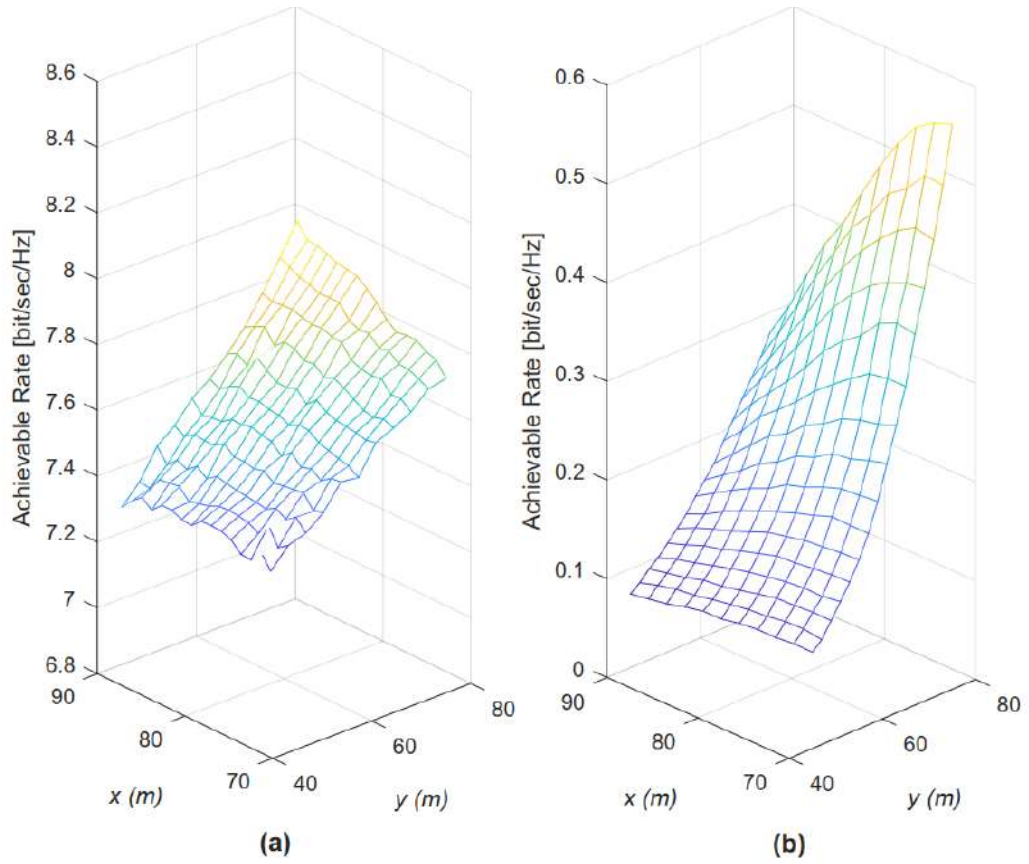
Figure 1.13 : Achievable rate in outdoor environment by varying receiver position with direct link **a** and without direct link **b** [20].

Figure 1.14 shows the effect of the RIS on achievable rate. As it can be seen from the figure, increase in the RIS elements results in an increase in the achievable rate. Also, for different positioning can be observed by comparing the adjacent graphics. Scenario 1 and scenario 2 represent different positioning cases in an indoor hotspot environment. For scenario 1, higher achievable rates are observed where RIS is placed

in xz-plane. Finally, the effect of height on achievable rate is observed too. Since the height of RIS is an important parameter in LOS probability, it affects the achievable rate. The LOS probability decreases immensely if the receiver placed up of the relative to the signal source.
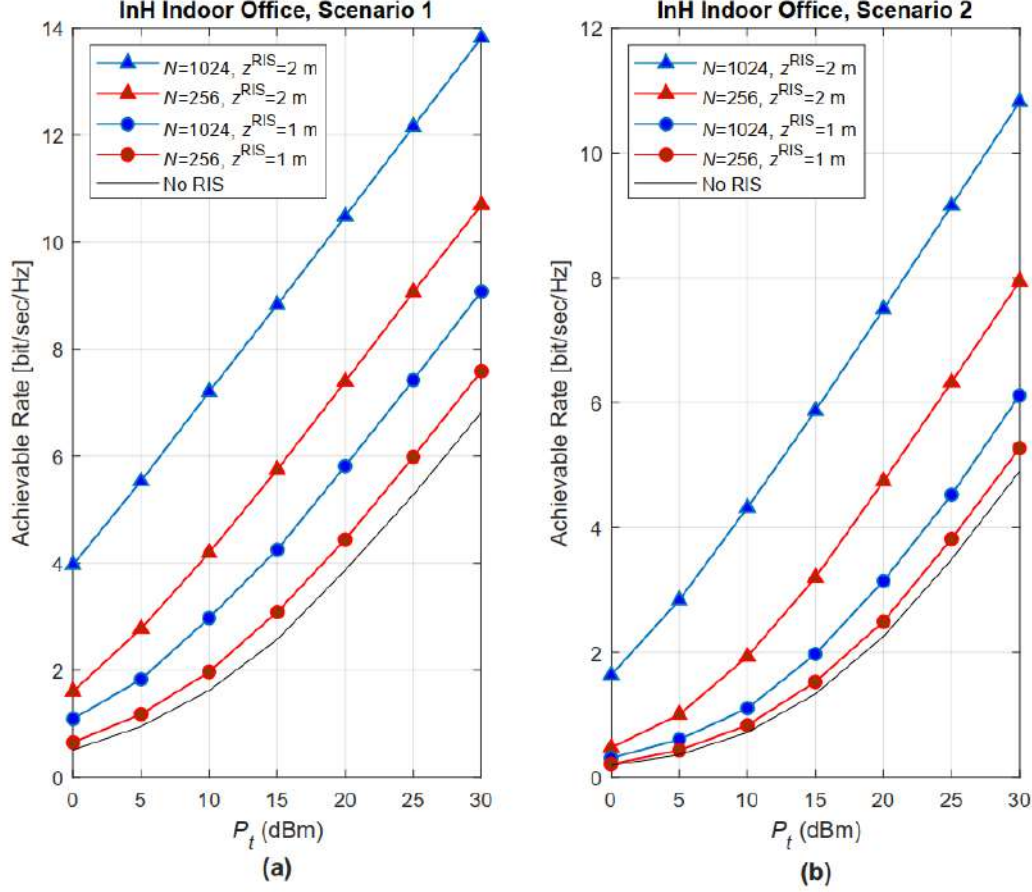
Figure 1.14 : Achievable rate in indoor environment for different N by varying P_t for Scenario 1 **a** and Scenario 2 **b** [20].

The model proposed in [20] considers a significant amount of parameters that is apparent in physical considerations. Also, this model is highly adaptive since its parameters are all environment dependent. However, RIS response is still modeled as a diagonal matrix, and it is assumed to be ideal. Cluster powers are assumed to be equidistributed among all clusters. Polarizations and transceiver antenna radiation patterns are neglected. Even though it is more descriptive and realistic compared to [19] study, there are still parameters required to be included in the model. Thus, by considering these requirements, it is proposed a novel channel model for RIS-assisted wireless links. The proposed model is explained in detail in the second chapter.

2. PROPOSED CHANNEL MODEL

Proposed channel models for RIS-assisted wireless communication links should include both an extensive model for the stochastic wireless channel and EM response of the RIS for reflecting the realistic channel end-to-end channel characteristics. In this section, an end-to-end channel model, which considers the both, is proposed. The model includes transmission line model of RIS elements and physical channel parameters such as antenna radiation patterns, polarizations. The general form of the proposed channel model, incorporating the polarizations, antenna radiation patterns, and the transmission line model of the RIS cells is shown as

$$H = \sum_{n=1}^{N} \sum_{c=1}^{C} \sum_{s=1}^{S_c} \sum_{k=1}^{\bar{C}} \sum_{l=1}^{\bar{S}_c} \mathbf{h_{n,c,s}^{NLOS}} \Theta_{n,c,s,k,l} \mathbf{g_{n,k,l}^{NLOS}} + \sum_{n=1}^{N} \mathbf{h_n^{LOS}} \Theta_n^{LOS} \mathbf{g_n^{LOS}} + h_{SISO} \qquad (2.1)$$

where $\mathbf{h_{n,c,s}}$ is the transmitter to nth RIS element complex 1-by-2 gain vector of c,sth scatterer, $\Theta_{n,c,s,k,l}$ is the response of nth cell to c,s th scatterer, and $\mathbf{g_{n,c,s}}$ is the complex 1-by-2 gain vector of c,sth scatterer from nth cell to receiver. These complex channel vectors will be explained in detail in the following subsections.

2.1 Electromagnetic Response of the RIS

The transmission line model that is used for modelling the RIS response is based on the study [13] where EM response of each cell is represented as a 2-by-2 matrix whose off-diagonal entries as zero, as shown in equation (1.22). The only difference of proposed response here with [13] is that the RIS response is assumed to be controlled by adjusting the impedance of each cell instead of adjusting the voltage of the capacitor to alter the capacitance of the control element. The angle of arrival dependent RIS element response that is used in the proposed model can be written as

$$\Theta_n(\theta, Z_{con,n}) = \begin{bmatrix} \Theta_n^{TE}(\theta, Z_{con,n}) & 0 \\ 0 & \Theta_n^{TM}(\theta, Z_{con,n}) \end{bmatrix} \qquad (2.2)$$

which shows the response of the nth element of the RIS. This matrix valued function takes two parameters as input arguments, which are tunable control impedance and the arrival angle of zenith of the impinging wave. Controllable impedance adjusts the RIS response, and it is deterministic. However, the arrival angle of zenith is probabilistic and in the overall channel model, it is modeled as a random variable. The first diagonal entry of the response matrix models the response given to the TE polarized waves, and the second diagonal entry models the response given to the TM polarized waves. It should be noted that responses for different polarizations can be controlled independently if proper RIS architecture is used. However, in this model, both responses are controlled by the same control element. Evaluation of these responses can be determined by

$$\Theta_n^{TE/TM}(\theta, Z_{con,n}) = \frac{Z_v^{TE/TM}(\theta, Z_{con,n}) - \eta_0}{Z_v^{TE/TM}(\theta, Z_{con,n}) + \eta_0} \tag{2.3}$$

which is used for the finding reflection coefficients for the impinging wave. η_0 is the impedance of the medium that impinging EM waves propagate. The calculation of $Z_v^{TE/TM}$ is represented as

$$Z_v^{TE/TM}(\theta, Z_{con,n}) = Z_{\text{surf}}^{TE/TM}(\theta, Z_{con,n}) \| Z_d^{TE/TM}(\theta) \tag{2.4}$$

where $Z_d^{TE/TM}$ stems from the impedance of the substrate that parallel with the propagation direction of the impinging wave. It is assumed that this direction is the z-direction. Also, $Z_d^{TE/TM}$ is dependent on the incidence angle of the incoming wave. $Z_d^{TE/TM}$ is calculated by

$$Z_d^{TE/TM} = jZ^{TE/TM} \tan(k_z d) \tag{2.5}$$

where $Z^{TE} = \frac{\omega\mu}{k_z}$; $Z^{TM} = \frac{k_z}{\omega\varepsilon_0\varepsilon_r}$ and k_z is the wave number of the impinging wave in the direction of z. It is calculated as $k_z = k_0\sqrt{\varepsilon_r - \sin^2\theta}$. Thus, angle dependency in Z_d stems from the k_z. Other parameters used in calculation of Z_d are, angular frequency (w), magnetic permeability (μ) of the medium, vacuum permittivity (ε_0), relative permittivity (ε_r), and the thickness of the bulky medium (d).

The surface impedance $Z_{\text{surf}}^{TE/TM}$ consists of two parameters, which are control device impedance and the patch impedance. Formulation of control device impedance may change with respect to the device used to tune of cell response. Thus, it is remained as a variable itself. Patch impedance is dependent on the design of the surface. The material properties of the patch and the geometry of the cell. For instance, if a cell is loop shaped, then it has an inductive parameter, if the cell is in rectangular shape, then the inductive parameter vanishes. The surface impedance for nth cell can be calculated as

$$Z_{\text{surf}}^{TE/TM} = Z_{\text{con,n}} \,\|\, Z_{\text{patch}}^{\text{TE/TM}} . \tag{2.6}$$

In the proposed model, it is assumed that the cells have square shape. Thus, patch impedance includes resistive and capacitive components. The resistance and the capacitance of the patch can be calculated respectively as

$$R_{\text{patch}} = \left(\frac{D}{D-w}\right)^2 \frac{1}{\delta \sigma_c}, \quad \delta = \frac{2}{\sqrt{\sigma_c w \mu_0}}, \tag{2.7}$$

$$C_{\text{patch}}^{\text{TE/TM}} = \begin{cases} \frac{-2D_y \varepsilon_{eff} \varepsilon_0}{\pi} \cdot \ln\left(\sin\left(\frac{\pi W_y}{2D_y}\right)\right)\left(1 - \frac{k_0}{k_{eff}} \cdot \frac{\sin^2 \theta_t}{2}\right), TE \\ -\frac{2D_x \varepsilon_{eff} \cdot \varepsilon_0}{\pi} \cdot \ln\left(\sin\left(\frac{\pi W_x}{2D_x}\right)\right), TM \end{cases} . \tag{2.8}$$

Parameters used in patch capacitance and resistance calculations are, conductivity of the patch (σ_c), loss tangent (δ), vacuum permeability (μ_0), angular frequency w, periodicity of the patch in the x and y directions (D_x, D_y), vacuum permittivity (ε_0), wave number of the propagating wave (k_0), gap between the cells (W_x, W_y), effective permittivity of the medium (ε_{eff}), and the effective wave number of the wave in the uniform host media (k_{eff}). Effective permittivity is calculated as $\varepsilon_{eff} = (1 + \varepsilon_r)/2$. With the aid of the equations (2.7) and (2.8), the impedance of the patch can be calculated as

$$Z_{\text{patch}}^{\text{TE/TM}} = R_{\text{patch}} + \frac{1}{j\omega C_{\text{patch}}^{TE/TM}} . \tag{2.9}$$

By using the impedance values for TE and TM polarized waves, elements of the response matrix can be calculated by following steps

$$Z_{\text{surf}}^{\text{TE/TM}} = \frac{Z_{\text{con}}\, Z_{\text{patch}}^{\text{TE/TM}}}{Z_{\text{con}} + Z_{\text{patch}}^{\text{TE/TM}}} \tag{2.10}$$

$$= \frac{Z_d^{TE/TM} \cdot Z_{\text{patch}}^{TE/TM} \cdot Z_{con}}{Z_d^{TE/TM}\left(Z_{con} + Z_{\text{patch}}^{TE/TM}\right) + Z_{con} \cdot Z_{patch}^{TE/TM}} \tag{2.11}$$

$$Z_d^{TE/TM} \cdot Z_{patch}^{TE/TM} = Z_\pi^{TE/TM} \tag{2.12}$$

$$Z_d^{TE/TM} + Z_{\text{patch}}^{TE/TM} = Z_\Sigma^{TE/TM} \tag{2.13}$$

$$\frac{Z_\Sigma^{TE/TM}}{Z_\pi^{TE/TM}} = \gamma^{TE/TM} \tag{2.14}$$

$$Z_v = \frac{Z_\pi^{TE/TM} Z_{con}}{Z_\pi^{TE/TM} + Z_\Sigma^{TE/TM} Z_{con}} = \frac{Z_{con}}{1 + \gamma^{TE/TM} \cdot Z_{con}} \tag{2.15}$$

$$\Theta_n^{TE/TM} = \frac{Z_v - \eta_0}{Z_v + \eta_0} = \frac{\frac{Z_{con,n}}{1+\gamma^{TE/TM} \cdot Z_{con,n}} - \eta_0}{\frac{Z_{con,n}}{1+\gamma^{TE/TM} Z_{con,n}} + \eta_0} \tag{2.16}$$

$$= \frac{Z_{con,n} - \eta_0 \gamma^{TE/TM} Z_{con,n} - \eta_0}{Z_{con,n} + \eta_0 \gamma^{TE/TM} Z_{con,n} + \eta_0} \tag{2.17}$$

$$\eta_0 \gamma^{TE/TM} = \eta^{TE/TM} \tag{2.18}$$

$$\Theta_n^{TE/TM} = \frac{Z_{con,n}\left(1 - \eta^{TE/TM}\right) - \eta_0}{Z_{con,n}\left(1 + \eta^{TE/TM}\right) + \eta_0}. \tag{2.19}$$

Thus, the response of the nth cell of the RIS to the csth ray can be written as

$$\Theta_n(\theta_{c,s}, Z_{con,n}) = \begin{bmatrix} \frac{Z_{con,n}\left(1 - \eta^{TE}(\theta_{c,s})\right) - \eta_0}{Z_{con,n}\left(1 + \eta^{TE}(\theta_{c,s})\right) + \eta_0} & 0 \\ 0 & \frac{Z_{con,n}\left(1 - \eta^{TM}(\theta_{c,s})\right) - \eta_0}{Z_{con,n}\left(1 + \eta^{TM}(\theta_{c,s})\right) + \eta_0} \end{bmatrix}. \tag{2.20}$$

In the proposed channel model equation, in order to simplify notation, RIS response is written as $\Theta_{n,c,s,k,l}$ for NLOS and Θ_n^{LOS} for LOS by omitting the input arguments of the matrix.

2.2 Transmitter to RIS Channels

Every element of RIS and transmitter forms a channel in the environment. Depending on the environment and distance between terminals, channels between transmitter and RIS can form LOS communication. However, regardless of the distance and environmental parameters, NLOS channels always exist, even though their strengths are subject to change. In the next two subsections, the equations for NLOS and LOS channels and their parameters are explained, respectively.

2.2.1 NLOS channels

NLOS channels always exist due to the nature of propagation. The electromagnetic waves that are propagating in an environment interact with the surrounding objects and new copies come into existence. Therefore, the interactions with these environment dependent parameters must be included in the model. In the proposed model, such interactions are taken into consideration and the complex channel vector for NLOS propagation is given as

$$\mathbf{h_{n,c,s}^{NLOS}} = \sqrt{P_c}\sqrt{L_{T-RIS}^{c,s}}\mathbf{Ge_t^T}\left(\theta_{Tx-c,s}\right)\alpha_{c,s}a_n\left(\theta_{c,s}^{RIS},\phi_{c,s}^{RIS}\right). \qquad (2.21)$$

P_c is the stochastic cluster power of cth cluster, $L_{T-RIS}^{c,s}$ is the path loss from transmitter-to-csth scatterer-to-nth RIS element whose equation is given as

$$L_{\text{T-RIS}} = -20\log_{10}\left(\frac{4\pi}{\lambda}\right) - 10n\left(1+b\left(\frac{f-f_0}{f_0}\right)\right)\log_{10}\left(d_{\text{T-RIS}}\right) - X_\sigma. \qquad (2.22)$$

Here, $d_{\text{T-RIS}}$ denotes the transmitter to RIS distance, n is the path loss exponent, b, f_0 is the environment dependent system parameters, and X_σ is the again environment dependent Gaussian distributed shadowing term. $\mathbf{Ge_t^T}(.)$ is the 1-by-2 radiation pattern vector of the transmitter antenna, which is given as a function of elevation angle. $\alpha_{c,s}$ is the polarization dependent complex gain matrix of csth scatterer whose representation is given as

$$\alpha_{\mathbf{c,s}} = \begin{bmatrix} \exp\left(j\Phi_{c,s}^{HH}\right) & \sqrt{K_{c,s}^{-1}}\exp\left(j\Phi_{c,s}^{HV}\right) \\ \sqrt{K_{c,s}^{-1}}\exp\left(j\Phi_{c,s}^{VH}\right) & \exp\left(j\Phi_{c,s}^{VV}\right) \end{bmatrix} \qquad (2.23)$$

where $\left\{ \Phi_{c,s}^{HH}, \Phi_{c,s}^{HV}, \Phi_{c,s}^{VH}, \Phi_{c,s}^{VV} \right\}$ are the random initial phases for the csth scatterer for different polarization combinations. These linear polarizations are denoted as the letters H and, V which stand for horizontal(TE polarization) and vertical (TM polarization), respectively. $K_{c,s}$ is the cross polarization power ratios (XPR) for each csth scatterer. $a_n(.,.)$ is the nth element of the following vector shown as

$$\mathbf{a}\left(\phi_{c,s}^{\mathrm{RIS}}, \theta_{c,s}^{\mathrm{RIS}}\right) = \begin{bmatrix} 1 & \cdots & e^{jkd\left((\sqrt{N}-1)\sin\theta_{c,s}^{\mathrm{RIS}} + (\sqrt{N}-1)\sin\phi_{c,s}^{\mathrm{RIS}}\cos\theta_{c,s}^{\mathrm{RIS}}\right)} \end{bmatrix}^{\mathrm{T}} \quad (2.24)$$

which is the array response of RIS representing the phase difference between different elements. The angles that are used above are $\theta_{Tx-c,s}$, $\theta_{c,s}^{RIS}$, $\phi_{c,s}^{RIS}$ which are elevation angle from transmitter to csth scatterer, elevation angle of arrival to RIS, and azimuth angle of arrival to RIS, respectively. The generation of these angles is explained in detail in [20].

2.2.2 LOS channels

As stated earlier, depending on the environment and the distance between transmitter and RIS, there may exist LOS channels. The probabilities deciding the existence of loss probabilities are given in equation (1.38) and (1.39). The nth complex 1-by-2 channel vector is given as

$$\mathbf{h_n^{LOS}} = \sqrt{L_{T-LOS}}\mathbf{G}\mathbf{e}_t^T\left(\theta_{Tx}^{LOS}\right)\alpha_{\mathbf{T-LOS}}a_n\left(\theta_{T-LOS}^{RIS}, \phi_{T-LOS}^{RIS}\right)I_h \quad (2.25)$$

where again L_{T-LOS} is the path loss component of LOS path whose calculation is the same in equation (2.22) with the only difference being random variables and the distance calculation. $\alpha_{\mathbf{c,s}}$ is the polarization dependent complex gain matrix of LOS component, whose matrix is given as

$$\alpha_{\mathbf{LOS}} = \begin{bmatrix} \exp\left(j\Phi_{LOS}^{HH}\right) & 0 \\ 0 & \exp\left(j\Phi_{LOS}^{VV}\right) \end{bmatrix} \quad (2.26)$$

where $\left\{\Phi_{LOS}^{HH}, \Phi_{LOS}^{VV}\right\}$ are the random initial phases for LOS propagation. Note that XPRs are removed since there are no scatterers and therefore no polarization changes in LOS propagation. Array response vector is the same as in equation (2.24) with the only exception of different angles as an input. The angles that are used above are

38

θ_{Tx}, θ_{LOS}^{RIS}, ϕ_{LOS}^{RIS} which are elevation angle from transmitter to RIS scatterer, elevation angle of departure from RIS, and azimuth angle of departure from RIS, respectively. The generation of these angles is explained in detail in [20]. $I_{\mathbf{h}}(d_{\text{T}-\text{RIS}})$ is a Bernoulli random variable that takes the values 0 or 1, with the PMF given in equations (1.38) and (1.39) depending on the environment.

2.3 RIS to Receiver Channels

RIS to receiver channel consists of two sub channels, which are the LOS and NLOS component of the RIS-receiver channel. Expression of the LOS channel is similar to transmitter to RIS channel. However, NLOS channel may change immensely with respect to the positioning of the RIS. If RIS is placed close to the receiver, after a certain distance, the LOS component of the channel dominates the NLOS components and the NLOS channel becomes negligible. The equation for the RIS to receiver channel is the same if there is no LOS domination, the only difference is the generation of random variables and the scatterers that propagating rays interact.

2.3.1 NLOS channels

The equation of the NLOS channel components is given as

$$\mathbf{g_{n,k,l}^{NLOS}} = \sqrt{P_k}\sqrt{L_{R-RIS}^{k,l}}\alpha_{\mathbf{k,l}}\mathbf{Ge_r}\left(\theta_{Rx-k,l}\right)a_n\left(\theta_{k,l}^{RIS},\phi_{k,l}^{RIS}\right) \tag{2.27}$$

where $\mathbf{Ge_r}(.)$ is the radiation pattern of the receiver antenna. It is a 2-by-1 vector and its first entry denotes the radiation pattern for the TE polarized waves, and its second entry denotes the radiation pattern for the TM polarized waves. $L_{R-RIS}^{k,l}$ is the path loss that klth ray experienced. Generation of azimuth and zenith angles are done similar to the in RIS to transmitter channel. The only changing factor in the generation of angles are the positions of scatterers, since $\mathbf{g}$ and $\mathbf{h}$ channels are not sharing common clusters. Elements of array response vector, cluster powers are generated by using the same method in the transceiver to RIS channel. Their intrinsic parameters are updated by considering the change of scatterers. The expression of $\alpha_{\mathbf{k,l}}$ is the same as in equation (2.23).

2.3.2 LOS channels

Expression of the RIS to receiver LOS channel is given as

$$\mathbf{g_n^{LOS}} = \sqrt{L_{R-LOS}}\mathbf{Ge}_r\left(\theta_{Rx}^{LOS}\right)\alpha_{\mathbf{R-LOS}}a_n\left(\theta_{R-LOS}^{RIS},\phi_{R-LOS}^{RIS}\right)I_r \qquad (2.28)$$

where L_{R-LOS} is the path loss, $\alpha_{\mathbf{R-LOS}}$ is the polarization dependent complex path gain matrix with zero off-diagonal entries. Off-diagonal entries are zero because since there are no scatterers that propagating waves interact, it is not possible for propagating waves to change polarization. Since the position of the RIS and receiver is fixed, angles are modeled deterministic instead of probabilistic. I_r is the Bernoulli random variable that determines the existence of the LOS path. Its PMF is a function pf a RIS to receiver distance. If the LOS probability is greater than fifty percent, then the channel could be assumed LOS dominant and the overall channel equation for RIS to receiver channel reduces to LOS channel equation for RIS to receiver channel.

2.4 SISO Channel

In the overall end-to-end channel, there is a classical direct channel. This direct channel is relatively stronger since the waves propagating directly to the receiver from the transmitter travel lesser distances and hence suffer from relatively smaller path loss. This channel is not related to RIS anyhow. It is classical Rician fading channel which can be given as summation of NLOS and LOS components as

$$h_{SISO} = h_{SISO}^{NLOS} + h_{SISO}^{LOS}. \qquad (2.29)$$

h_{SISO}^{NLOS} and h_{SISO}^{LOS} is presented in detail in the following two subsections.

2.4.1 NLOS channel

The channel equation representing the NLOS situation is given as

$$h_{SISO}^{NLOS} = \sum_{p=1}^{P}\sum_{q=1}^{Q}\sqrt{P_p}\sqrt{L_{SISO}}\mathbf{Ge_t}^T\left(\theta_{Tx-p,q}\right)\alpha_{\mathbf{p,q}}\mathbf{Ge_r}\left(\theta_{p,q-Rx}\right) \qquad (2.30)$$

where P, Q are the number of clusters and scatterers respectively. L_{SISO} is the path loss component accompanying the path from transmitter to scatterers and scatterers

to receiver. Radiation pattern vectors are the same as the ones explained in **h** and **g** channels, except for input angles. The expression of $\alpha_{\mathbf{p,q}}$ is the same as in equation (2.23). $\theta_{Tx-p,q}$ and $\theta_{p,q-Rx}$ are elevation angles calculated from transmitter to pqth scatterer and pqth scatterer to receiver.

Here, it is assumed that direct channel experiences completely different clusters than that of the **h** and **g** channels experience. However, this may not be the case in real-life application. If the receiver and RIS are close enough, which generally holds in the indoor environment, then they may experience common clusters that transmitter to RIS channels experience. Namely, if they experience the common clusters, the indices in equation 1.41 will be c and s instead of p and q.

2.4.2 LOS channel

The existence of LOS channel again depends on the environment and the distance between transmitter and receiver. If it exists, then it contributes the h_{SISO} channel by an extra term whose equation given as

$$h_{SISO}^{LOS} = \sqrt{L_{SISO}^{LOS}} \mathbf{Ge_t}^T \left(\theta_{Tx}^{LOS} \right) \alpha_{\mathbf{TR-LOS}} \mathbf{Ge_r} \left(\theta_{Tx}^{LOS} \right) I_{SISO}(d_{\mathrm{T-R}}) \qquad \textbf{(2.31)}$$

where L_{SISO} is the path loss component accompanying the path from transmitter to receiver. The expression of $\alpha_{\mathbf{TR-LOS}}$ is the same as in equation (2.26). $I_{SISO}(d_{\mathrm{T-R}})$ is again a Bernoulli random variable depending on the distance between transmitter and receiver that is taking the values 0 or 1, with the PMF given in equations (1.38) and (1.39) depending on the environment.

2.5 Simulations of the Channel Model

A common metric for examining the impact of the RIS on wireless channel is achievable rate. The change of the achievable rate under RIS usage is investigated in simulations. Achievable rate is calculated as

$$R = \log_2(1+\rho) \qquad \textbf{(2.32)}$$

where ρ is the instantaneous SNR. The equation for instantaneous SNR is given as

$$\rho = \frac{|H|^2 P_t}{P_N} \tag{2.33}$$

where H is the overall end-to-end channel coefficient. P_t is the power of the transmitter and P_N is the noise power. If perfect channel estimation is assumed at the RIS, then phase shifts applied by RIS elements can be adjusted so that RIS-assisted channel cancel the phase shift caused by the direct channel (SISO). In order to be able to apply these phase shift, the channels between transmitters and RIS and between RIS and receiver should be estimated. This is one of the major challenges in the usage of RIS. Assuming RIS is able to apply any phase shift, this assumption can be satisfied.

Since the proposed model is an extension to the model proposed in [20] in terms of polarization, transmit and receive antenna radiation pattern, and non-ideal RIS response, their methodology of simulation is followed here with some differences to be able to compare the results. The simulations are carried out in MATLAB software and the codes of environments and generation of stochastic parameters are written with the help of open source published codes of these researchers.

Moreover, cluster powers are assumed to be equidistributed. Namely, all coefficients will be the same for all clusters and their sum is equal to unity. A more realistic cluster power modelling can be satisfied by stochastic models. Also, for the sake of simplicity and maintain the comparability, all radiation patterns are assumed to be omnidirectional which means that the radiated waves' polarizations are multiplied with the same coefficient.

Since the purpose of the simulations are to verify the accuracy of the proposed model, RIS is only placed on the *xz* plane, and it remains there unchanged. Also, the receiver and transmitter are assumed to be stationary; namely, they don't change their positions with time. This may not be the case in real-life applications. For example, the receiver may be a mobile unit and therefore a Doppler frequency calculation and/or localization might be an important issue.

This model utilizes two different environments, which are the indoor environment and the outdoor environment. The definitions of these environments are explained in detail in 3GPP and WINNER II channel model reports. The indoor environment is a type of environment that receiver is not much farther from transmitter and RIS; therefore,

experience a high LOS probability. Outdoor environments;on the other hand, is a type of environment like suburban or rural areas that the receiver might be much farther away from the transmitter or RIS. Therefore, the outdoor environment utilizes less LOS probability. Environment parameters are taken from empiric measurements published by the network providers. However, while conducting the simulations, the respective positions of transmitter, RIS, and receiver should be chosen such that they comply with the real-life distances. Otherwise, the empiric parameters would not be the best fit for these simulations.

As it is mentioned above, the receiver is generally close to the transmitter and RIS. Therefore, 100% LOS probability is assumed in the indoor environment while conducting the simulations. However, since it is not the case in outdoor environments, NLOS parameter is not excluded there, even though it still has a LOS channel with the calculated probability.

On the other hand, the environment still makes a difference for the direct channel as well. For example, if the receiver is close to the RIS, then the direct channel probably experiences the same clusters with the channels between transmitter and RIS. Therefore, common clusters model are adopted in indoor environments while conducting the simulations. However, since outdoor distances are relatively larger, a completely different cluster model is applied and simulated.

All the simulations presented here are realized with the operating frequency of 28 GHz. In this frequency band, path loss is quite strong and RIS-assisted channel suffer from this path loss due to the fact that the waves propagating in the RIS-assisted channel have to travel longer distances. Therefore, the deployment of RIS in an environment where direct channel can be established may be unnecessary. However, if correct positioning of these terminals are adjusted. Then it makes a difference. In these simulations, the effect of direct channel is studied in detail.

In the following subsections, the effect of SNR on the achievable rate (ergodic capacity), the effect of positioning and direct channel on the achievable rate, and finally the effect of RIS size (number of elements) are presented with their corresponding simulated graphics. Also, the titles of the figures are given in a descriptive form. For example, in the title of Figure 2.11 there is *env* = 1 where *env* denotes the type

of environment by assigning numbers 1 and 2. If *env* = 1, then the environment is an indoor type environment, and if *env* = 2, then the environment is an outdoor type environment. *N* represents the number of elements belong to RIS. NO_{SISO}, as the name suggests, there is no direct channel between transmitter and receiver. Namely, the direct channel is blocked. *ort* represents the number that the channel coefficient is averaged exactly this number of times. For example, *ort* = 1000 means that a random channel coefficient is created 1000 times and its average is taken as a reference channel coefficient.

2.5.1 SNR vs. achievable rate

In this simulation, change of the achievable rate with increasing SNR in RIS assisted channel is investigated. Other parameters such as RIS size, position, and operating frequency have been kept fixed. SNR is adjusted by changing the transmitted power. Noise power has been kept fixed.

2.5.1.1 Indoor environment and SISO blocked channel

In this section, change of achievable rate in the indoor environment with SISO blocked channel is investigated. Transmit power (P_T) vs. achievable rate (R) curve is plotted for different RIS sizes. Figure 2.1 demonstrates the change of achievable rate with increasing SNR in the 256-cell RIS deployed channel. It is assumed that RIS has the capability of providing ideal response. Thus, there is no loss in the RIS response and all phase mismatches are cancelled in the receiver. From 2.1 it can be seen that the existence of the RIS increases the ergodic capacity. Note that, since the SISO channel is blocked, most of the power radiated from the transmitter is directed from RIS to the receiver in a controlled manner. The achievable rate almost hits the 2 [bit/sec/Hz] for 0 dB transmit power. This result shows that RIS can provide a communication link in the case of LOS channel is blocked between the transmitter and the receiver. This capability of RIS makes it a potential technology in future applications, especially for indoor environments, which suffer from the lack of clear LOS links between transceivers. However, since ideal RIS response is assumed, power loss stem from the interaction with the RIS is ignored. Consequently, lower achievable rate values are expected in practical cases.
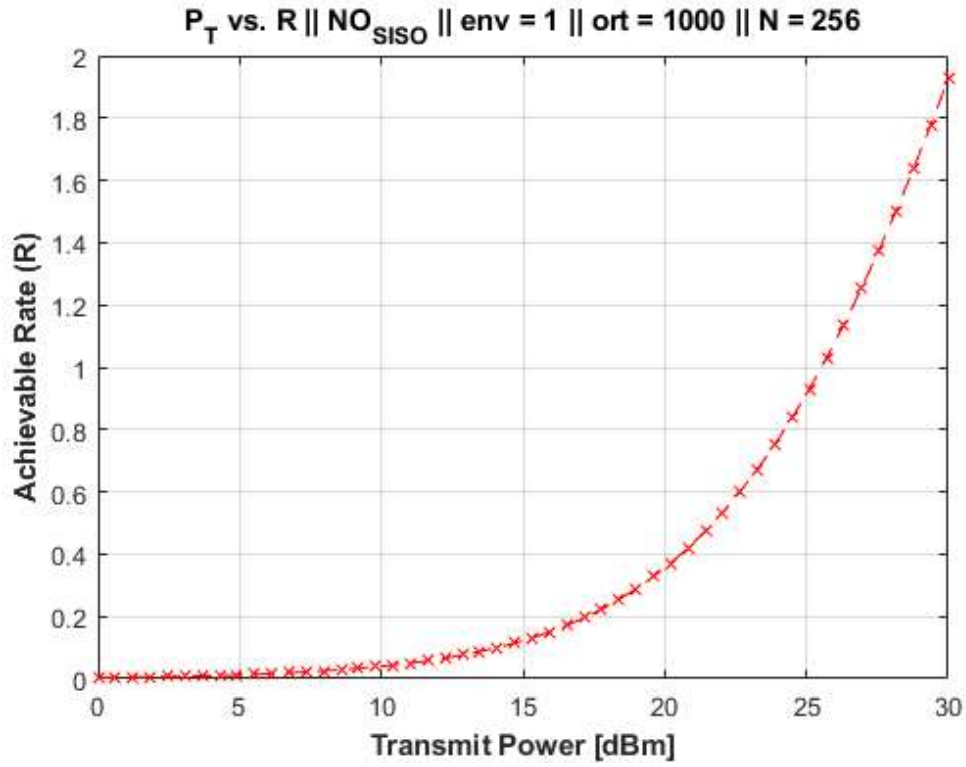
Figure 2.1 : Change of achievable rate with increasing SNR in indoor environment (SISO blocked, N = 256).

Figure 2.2 shows the change of achievable rate in the same conditions, except for the size of the RIS. In this graphic, the effect of the RIS with 1024 elements is shown. As it can be seen from this figure, almost 6 [bit/sec/Hz] achievable rate value is provided by the RIS for 0 dB transmit power. Apparently, increasing the size of the RIS enhances the communication performance. It is reasonable because the larger the RIS becomes, the more signals it captures and directs towards the receiver. Thus, a larger portion of the radiated power arrives to the receiver in a controlled manner. Compared to the results in Figure 2.1, it can be seen that a four-fold increase in the RIS size resulted in approximately three-fold increase in the achievable rate at 0 dB transmit power. Another distinction between these figures are the points that which achievable rate curve becomes linear. For the RIS with 256 elements, up to 25 dBm, the slope of the achievable rate curve increases. Then it becomes relatively fixed compared to the region below the 25 dBm. For the RIS with 1024 elements, the value that slope becomes fixed is somewhere between 15 and 25 dBm.

In the Figures 2.1 and 2.2, it has been shown that increasing the size of the RIS increases the achievable rate. However, after a certain size, RIS's capability of

increasing the achievable rate vanishes and increasing the RIS size does not change the achievable rate.
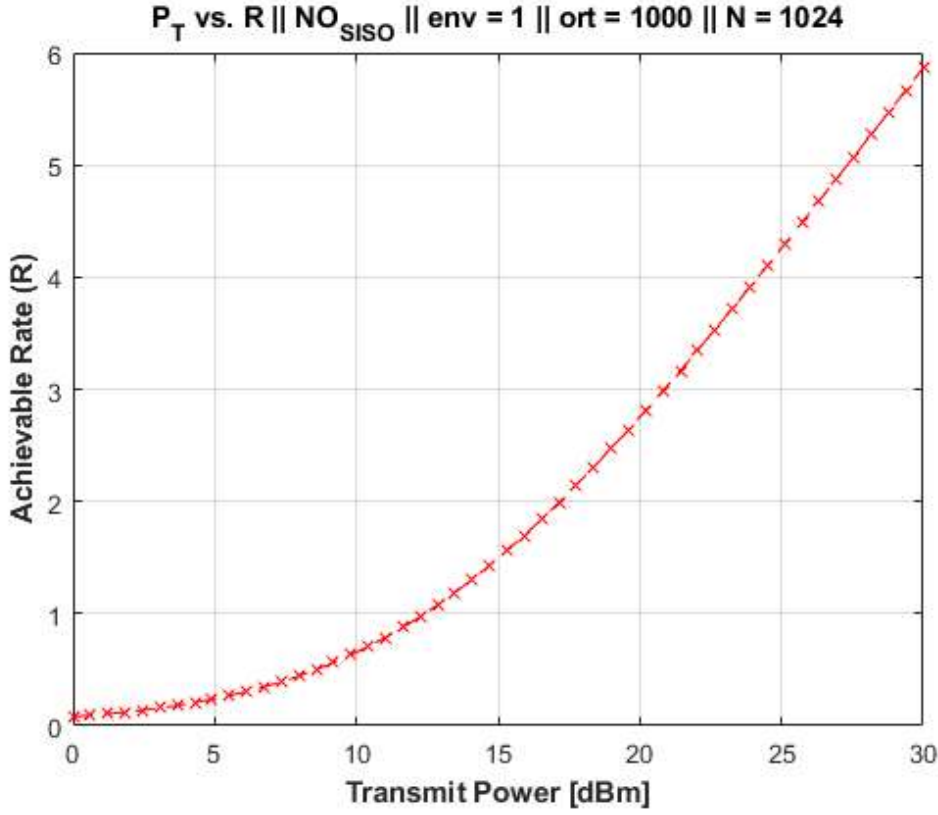

Figure 2.2 : Change of achievable rate with increasing SNR in indoor environment (SISO blocked, N = 1024).

2.5.1.2 Indoor environment and SISO channel

The effect of the RIS deployment in the channels with SISO link in the indoor environment are investigated and results have been shown in this section. Except for the SISO channel, all parameters have been kept the same as the parameters used in the SISO blocked channel case. The existence of the SISO channel enormously increases the achievable rate, since the transmitted power increases a lot due to the existence of a direct link between transmitter and receiver. Power transferred through SISO channel is much greater than the power transferred through RIS. The reason for this difference is the fact that SISO link is shorter than the distance between the transmitter to RIS to receiver link. In the high frequency regimes, the signal power attenuates rapidly. This decrease is proportional to the square of the covered distance and with the square of the frequency. Since 28 GHz is a relatively high operating frequency and the length of

the SISO channel is the shortest, the vast difference between powers transferred from different path occurs.

Figure 2.3 shows the change of achievable rate with transmit power in the channel deployed with 256 elements RIS.
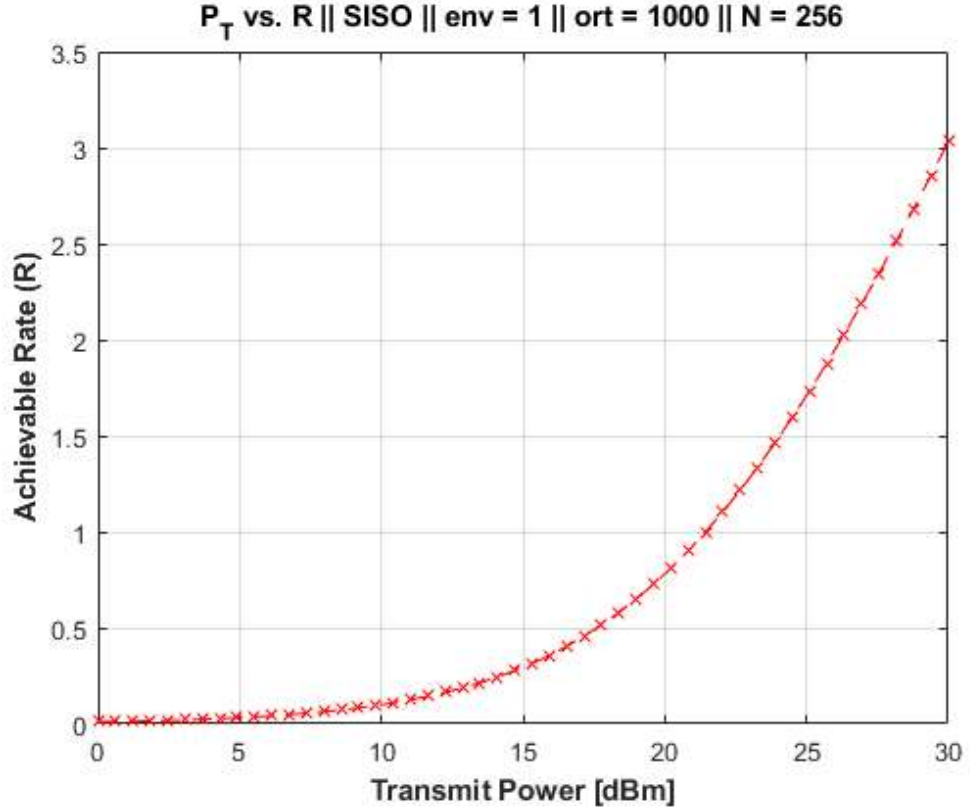

Figure 2.3 : Change of achievable rate with increasing SNR in indoor environment (SISO, N = 256).

Compared to the results shown in Figure 2.1, it can be seen that in the channel with SISO link, achievable rate increases. This result stems from the fact that received power increases if SISO channel is not blocked, and if received power increases, then achievable rate increases. More than 3 [bits/sec/Hz] achievable rate is obtained in this channel. Compared to SISO blocked case, there is a 1.5-fold increase in the achievable rate.

2.5.1.3 Outdoor environment and SISO blocked channel

The simulations conducted for indoor environment are repeated for the outdoor environment. In this section, the effect of the RIS deployment in outdoor environment with blocked SISO link is investigated. For two different cases, which are RIS with

256 and RIS with 1024 elements, change of achievable rate with respect to changing transmit power is simulated.

Figure 2.4 illustrates the change of achievable rate in the channel deployed with 256 elements RIS.
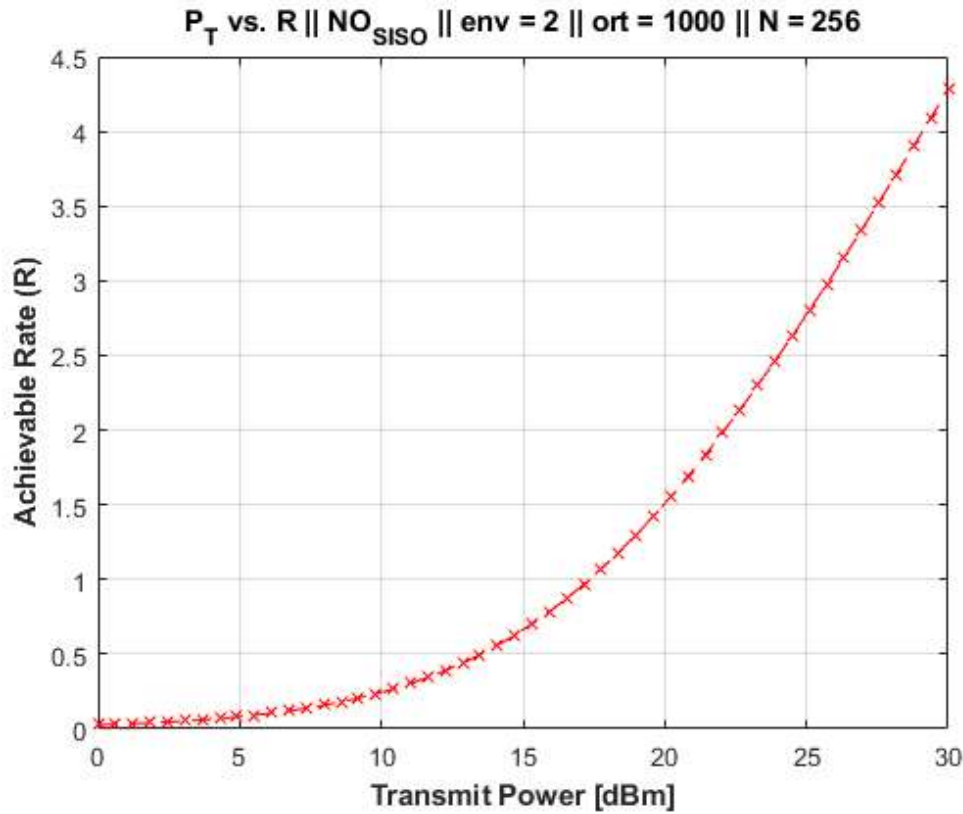

Figure 2.4 : Change of achievable rate with increasing SNR in outdoor environment (SISO blocked, N = 256).

In this settlement, for 0 dB transmit power, approximately 4.3 [bit/sec/Hz] achievable rate is obtained. Since LOS probabilities, path loss coefficients are different from indoor environment, achievable rate varies.

Figure 2.5 repeats the same simulation with the RIS consists of 1024 elements. Again, due to the enlargement of the RIS size, the achievable rate increased. This result shows that independent of the environment, increasing the RIS size increases the achievable rate. Approximately 8.3 [bit/sec/Hz] achievable rate is obtained at 0 dB transmit power. Thus, almost 2-fold increase in achievable rate is obtained due to 4-fold increase in the RIS size. Even though simulations show that RIS perform well in

outdoor environments, practical cases should be different due to the fact that distances in outdoor environments are larger compared to indoor.
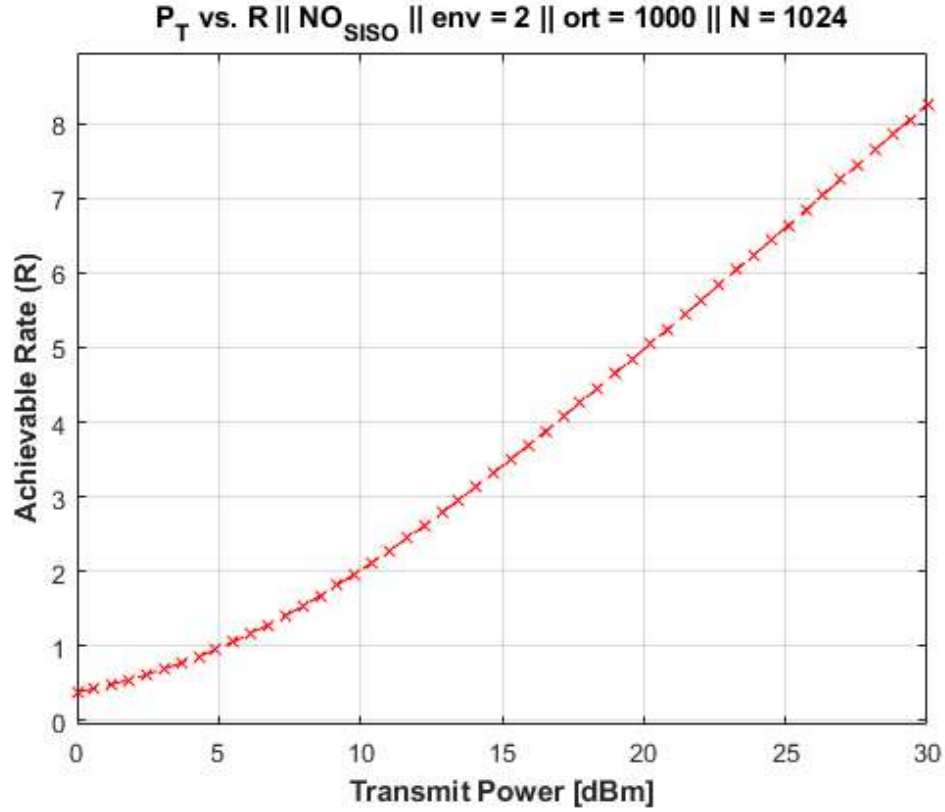

Figure 2.5 : Change of achievable rate with increasing SNR in outdoor environment (SISO blocked, N = 1024).

2.5.1.4 Outdoor environment and SISO channel

The effect of RIS deployment in the outdoor environments with LOS path between receiver and transmitter is in this section. Achievable rate's dependency on transmit power is simulated. Figure 2.6 demonstrates the change of achievable rate with respect to transmit power in the channel deployed with 256 elements RIS. Approximately 5.4 [bit/sec/Hz] achievable rate is obtained. This result is slightly higher than the case where SISO channel is blocked. The increase in the achievable rate stems from the fact that the existence of the direct channel between transmitter and receiver increases the transferred power.

It has been shown that RIS deployment provides an increase in the achievable rate in both indoor and outdoor environments. The Existence of SISO channel provides an increase in achievable rate. However, as it will be shown in the following sections,

it is hard to compensate for the randomness of SISO channel with RIS deployment because SISO channel is the dominant channel. Thus, it is more feasible to use RIS when the communication link suffers from blocked LOS channel between transmitter and receiver.
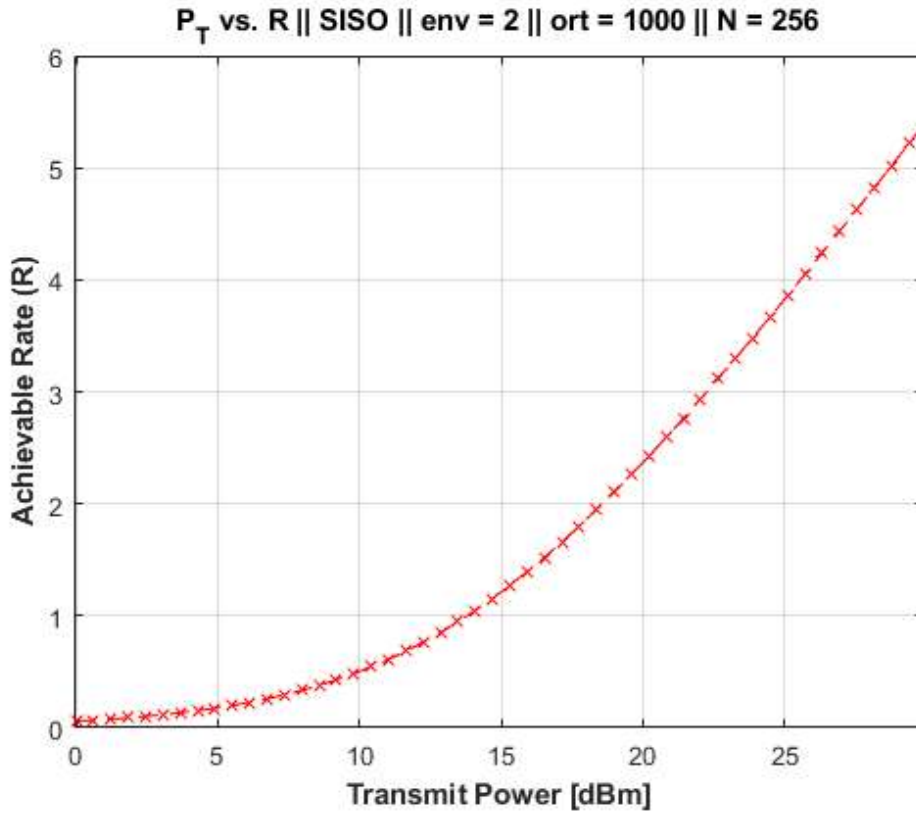

Figure 2.6 : Change of achievable rate with increasing SNR in outdoor environment (SISO, N = 256).

2.5.2 RIS size vs. achievable rate

It has been shown that deployment of the RIS in wireless channel increases the achievable rate. In addition, for reaching the same achievable rate value with lower transmit power, larger RIS should be used. However, increasing the RIS size does not always increase the achievable rate. After a certain size, increasing the dimensions changes nothing, RIS size vs. achievable rate curve approaches an asymptote. This behavior is shown in the Figure 2.7. For fixed transmit power, increasing the RIS size (N) increases the achievable rate, but the rate of increase in the achievable rate gradually decreases.
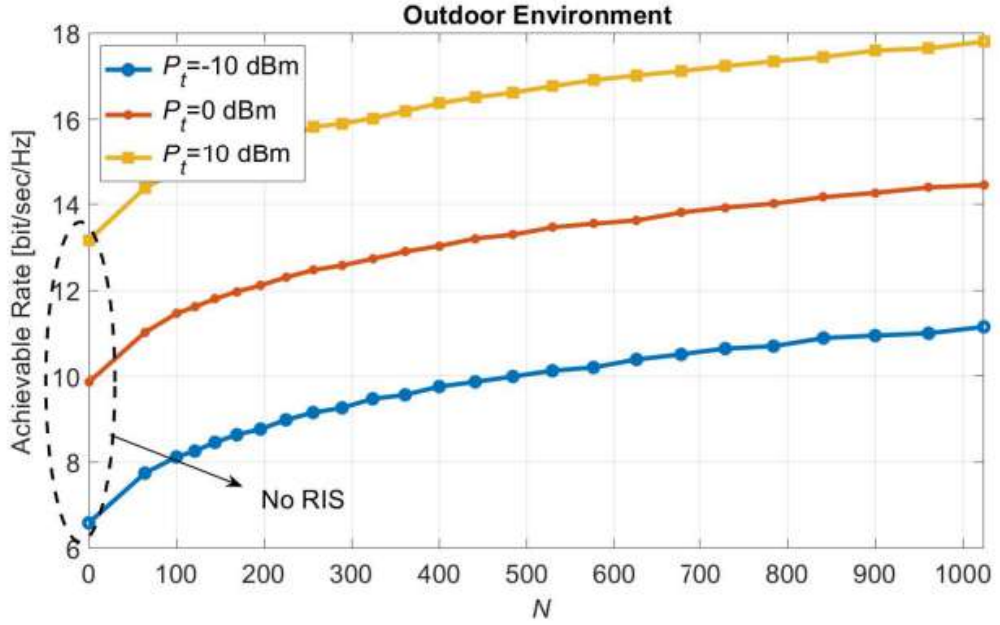
Figure 2.7 : RIS size vs. achievable rate [19].

In the simulations,it is expected to observe a similar trend as in 2.7. For different environments and both in SISO and SISO blocked channels, change of the achievable rate with respect to RIS size is simulated. Three graphics were plotted for transmit powers 10,20 and 30 dBm. Also, it expected to see randomness in the SISO channel simulations, since power transferred through RIS is relatively small compared to SISO channel.

2.5.2.1 Indoor environment with SISO blocked channel

In this section, RIS size vs. achievable rate is simulated for indoor environment in SISO blocked channel conditions. Figure 2.8 shows that the trend of increase continues up to 1024 elements. The fluctuations in the graphic stems from the randomness of the channel. It is observed that even in small transmit powers such as 10 dBm, RIS utilization can provide achievable rate up to 0.5 [bits/sec/Hz]. An increment in transmit power causes an increase in the slope of the RIS size vs. achievable rate curve. Even though the trend of decrease on the slope of the curve is not clearly observed, it is expected to observe this trend for the RIS size larger than 1024. Because after some point, RIS's capability of directing the rays into the receiver becomes independent of its size. The reason behind this phenomenon is the fact that for large RISs, the total

amount of directible rays to receiver stays fixed after a certain limit. Because RIS already directs most of the directible rays in the medium, and the amount of directible rays also depends on stochastic parameters of the medium.
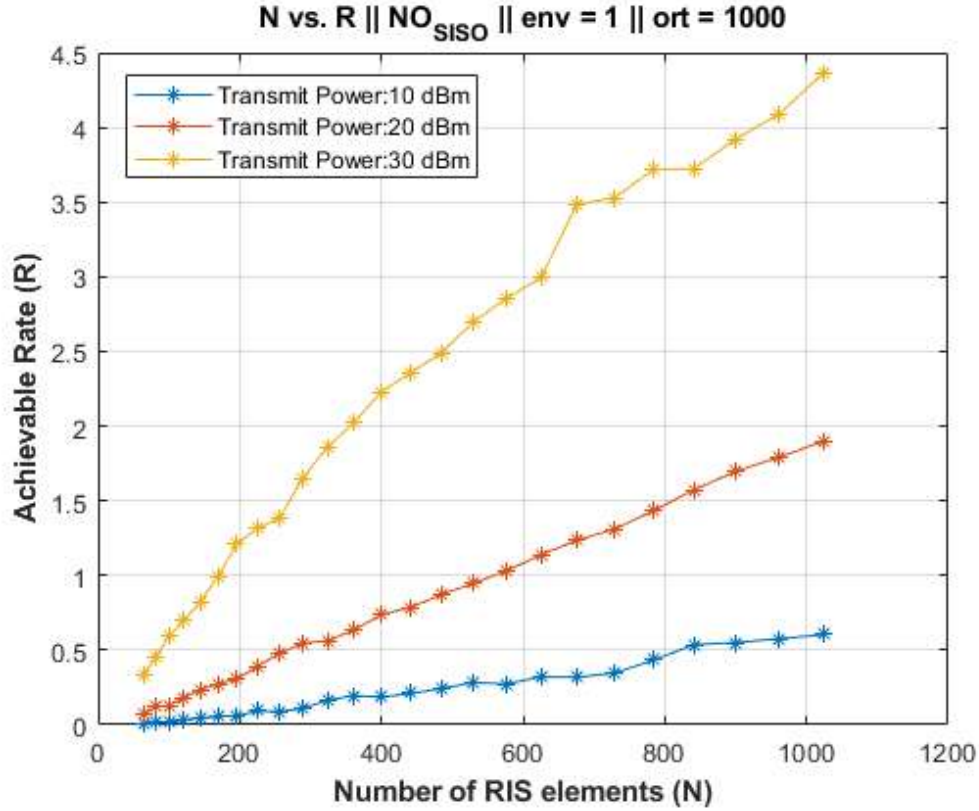

Figure 2.8 : RIS size vs. achievable rate (Indoor, SISO blocked).

2.5.2.2 Outdoor environment with SISO blocked channel

In this section, RIS size vs. achievable rate is simulated for outdoor environment in SISO blocked channel conditions. Figure 2.9 shows the simulation results. The trend of decrease on the slope of the curve is observed in this figure, which implies that for outdoor environments, the adjuvant effect of the RIS size on achievable rate reduces faster compared to indoor environments. The results are compatible with the result found in [19].

The difference between the figures 2.8 and 2.9 may stem from, in the indoor environment model, there is a LOS dominant channel between RIS and the receiver. However, in outdoor, RIS to receiver channel is not LOS dominant. However, LOS probabilities in the RIS to receiver and RIS to transmitter channels are higher in the outdoor environment.
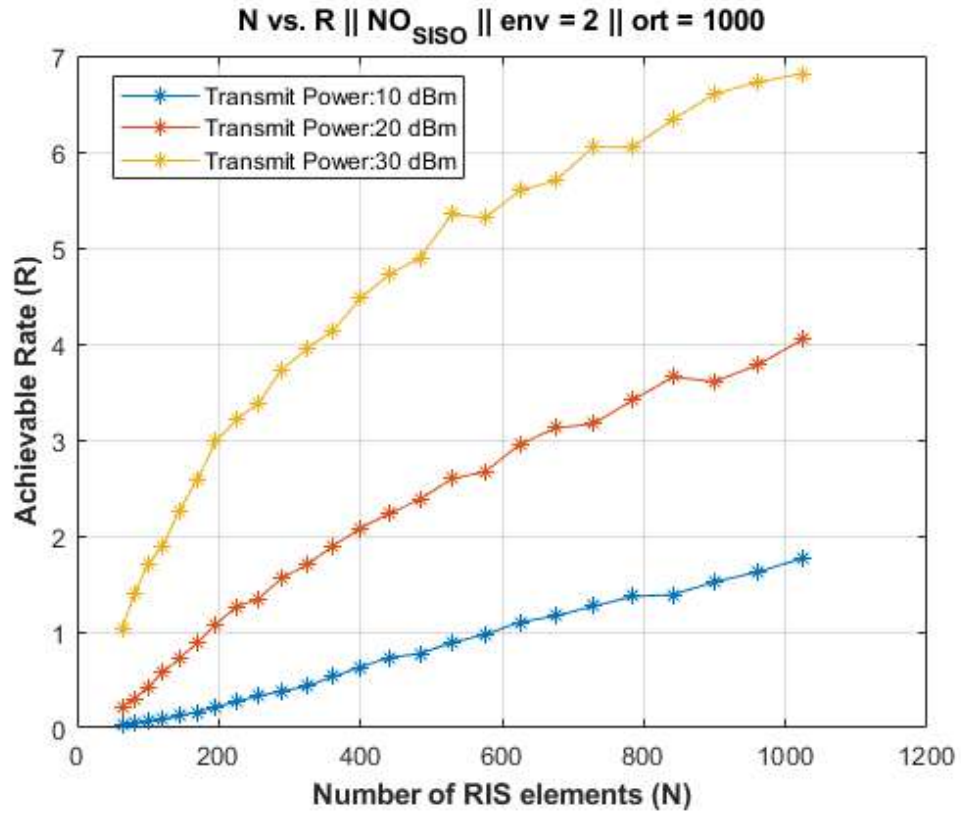
Figure 2.9 : RIS size vs. achievable rate (Outdoor, SISO blocked).

2.5.2.3 Indoor and outdoor environment with SISO channel

The existence of the direct link between the transmitter and the receiver creates a channel dominated by the direct channel (h_{SISO}). Signal power transmitted from direct channel outweighs the power transmitted via RIS deployed channel. RIS's impact on the achievable rate becomes little compared to the impact of the direct channel. Since there are random variations in the h_{SISO} channel, observed achievable rate changes randomly. However, these variations on power are too large compared to the power of the signals transferred through RIS. Thus, it is not possible to observe an increasing trend on achievable rate in the channels even if RIS size increases.

Figure 2.10 shows the RIS size vs. achievable rate in the indoor and outdoor environments with SISO channel, respectively. In both figures, there are no increasing or decreasing trends. The achievable rate fluctuates randomly because of the impact of the dominant SISO channel. Also, it is observed that the average achievable rate is increased due to the existence of the SISO channel.
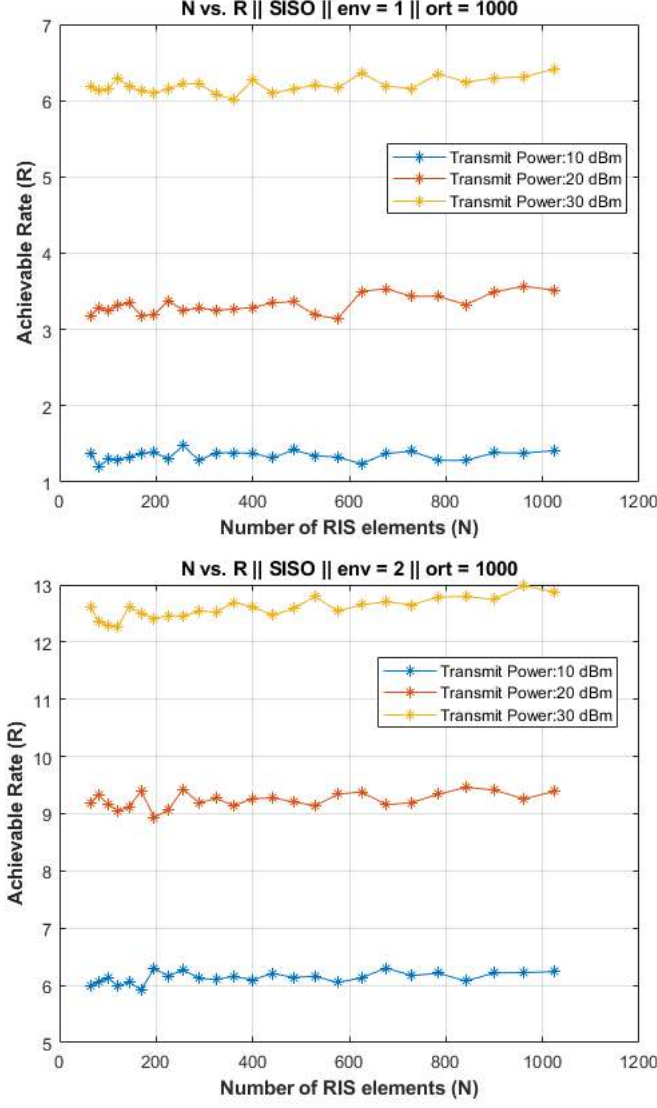
Figure 2.10 : RIS size vs. achievable rate (Indoor and Outdoor, SISO).

2.5.3 Position vs. achievable rate

In this subsection of the performed simulations, the effect of positioning is examined. One of these positioning simulations is the change of achievable rate with changing the *x* coordinate of the RIS in 3D space. The all units in positioning are in meters. Therefore, the distance of RIS is calculated in meters. This analysis was chosen so that it becomes comparable with the results that were obtained by the developed model in [20]. The effect of RIS's *x* coordinate (X_{RIS}) does not suffice by itself to analyze the effect of positioning in the overall performance, since it is not only a function of RIS position but also the others. Therefore, this subsection is divided into two subsections which introduce different receiver, transmitter, RIS coordinates in 3D space.

In the positioning section of the simulation analysis, transmit power of the transmitter is chosen as 30 dBm and AWGN power spectral density (N_0) is chosen as -100 dBm in order to be able to compare the obtained result with the referenced research.

2.5.3.1 First case of different positioning

In the first case, the coordinates of the transmitter, RIS, and receiver are respectively given as (0,25,2), (38,48,1), (20,50,1). This setup is investigated for the case of the existence of direct channel and the absence of direct channel because the effect of direct channel in the overall communication link is interesting.

SISO blocked channel

For example, Figure 2.11 is a one example of the first case of positioning figures. It is obtained for $N = 256$ and with no direct channel between transmitter and receiver in the indoor environment by averaging over 1000 samples.
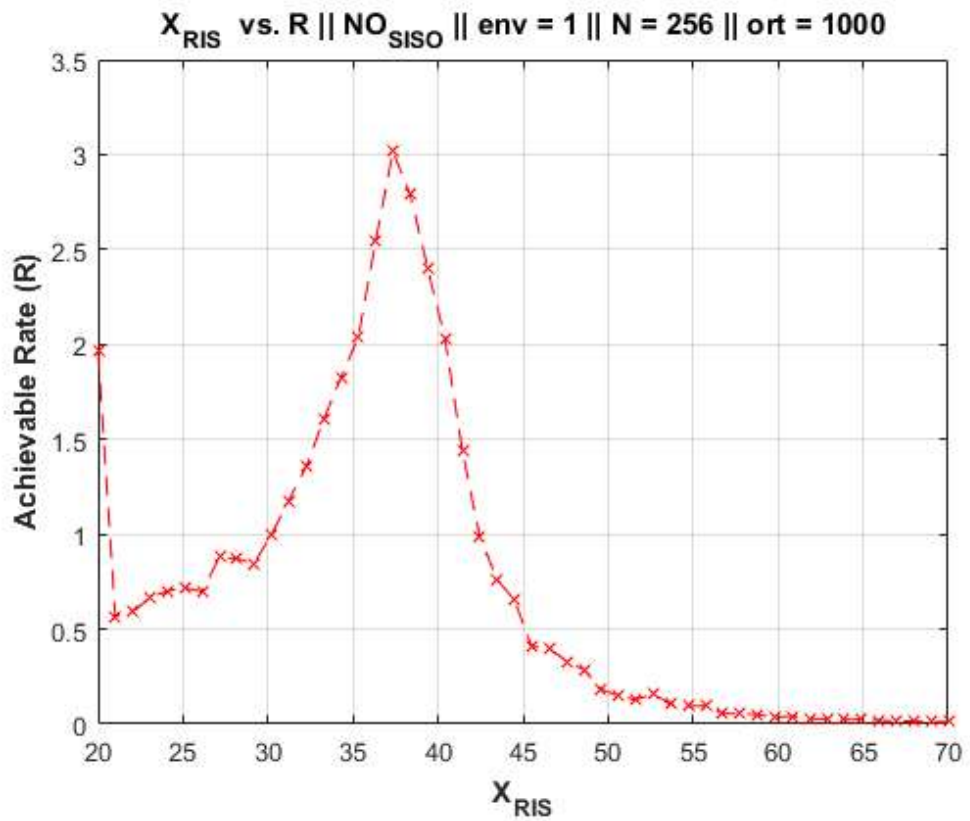

Figure 2.11 : Achievable rate in indoor environment for 256 elements with the absence of direct channel by varying x_{RIS}.

As it can be seen from this figure, it follows an increasing trend until a peak point, then rapidly decreases. The reason why it increases until that point is that receiver and RIS are quite close. However, as RIS continues to move along the x axis, it starts to move further away from the receiver and causes the signal reception to decrease. Also, it can be noted that although receiver and RIS get closer until the peak point, transmitter and RIS get farther away. However, it still continues to increase, which allows us to conclude that the receiver and RIS channel is relatively stronger than the channel between transmitter and RIS. This may result from the fact that the channel is assumed to be LOS in the indoor environments. After rapid increase, the distance of RIS increases to both transmitter and receiver; therefore, the decrease is much steeper than the increase around the peak point. The direct decrease in the 20 meter is caused by a decent mistake that was performed during the coding of the process. It is kindly asked to ignore it.

On the other hand, when this simulation is performed in an outdoor environment with the exactly same parameters as it can be seen from the title of the Figure 2.12, the mentioned difference in strength between the channels is no longer visible. The rate of decrements is approximately the same around the peak point. Again, this is expected because different cluster models are adopted in the outdoor environment.

Furthermore, the peak occurs for exactly the same reason as in the indoor environment. When RIS moves closer to the receiver, the suffering from path loss eases; hence, increasing the achievable rate. Also, the enhancement in the achievable rate can be easily figured out, since there is almost twofold increase in the achievable rate. This may be the fact that for outdoor environments, when the LOS probability increases, it contributes to achievable rate in an excessive amount. Also, it may be the fact that outdoor environment parameters produces better results. In addition, it should be noted that for the two given figures, there are no direct (SISO) channels; namely, the direct channels are blocked for the two environments.

Furthermore, this analysis is further continued with the increment of the RIS size since achievable rate is expected to increase with the rise of element number. Therefore, the exactly same simulations performed with the RIS size of 1024 and the one for the indoor environment is shown in Figure 2.13.
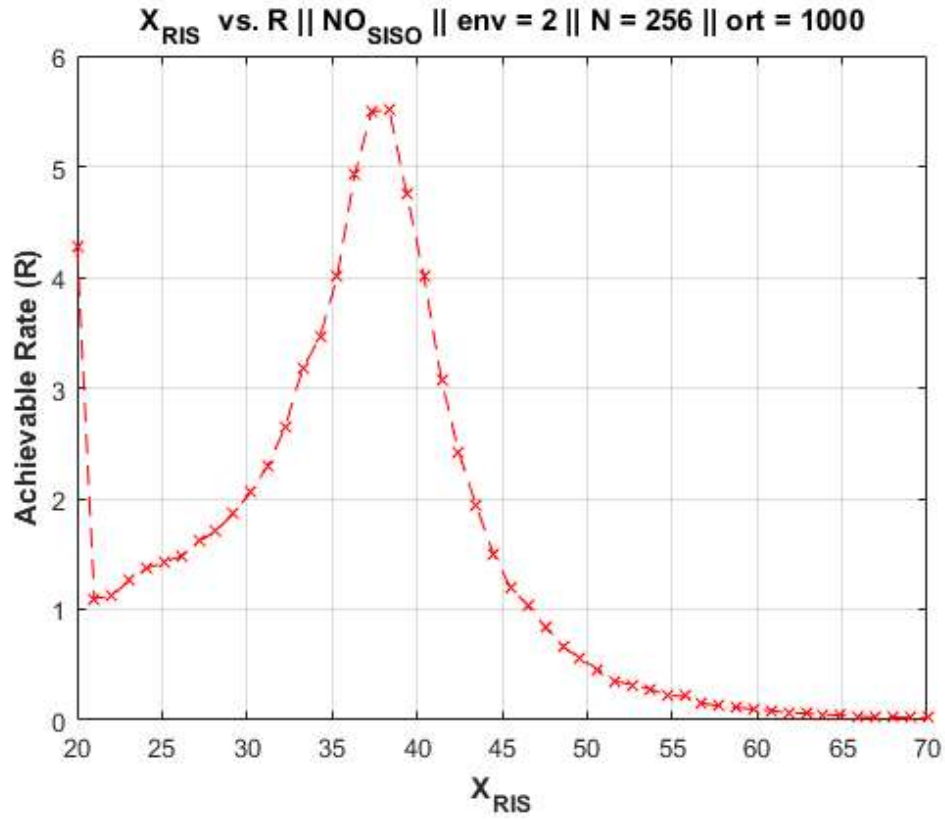
Figure 2.12 : Achievable rate in outdoor environment for 256 elements with the absence of direct channel by varying x_{RIS}.

When the RIS size is further increased to, 1024 in the indoor environment, the achievable rate increases to an initial point of 3 (ignoring the error made in the beginning). However, there is a loss of increase rate in the achievable rate. For example, when the RIS size is 256 and all other parameters are the same; namely Figure 2.11, the achievable rate goes from 0.5 to 3, almost 6-fold. However, when the RIS size is 1024, this rate of increase is only from 3 to 6.5, approximately 2-fold. There is a decrease in the amount of the increase. This may be the fact that increasing the RIS size increases the number of channels, and these channels experience a specified amount of fading.

Since RIS collects the scattered waves in the environment, increasing RIS size cannot affect the achievable rate as long as scattering does not increase. Therefore, it causes this decrease. It is a strong argument because when the same analysis is performed for the outdoor environment as well, this decrease in the amount of increase again can be seen. This is illustrated in Figure 2.14.
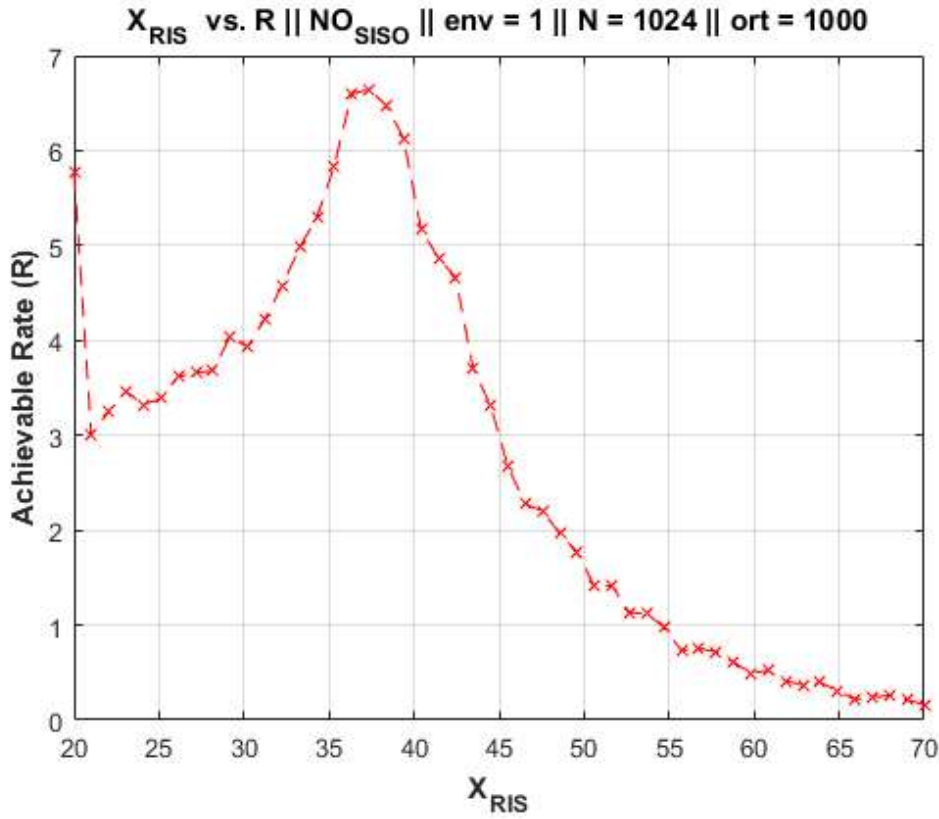
Figure 2.13 : Achievable rate in indoor environment for 1024 elements with the absence of direct channel by varying x_{RIS}.

It starts from 4.5 and rises to the level of approximately 9.5, almost 2-fold increase. Since the scattering isn't increased in the environment, increasing the number of elements helps achievable rate until some point.

SISO channel

Until this point, all the simulations presented in positioning analysis are carried out for blocked direct channel (SISO). However, for the sake of completeness it is presented now the SISO enabled channels. For example, in the Figure 2.15, a direct channel enabled simulation result is presented, and the results are somewhat complicated. These large fluctuations come from the fact that direct channel is dominant to RIS-assisted channel, and moving RIS to closer to the receiver does not affect the result. Therefore, the changes on the SISO channel which comes from the LOS probability is observed in the figure.

Moreover, it can be seen that after 40 meters, a small decrease in the mean of these fluctuating points occurs. This comes from the fact that, after 40 meters, RIS channel
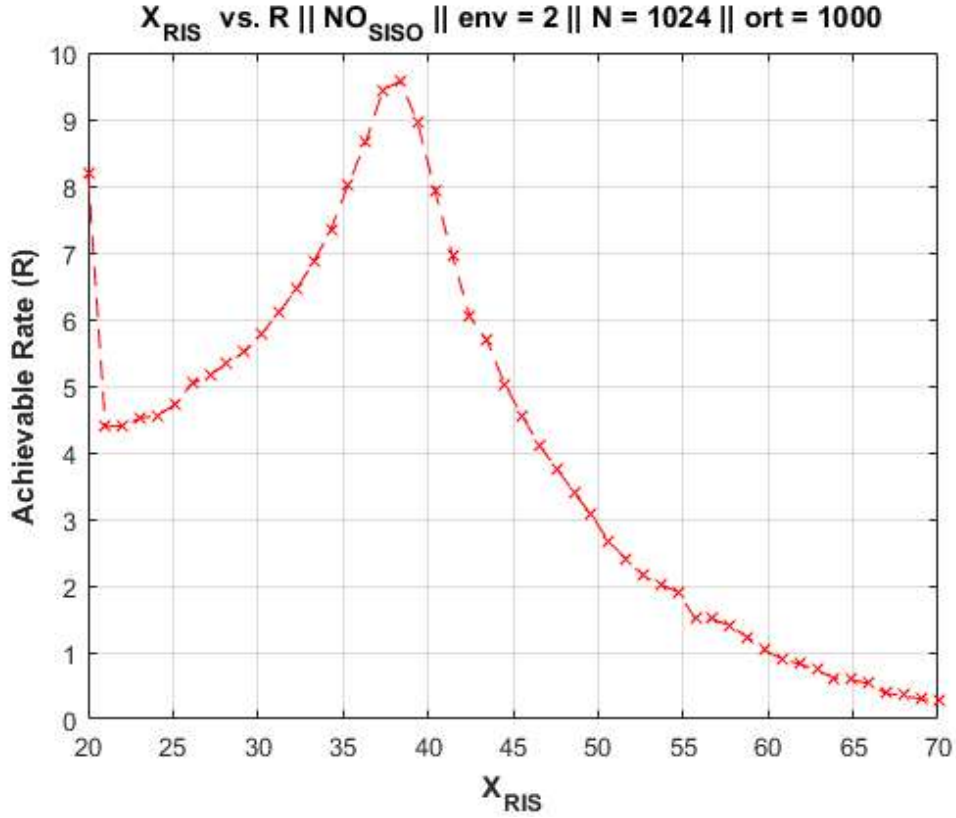
Figure 2.14 : Achievable rate in outdoor environment for 1024 elements with the absence of direct channel by varying x_{RIS}.

is rapidly goes to zero due to path loss. However, direct channel does not suffer from these large path loss and its mean is at the level of 0.5.

Also, it can be seen that, if the mean of these points are taken as reference, the achievable rate is larger compared with the one that direct channel is absent. Therefore, it can be concluded that usage of RIS in an environment that direct channel can be formed might be useless.

For example, if the above simulation is performed for the outdoor environment as well, again a completely random behavior can be seen in Figure 2.16. However, the mean value of these fluctuating points are larger than the one with no direct channel. This observation again supports the argument that the direct channel is much stronger than the RIS-assisted channel in all types of environments.

Also, the outdoor environment uses a completely different cluster model for RIS-receiver and direct channel unlike the indoor model which assumes a complete LOS channel for RIS-receiver and a common cluster model for the direct channel.
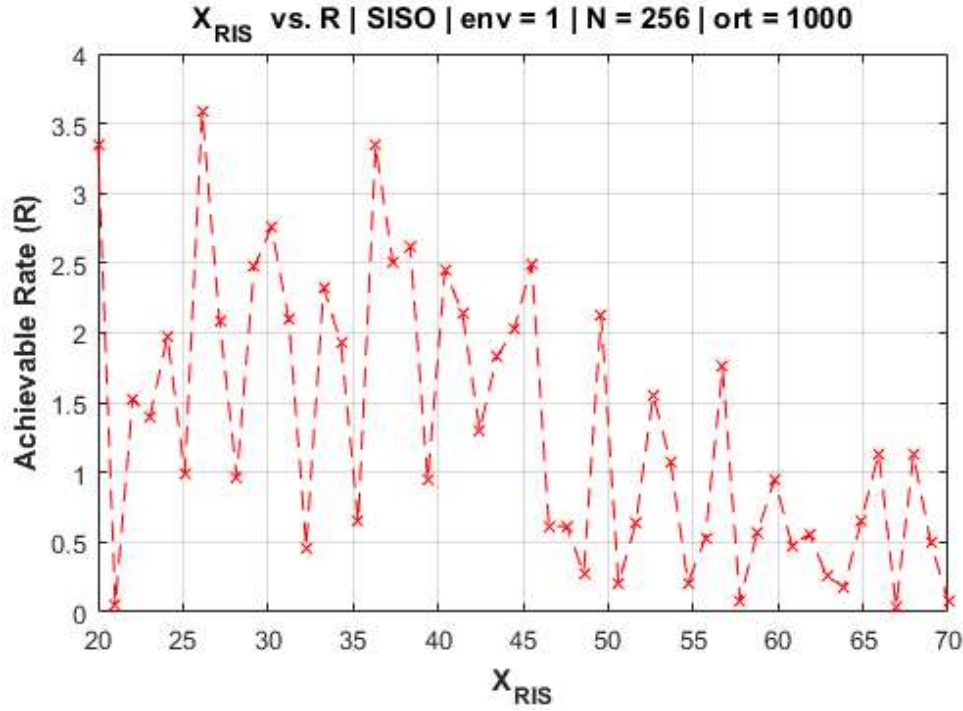
Figure 2.15 : Achievable rate in indoor environment for 256 elements with the presence of direct channel by varying x_{RIS}.

Therefore, adding another scattering mechanism to the channel, increases the overall randomness and causes the fluctuations as we see in the figure.

It is checked that if RIS-assisted channel is able to compete with the direct channel by increasing the RIS size again to 1024. This is illustrated in Figure 2.17. Although, the achievable rate again fluctuates to some degree, a trend now can be seen. The reason for that is when RIS moves closer to the receiver, the suffering from path loss is mitigated;and hence, it can beat the strength of direct channel. Fortunately, the indoor environment does not introduce any extra randomness and thanks to that, a clear trend can be seen. However, this is not the case in the outdoor environment, as seen in Figure 2.18.

In Figure 2.18, a clear trend cannot be seen because in the outdoor model both the RIS-receiver channel and the direct channel is a different scattering environment, although the overall channel gain is strong. This again is in the favor of our argument, stating that if a direct channel can be established for communication, RIS usage might be unnecessary unless its terminal points are perfectly chosen. However, again a peak
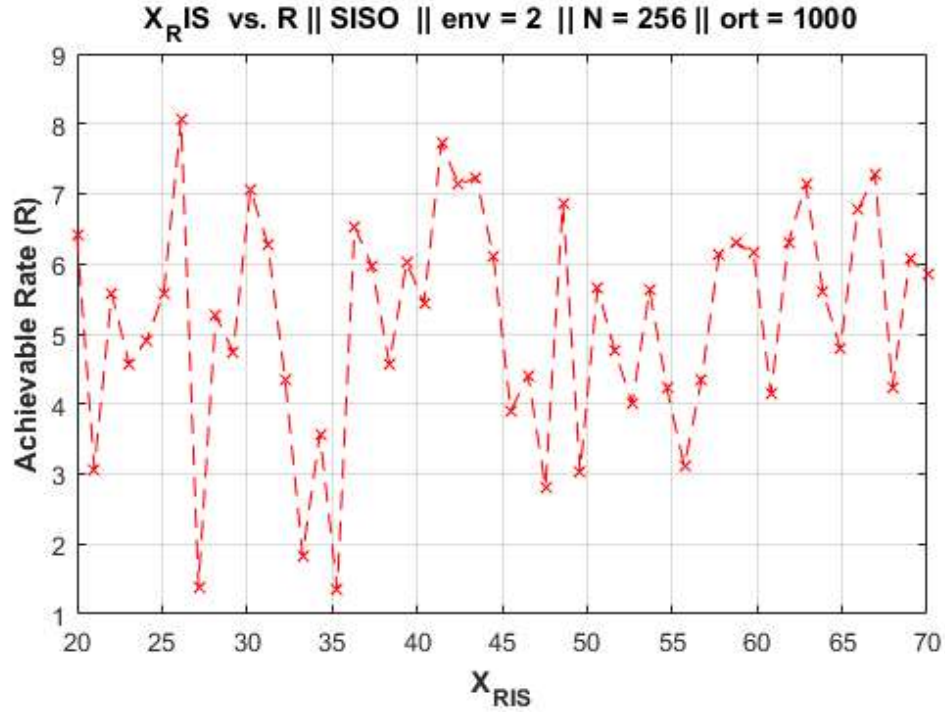
Figure 2.16 : Achievable rate in outdoor environment for 256 elements with the presence of direct channel by varying x_{RIS}.

can be seen around the 40 meters since RIS and receiver are in their closest position and hence almost no path loss incurred.

The first case of the positioning analysis is completed. However, since the coordinates for the terminals are chosen somewhat arbitrary, there are no figures to compare. Therefore, a new set of points proposed by [20] are used in the following subsection. These points are optimized and comply with the network parameters as suggested by the researchers.

2.5.3.2 Second case of different positioning

In the second case, on the other hand, the coordinates of the transmitter, RIS, and receiver are respectively given as (0,25,20), (20,60,10), (50,50,1). The referenced figure proposed by [20] is given in Figure 2.19.

The smoothness of these curves stems from the *ort* number;namely, how many times it is generated and averaged. However, this figure assumes that the direct channel between transmitter and receiver is blocked. Therefore, the trend of curves is close to our simulations that are calculated in the outdoor environment. However, the element
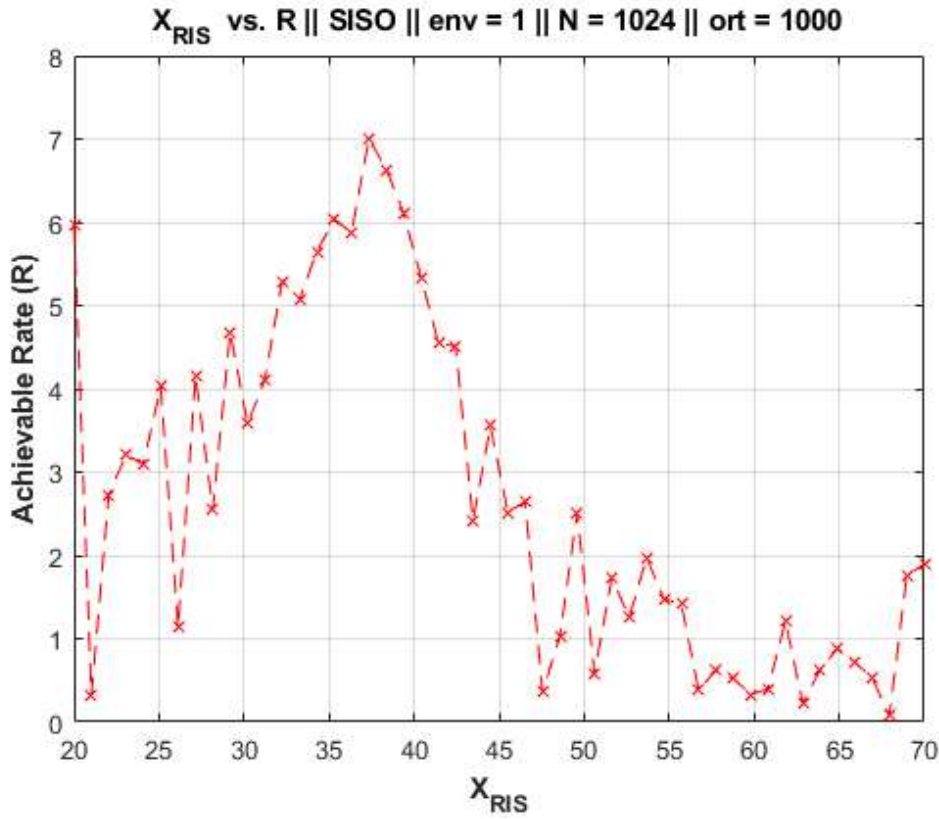
Figure 2.17 : Achievable rate in indoor environment for 1024 elements with the presence of direct channel by varying x_{RIS}.

number of 64 is quite low for these frequency ranges because RIS-assisted channel suffers from high path loss. Therefore, element number of 256 and 1024 are taken as reference to be able to compare the results.

Also, the rate of increases is different and smaller than our simulations. These results can be expected since the proposed model here is more extensive and different.

Since the referenced simulation is only performed for the outdoor environment. The simulations performed by us only include outdoor environment and blocked direct channel.

SISO channel is somewhat problematic, therefore it is blocked, as the researchers in [20] suggested. As it can be seen from the Figure 2.20, the results obtained in our simulations are close to the referenced simulation.

Here, in our model, it starts from 0.15 and rises to a level of 0.55. In the referenced figure, on the other hand, it starts from 1 and goes to a level of 1.5. As we mentioned earlier, the starting point of our model is much less than the referenced simulation.
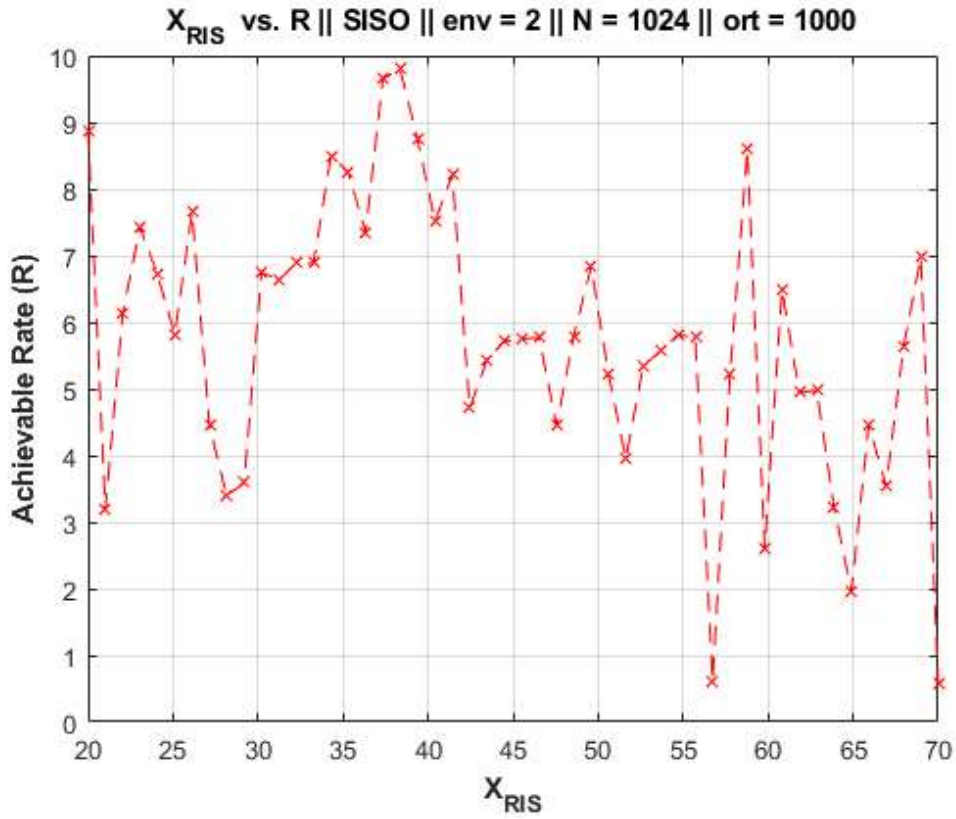
Figure 2.18 : Achievable rate in outdoor environment for 1024 elements with the presence of direct channel by varying x_{RIS}.

However, our model is more extensive and includes performance degrading parameters such as polarization dependent fading and cluster power. Therefore, the reduction in the starting point is not much of a problem.

Also, the difference between the amount of increase may be dependent on the models. However, the trend is almost the same. There is a peak point where the RIS and receiver reach their closest distance; and hence, less path loss and when the RIS moves much farther away from the receiver, signal quality rapidly dies out.

For the sake of completeness and to see the effect of the increasing N, the same simulation is performed for an element number of 1024. The result of the simulation is given in the Figure 2.21. As it can be seen, the trend is exactly the same that of 2.20 with an increase of more than 6-fold.

This result shows that when the direct link is absent in the channel, increasing the RIS size contribute achievable rate thoroughly. Therefore, RIS can be utilized in an environment where establishing a direct channel is not effective or cannot be done.
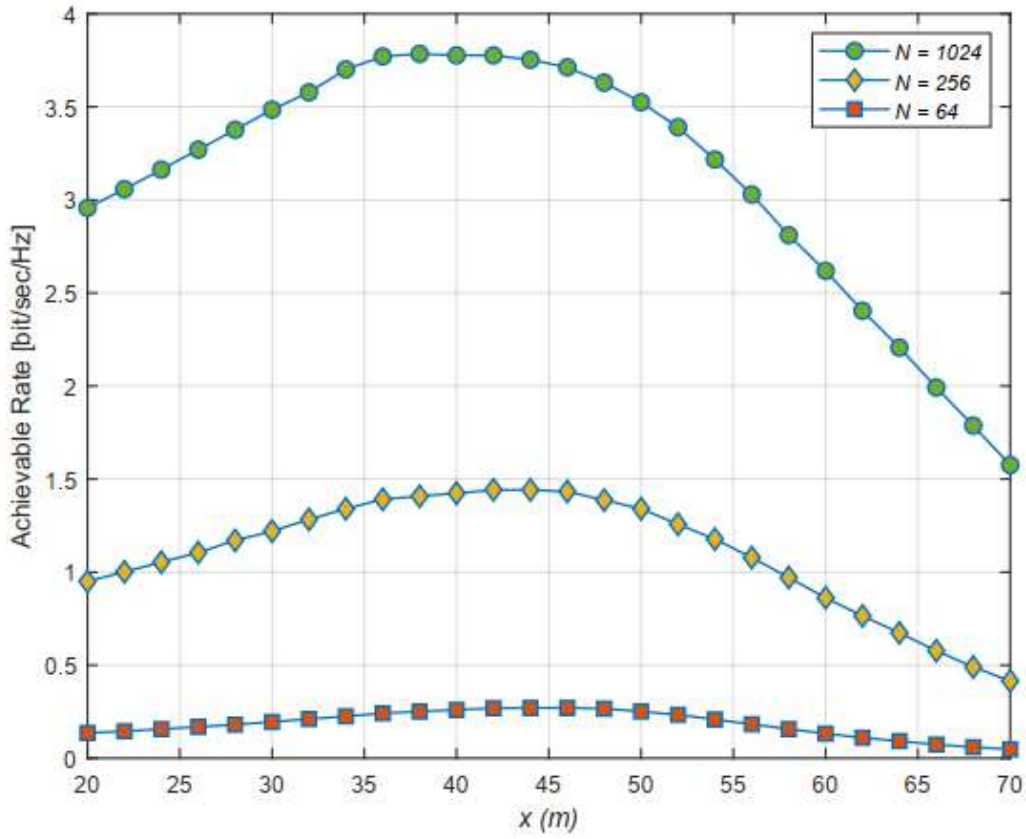
Figure 2.19 : Referenced achievable rate in outdoor environment for different number of elements with the absence of direct channel by varying x_{RIS}.
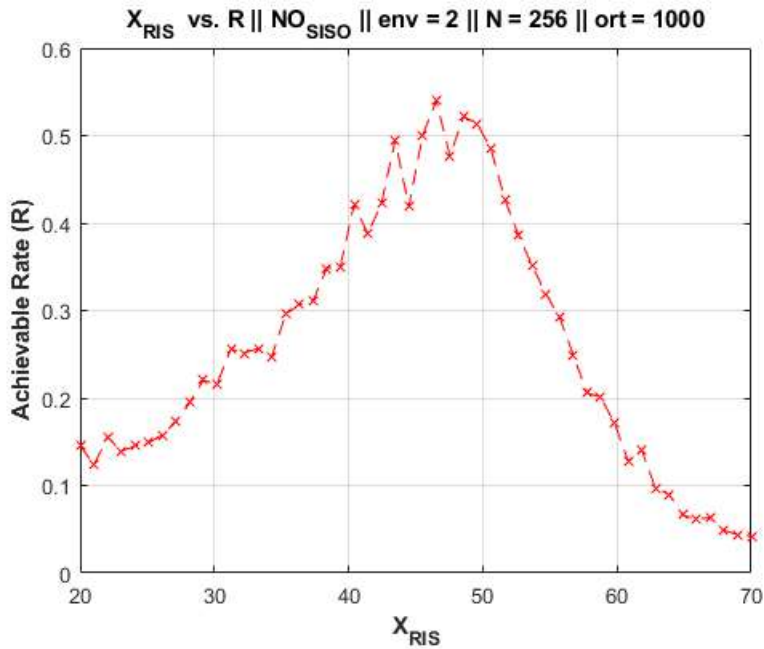

Figure 2.20 : Achievable rate in outdoor environment for 256 elements with the absence of direct channel by varying x_{RIS}.
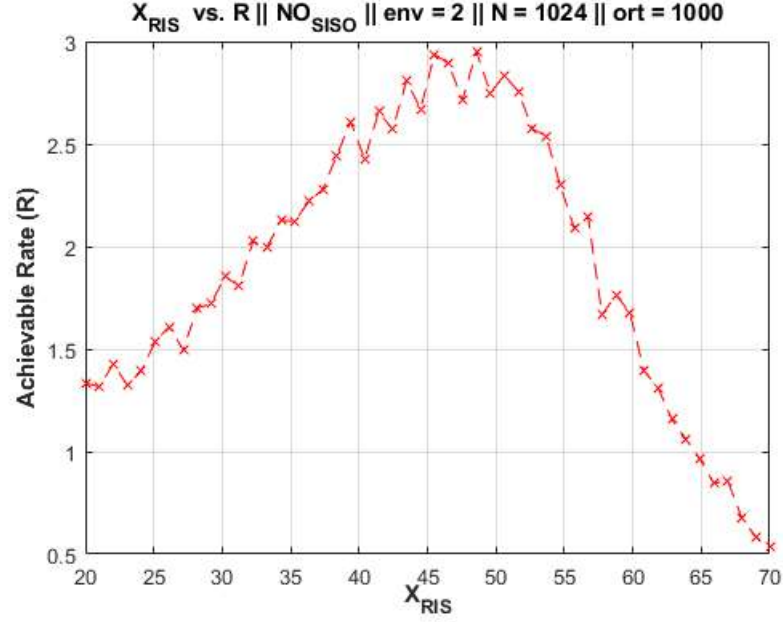
Figure 2.21 : Achievable rate in outdoor environment for 1024 elements with the absence of direct channel by varying x_{RIS}.

Moreover, one can easily see the effects of positioning here. The arbitrarily chosen terminal coordinates do not yield the best performance. However, the suggested coordinates in [20] yield better performances. This shows that the positioning of the RIS is also a network design optimization parameter. It should be chosen such that the communication link can benefit both from the RIS-assisted channel and direct channel. However, one should be careful when it is decided to deploy RIS because direct channel is much stronger, and it makes the use of RIS is useless in its presence. Therefore, we close this section by stating the importance and effect of the positioning.

2.6 Optimizing the RIS Response

Formulation of the optimization problem for the RIS response may vary with respect to the channel conditions. The existence of the direct path between transmitter and receiver (h_{SISO} channel), model of the RIS, estimation of the channel information changes the formulation of the problem. For instance, if a passive RIS structure is used, then the magnitude of the RIS response matrix entries should be less than or equal to one. If there is h_{SISO} a channel, then phase adjustment should be done with respect to the signal propagated through that channel. However, as shown in the simulations, the existence of h_{SISO} causes randomness in achievable rate that is not controllable by

the RIS usage. Thus, in the optimization problem, it is assumed that the LOS channel between transmitter and receiver is blocked.

If there is no channel information, then maximizing the expected value of the achievable rate could be the starting point. However, since the channel model is quite complex, and it includes many random variables, it is challenging to obtain a closed form formulation for the expected value. Thus, it is assumed that RIS to transmitter and RIS to receiver channel are estimated, and perfect channel information has been obtained. However, since channel information also includes the estimation of arrival angles, which is not feasible in practice, in the course of determining the RIS response, the mean of the angles can be used. Using the mean of the angles produces acceptable results when the variations of the random variables that are generating the angles are small.

Formulation of the optimization problem starts with the determining the objective function and constraints. The function to be maximized is the achievable rate. Maximizing the achievable rate is equivalent to maximizing the instantaneous SNR. The formulation of the optimization problem is given as

$$maximize\{\rho\} \quad , \quad subject \text{ to } \left|(\Theta_{n,c,s,k,l})_{ij}\right| \leq 1, \quad i,j \in \{1,2\} \qquad \textbf{(2.34)}$$

where constraints stem from the passive RIS condition. Instantaneous SNR is a function of the channel coefficients, transmit power and the noise power. Since transmit and noise power are the parameters which have been kept fixed, maximizing the instantaneous SNR problem turns into maximizing the channel coefficients problem. Thus, optimization problem turns into

$$maximize\{|H|^2\} \quad , \quad subject \text{ to } \left|(\Theta_{n,c,s,k,l})_{ij}\right| \leq 1, \quad i,j \in \{1,2\}. \qquad \textbf{(2.35)}$$

The open form of this formulation is given as

$$maximize\{|\sum_{n=1}^{N}\sum_{c=1}^{C}\sum_{s=1}^{S_c}\sum_{k=1}^{\bar{C}}\sum_{l=1}^{\bar{S}_c}\mathbf{h_{n,c,s}^{NLOS}}\Theta_{n,c,s,k,l}\mathbf{g_{n,k,l}^{NLOS}} + \sum_{n=1}^{N}\mathbf{h_n^{LOS}}\Theta_n^{LOS}\mathbf{g_n^{LOS}}|^2\}$$
$$subject \text{ to } \left|(\Theta_{n,c,s,k,l})_{ij}\right| \leq 1, \quad i,j \in \{1,2\}. \qquad \textbf{(2.36)}$$

This maximization problem can be solved by using the estimated channel information. Another approach for forming optimization problem is turning a maximization problem to minimization problem by using the ideal RIS response solution. In the ideal case, RIS cancels phase mismatches with no loss. Thus, coefficients of the response matrix become complex exponentials with unit magnitude. The phases of these complex exponentials are equal to the sum of the phases of the RIS to transmitter and RIS to receiver channel multiplied by minus one. Thus, RIS response cancels the total phase shift in the channel. In the ideal response case, the overall channel equation reduces to

$$H_{ideal} = \sum_{n=1}^{N}\sum_{c=1}^{C}\sum_{s=1}^{S_c}\sum_{k=1}^{\bar{C}}\sum_{l=1}^{\bar{S}_c} |\mathbf{h_{n,c,s}^{NLOS}}||\mathbf{g_{n,k,l}^{NLOS}}| + \sum_{n=1}^{N}|\mathbf{h_n^{LOS}}||\mathbf{g_n^{LOS}}| \qquad (2.37)$$

which can be calculated by using the estimated channel information, and with the help of this equation, maximization problem can be turned into

$$minimize\{(H_{ideal} - |H|)^2\} \quad , \quad subject\ to\ \left|(\Theta_{n,c,s,k,l})_{ij}\right| \leq 1, \quad i,j \in \{1,2\} \quad (2.38)$$

which is a minimization problem. In this minimization formulation, it is aimed to using the information provided by the ideal case solution. By using this information and omitting the passive RIS constraint, the ideal RIS response for NLOS and LOS can be expressed in terms of the channel coefficients respectively as

$$\Theta_{n,c,s,k,l} = \frac{1}{\sqrt{\left|h_{n,c,s}^{NLOS}\|g_{n,k,l}^{NLOS}\right|}}\left((h_{n,c,s}^{NLOS})^*\right)^{\top}\left((g_{n,k,l}^{NLOS})^*\right)^{\top}, \qquad (2.39)$$

$$\Theta_n^{LOS} = \frac{1}{\sqrt{|h_n^{LOS}\|g_n^{LOS}|}}\left((h_n^{LOS})^*\right)^{\top}\left((g_n^{LOS})^*\right)^{\top}. \qquad (2.40)$$

It should be noted that, equations (2.39) and (2.40) produce 2-by-2 matrices in general, and in transmission line models off-diagonal entries become zero. However, according to these equations, it is not mandatory to off-diagonal entries become zero. Thus, it has been shown that transmission line models can not provide ideal RIS response. Moreover, it is required that for providing ideal RIS response, each entry of the 2-by-2 matrix should be controlled independently. However, it is not the case in general. But

this result implies that using a RIS structure such as dual polarized RIS may increase the optimization performance because it provides flexibility on the control of the RIS response. Capability of adjusting responses for different polarizations separately is a desired property.

Finally, in the case of no channel information is estimated, optimization of can be performed by maximizing the expected value of the instantaneous SNR, which corresponds to maximizing the expected value of the $|H|^2$. Since open expression of the H is quite complex, instead of calculating the expectation directly, RIS to transmitter and RIS to receiver channels can be modeled as a single random variable. Then probability density functions for these random variables can be generated by using the data obtained by experiments or simulations. Then expected values of these random variables can be calculated, which is more simple compared to calculating the expectation of the open expression.

3. REALISTIC CONSTRAINTS AND CONCLUSIONS

3.1 Practical Application of this Project

Since the RIS is a potential technology for 6G systems, it has many potential use cases in wireless communication systems. Creating a non-direct channel in the LOS channel blocked scenarios, reducing the electromagnetic pollution, passive beamforming, blocking the eavesdropping, providing access to the local blind spots are some prominent potential use cases of the RIS. These capabilities of the RIS make it a candidate technology for indoor environment wireless communications. Moreover, RIS can be used in more complex tasks such as index modulation [21], media based modulation [22], binary polarization shift keying [23], and MIMO transmission [24].

In this project, a physical end-to-end channel model is proposed for the frequency range from few GHz to 100GHz. If measurements verify the model, then the model can be used in the analysis of the systems explained at the beginning. By using the proposed model, limits of the potential RIS usage cases, system performance can be determined. More importantly, synthesis and the optimization of the wireless link could be performed by considering the proposed model. Consequently, in the case of the proposed model being accurate, it is expected to find widespread area of application in the future.

3.2 Realistic Constraints

Deploying a RIS in the wireless channel comes with constraints to consider. Foremost, the RIS structure should be designed with respect to the application. For instance, since outdoor distances are larger compared to the indoor, active RIS usage may be required in outdoor scenarios. However, since RIS technology's prominent aspect is the fact that being passive, the cost of the link should be considered. Because if active RIS is used, then power consumption increases the cost. In that case, relays should be considered instead of the RIS. Moreover, since wireless channel is dynamic,

RIS's capability of adopting the dynamic environment should be tested. It may be required to update RIS response in real time. Nonetheless, updating the response in real time may require active components that estimating the channel and computing the proper response continuously. RIS should be tested for its reliability critic operating conditions. If the transmitter or receiver is mobile, then Doppler shift arises. Since RIS is stationary in general, response should be adjusted considering the mobile users. If more than one user is communicating by using the RIS link, then multi-objective optimization for achievable rate should be performed. In such cases, Pareto optimum for achievable rates can be calculated. However, Pareto optimum value differs from the case where a single objective function is investigated. Since RIS size is proportional to the wavelength, producing a RIS in the higher frequencies regimes gets difficult because of the requirement of smaller meta-atoms. Moreover, for wideband signals, the response of the RIS differs. For different modulation schemes, the response of the RIS also differs. Thus, used modulation scheme should be considered as a parameter that effects the RIS performance.

3.2.1 Social, environmental and economic impact

The deployment of a RIS in the environment makes the channel more reliable and makes the users get access to higher data rates and bandwidth. This will ease both the communication between people and reaching the information available on the network. In addition, since the deployment of the RIS technology does not require high powers, it will be more environmentally friendly.

The economic impact that RIS poses on society may be the easiness of reaching information and maybe a cheaper solution for users to obtain since it will reduce the transmitter and receiver complexity considerably.

3.2.2 Cost analysis

The project is aiming to obtain a theoretical electromagnetic model of RIS assisted channels. Obtained models will be simulated by using adequate programs, i.e., MATLAB, Python etc. There will be no practical implementation. Thus, the cost of the project is confined to the salary of engineers and the cost of the used software programs used. The annual license for MATLAB is 940 American dollars. If EM analysis for the RIS model is required, ANSYS HFSS software for electromagnetic

simulations costs, 40000 American dollars. Engineers' minimum wage is determined to be 5750 Turkish liras per month by TMMOB in 2021. The research is expected to last 7 months. Two engineers will be working on this project. Since there is no practical implementation, there are no material costs.

3.2.3 Standards

Since RIS is a novel technology under development, the standards for RIS assisted wireless channel is not determined yet. RIS technology has potential use cases in 6G systems. Thus, it is expected that standards for RIS assisted communications are coherent with 6G standards in terms of reliability, data rates and other application specific requirements. In order to determine the standards for RIS assisted systems, ETSI found a study group called, industry specification group on reconfigurable intelligent surfaces. However, there are no results published yet.

3.2.4 Health and safety concerns

In the case of RIS used as a beamformer, the incoming waves can be focused on certain locations and focused radiation patterns may interact with molecules in the human body in several frequencies. For example, a 2.45 GHz signal used in microwave ovens can vibrate the water molecules and can cause an increase in heat. If the same frequency is used in communications and the focused radiation field's power is high enough, water molecules in the human body may also vibrate. However, it is not expected to exposure to any kind of detrimental radiation in the project.

3.3 Future Work and Recommendations

Foremost, the optimization problem of EM response should be solved. Thus, the limits of the RIS technology can be simulated in a more realistic manner. Then, measurements of the RIS assisted channel should be done and results should be compared to the simulations results. Thus, the accuracy of the model can be tested. Moreover, if measurement and simulations results are consistent, then the generation procedure of the stochastic parameter in the channel such as path loss, cross polarization ratio and others can be updated by considering the data obtained from measurements. In the application specific use cases, the more detailed surface

models can be used. Therefore, more profound surface models could be developed by using the SEM based models. Finally, RIS response should be analyzed in different modulation cases. The models for EM response are developed for the single tone signals. Thus, EM response models are valid under the condition of interaction with the sinusoidal wave. For obtaining a more general model, RIS interaction with the modulated signals should be studied and included in the channel model.

Also, the proposed channel model can be tested in a real-life using a RIS. The results obtained from the measurements can be compared with the simulations performed in this study.

Moreover, There is a phenomenon called mutual coupling, which is the electromagnetic interference between the elements of the RIS. However, if these elements affect each other comparable to the control mechanism, then controlling the elements of RIS would be useless. Therefore, a new electromagnetic surface modelling can be utilized as a future work to take mutual coupling effects into consideration and apply the desired control accordingly. The surface electromagnetic based models are promising in terms of mutual coupling and can be utilized more in the future.

REFERENCES

[1] **Goldsmith, A.,** (2005), Wireless Communications.

[2] **Tse, D.N.C. and Viswanath, P.** (2009). Fundamentals of Wireless Communication (Tse, D. and Viswanath, P.) [Book review]., *IEEE Trans. Inf. Theory*, *55*(2), 919–920, `http://dblp.uni-trier.de/db/journals/tit/tit55.html#TseV09`.

[3] **Stuber, G.L.** (1996). *Principles of Mobile Communication*, Kluwer Academic Publishers, USA, 1st edition.

[4] **Caloz, C.** (2005). *Electromagnetic Metamaterials: Transmission Line Theory and Microwave Applications: The Engineering Approach*, volume 15.

[5] **Zheludev, N. and Kivshar, Y.** (2012). From Metamaterials to Metadevices, *Nature materials*, *11*, 917–24.

[6] **Capolino, F.** (2009). *Applications of Metamaterials*, Metamaterials Handbook, CRC Press, Boca Raton, FL.

[7] **Ma, J.** (2021). From Metamaterials to Metadevices and Applications, *IEEE Transactions on Microwave Theory and Techniques*, *69*(3), 1491–1492.

[8] **Epstein, A. and Eleftheriades, G.** (2016). Huygens' metasurfaces via the equivalence principle: Design and applications, *Journal of the Optical Society of America B*, *33*, A31.

[9] (2019). *Surface Electromagnetics: With Applications in Antenna, Microwave, and Optical Engineering*, Cambridge University Press.

[10] **Wu, Q. and Zhang, R.** (2020). Towards Smart and Reconfigurable Environment: Intelligent Reflecting Surface Aided Wireless Network, *IEEE Communications Magazine*, *58*(1), 106–112.

[11] **Di Renzo, M., Danufane, F.H. and Tretyakov, S.** (2021). Communication Models for Reconfigurable Intelligent Surfaces: From Surface Electromagnetics to Wireless Networks Optimization, *arXiv preprint arXiv:2110.00833*.

[12] **Han, Y., Li, X., Tang, W., Jin, S., Cheng, Q. and Cui, T.J.** (2021). Dual-Polarized RIS-Assisted Mobile Communications, *IEEE Transactions on Wireless Communications*.

[13] **Costa, F. and Borgese, M.** (2021). Electromagnetic Model of Reflective Intelligent Surfaces, *IEEE Open Journal of the Communications Society*, *2*, 1577–1589, `https://doi.org/10.1109%2Fojcoms.2021.3092217`.

[14] **Chen, W.**, **Bai, L.**, **Tang, W.**, **Jin, S.**, **Jiang, W.X. and Cui, T.J.** (2020). Angle-Dependent Phase Shifter Model for Reconfigurable Intelligent Surfaces: Does the Angle-Reciprocity Hold?, *IEEE Communications Letters*, *24*(9), 2060–2064.

[15] **Holloway, C.L.**, **Love, D.C.**, **Kuester, E.F.**, **Gordon, J.A. and Hill, D.A.** (2012). Use of Generalized Sheet Transition Conditions to Model Guided Waves on Metasurfaces/Metafilms, *IEEE Transactions on Antennas and Propagation*, *60*(11), 5173–5186.

[16] **3GPP**, (2019), Study on channel model for frequencies from 0.5 to 100 GHz.

[17] **Basar, E.** (2019). Transmission Through Large Intelligent Surfaces: A New Frontier in Wireless Communications, *2019 European Conference on Networks and Communications (EuCNC)*, pp.112–117.

[18] **Bjornson, E. and Sanguinetti, L.** (2021). Rayleigh Fading Modeling and Channel Hardening for Reconfigurable Intelligent Surfaces, *IEEE Wireless Communications Letters*, *10*(4), 830–834, `https://doi.org/10.1109%2Flwc.2020.3046107`.

[19] **Kilinc, F.**, **Yildirim, I. and Basar, E.**, (2021), Physical Channel Modeling for RIS-Empowered Wireless Networks in Sub-6 GHz Bands, `https://arxiv.org/abs/2111.01537`.

[20] **Basar, E.**, **Yildirim, I. and Kilinc, F.** (2021). Indoor and Outdoor Physical Channel Modeling and Efficient Positioning for Reconfigurable Intelligent Surfaces in mmWave Bands, *IEEE Transactions on Communications*, *69*(12), 8600–8611.

[21] **Basar, E.** (2020). Reconfigurable Intelligent Surface-Based Index Modulation: A New Beyond MIMO Paradigm for 6G, *IEEE Transactions on Communications*, *68*(5), 3187–3196.

[22] **Yan, Y.**, **Cao, Y. and Lv, T.** (2021). Enabling Media-Based Modulation for Reconfigurable Intelligent Surface Communications, *2021 IEEE Wireless Communications and Networking Conference (WCNC)*, pp.1–6.

[23] **Ibrahim, E.**, **Nilsson, R. and Van De Beek, J.** (2022). Binary Polarization Shift Keying With Reconfigurable Intelligent Surfaces, *IEEE Wireless Communications Letters*, *11*(5), 908–912.

[24] **Tang, W.**, **Dai, J.Y.**, **Chen, M.Z.**, **Wong, K.K.**, **Li, X.**, **Zhao, X.**, **Jin, S.**, **Cheng, Q. and Cui, T.J.** (2020). MIMO Transmission Through Reconfigurable Intelligent Surface: System Design, Analysis, and Implementation, *IEEE Journal on Selected Areas in Communications*, *38*(11), 2683–2699.

CURRICULUM VITAE

Name Surname	:	Serden Sait Eranil
Place and Date of Birth	:	Batman, 26.10.1999
E-Mail	:	eranil17@itu.edu.tr

EDUCATION :

- **High School Diploma** : 2017, Yalova Termal Science High School, Quantitative Section
- **B.Sc.** : 2022, Istanbul Technical University, Faculty of Electrical and Electronics, Department of Electronics and Communication Engineering

PROFESSIONAL EXPERIENCE:

- 2020 June-2020 October ASELSAN A.Ş, MGEO Sector, Navigation Systems Lab., Intern
- 2022 October-Present, ITU Wireless Communication Research Laboratory, Volunteer Undergrad Researcher
- 2022 April-Present TUSAŞ, Avionics Software, Part-Time Software Engineer

CURRICULUM VITAE

Name Surname	: Ramazan Umut Aktaş
Place and Date of Birth	: İzmir, 22.12.1998
E-Mail	: aktasr17@itu.edu.tr

EDUCATION :

- **High School Diploma** : 2017, Halil Kale Science High School, Quantitative Section
- **B.Sc.** : 2022, Istanbul Technical University, Faculty of Electrical and Electronics, Department of Electronics and Communication Engineering

PROFESSIONAL EXPERIENCE:

- 2021 August October ASELSAN A.Ş, UGES Sector, Process Design and System Production Department, Intern
- 2022 October-Present, ITU Wireless Communication Research Laboratory, Volunteer Undergrad Researcher
- 2022 February-Present TÜBİTAK BİLGEM, Communication and Signal Processing Research Lab., Long Term Intern